Title
Global Distribution of Carbon Stock in Live Woody Vegetation

Author
Yu, Yifan

Publication Date
2013

Peer reviewed|Thesis/dissertation

University of California

Los Angeles

Global Distribution of Carbon Stock in Live Woody Vegetation

A dissertation submitted in partial satisfaction

of the requirements for the degree

Doctor of Philosophy in Atmospheric and Oceanic Sciences

by

Yifan Yu

2013

Abstract of the Dissertation

Global Distribution of Carbon Stock in Live Woody Vegetation

by

Yifan Yu

Doctor of Philosophy in Atmospheric and Oceanic Sciences

University of California, Los Angeles, 2013

Professor Ulrike Seibt, Chair

The terrestrial biosphere is responsible for removing roughly one quarter of the total anthropogenic emissions of carbon dioxide from the atmosphere. This process is dominated by the forests. The terrestrial portion of the global carbon cycle is also the most uncertain. Growing forests are a major sink of CO_2 while deforestation contributes as a major source of CO_2. While the locations of deforestation can be tracked with remote sensing data relatively well, the amount of carbon removed is not well known due to the lack of knowledge on the biomass density of the forests that were disturbed. Spatially explicit distribution of carbon stocks in global forests can greatly reduce this uncertainty by improving estimates of emissions from land use activities. It will also help with green house gas inventory at regional and national scales.

Increasing amounts of remote sensing based forest studies are being conducted, however, there is currently no global spatially explicit map of forest biomass/carbon. This dissertation aims to address that by producing the first global spatially explicit map of live biomass and carbon stock in forests and other living woody vegetation at ∼1 km resolution for circa year 2005. A combination of remote sensing data from the Quick Scatterometer (QuikSCAT), Moderate Resolution Imaging Spectroradiometer (MODIS), and Shuttle Radar Topography

Mission (SRTM) are used to provide wall-to-wall spatial information. Ground inventory and LiDAR from the Geosciences Laser Altimeter System (GLAS) onboard the Ice, Cloud, and land Elevation Satellite (ICESat) are used to create a global network of aboveground biomass (AGB) samples. Landcover map based on the GlobCover product from the European Space Agency (ESA) is used as ancillary data. These are combined in a statistical model using Maximum Entropy to create the first global map of AGB and total carbon stock (above + below ground) in living biomass. Uncertainty at the pixel level is also produced alongside the above products. The total global carbon in live woody vegetation is estimated at 337 PgC, with 311.4 PgC being in the forests (92% of total) for circa year 2005, compared with 302.8 PgC in total global live forest biomass as reported in the United Nations Food and Agriculture Organization's 2010 Forest Resources Assessment report (FRA 2010). Shrublands and savannas account for the other 25.6 PgC (8% of total) globally. National carbon stocks are calculated and reported for all the countries using several different thresholds for forest cover.

The dissertation of Yifan Yu is approved.

Sassan S. Saatchi

Curtis Deutsch

Thomas W. Gillespie

Alex Hall

Ulrike Seibt, Committee Chair

University of California, Los Angeles

2013

In Memory of my Mother ...

always strong and loving

Table of Contents

List of Figures

List of Tables

Acknowledgments

First and foremost, I would like to thank my mentor and advisor, Dr. Sassan Saatchi. I first worked for Sassan when I was still an undergrad. That work led me to eventually go into this field of study. This dissertation work would not have been possible without his guidance. I have learned much regarding scientific research through working with him. I would also like to thank my advisor Professor Ulli Seibt for her help. My committee members, Professor Curtis Deutsch, Professor Alex Hall, and Professor Thomas Gillespie, thank you for taking time out of your busy schedules to be on my committee. My acknowledgement also goes to the collaborators I've worked with on the various projects and for providing some of the data used in this dissertation.

This has been a long journey for me with many ups and downs. My family have been supportive of me this entire time and I am very grateful. My mother passed away in 2012, and I still feel some regret that she was not able to see me complete my PhD. Even through her 8 year battle with ALS, she has always worried about me more than herself. My father also went through this difficult period while shouldering much of the responsibility, trying to minimize the disturbance on my graduate studies.

Finally, I also want to mention all my friends who have been part of my journey: Mark Rudner, Nathan Wu, Brian Eng, Kelly Zheng, and Graeme Smith, going all the way back to the band days of undergrad. I have always thought Mark is one of the best role models for good time management, and he has been helpful to me on many occasions. Nathan is the only band member still in the LA area, and we often hang out over food to discuss various topics or just life in general.

There are also all my friends from UCLA. Calvin, Sergio, KaYee, Clare, Steven, Edan, Stephanie, Hoon-Ju; you guys were great. I think we were one of the most close knit years at AOS. KaYee has been like a big sister to me. I met Masanao

Yajima through a martial arts class at UCLA. We have become good friends, and his insights on statistics have been very helpful. I would often go to practice on Saturdays with Masa and Marin and discuss our respective research while on the road. In the last few months of working on this dissertation, it was very helpful to work with Jida Wang, who's also finishing around the same time, to help motivate each other. Lani, Peng, Lunjin, Thanasis, Cici, Seunghee, Guoqiong, Kim, Xuan, Ting, and many other friends, you have all helped make this journey great.

This research was partially supported by NASA Carbon Monitoring System grant #101535 at the Jet Propulsion Laboratory and the UCLA Institute of Environment and Sustainability.

Vita

2003	B.S. Applied Physics, California Institute of Technology.
2007	M.S. Atmospheric and Oceanic Sciences, University of California Los Angeles.
2006-2010	Teaching Assistant/Associate, Atmospheric and Oceanics Sciences Department, UCLA.
2007-2013	Graduate Student Researcher, Atmospheric and Oceanic Sciences Department, Joint Institute for Regional Earth Systems Science and Engineering, Institute of the Environment and Sustainability, UCLA.

Publications

Yu, Y., Saatchi S., Ganguly S., Zhang G., Nemani R., Lefsky M., Myneni R., Sun G., Mitchard E., Harris N., Brown S., and Seibt U. Global distribution of carbon stock in live woody vegetation, in progress

Zhang G., Wang W., Ganguly S., Weng E., **Yu Y.**, Saatchi S., Nemani R., White M., Mapping stand age of global primary forests using remote sensing data, *Journal of Geophysical Research*, submitted

Zhang G., Ganguly S., Nemani R., White M., Wang W., Saatchi S., **Yu Y.**, Myneni R., A Simple parametric estimation of live forest aboveground biomass

in California using satellite derived metrics of canopy height and leaf area index, *Remote Sensing of Environment*, submitted

Yu, Y., Saatchi S., Heath L. S., LaPoint E., Myneni R., Knyazikhin Y., 2010 Regional distribution of forest height and biomass from multisensor data fusion, *Journal of Geophysical Research*, 115, G00E12, doi:10.1029/2009JG000995.

Rian S., Xue Y. K., McDonald G.M., Toure M.B., **Yu Y.F.**, De Sales, F., Levine, P.A., Doumbia S., and Taylor C.E., 2009 Analysis of climate and vegetation characteristics along the savanna-desert ecotone in Mali using MODIS data, *GIScience & Remote Sensing*, p 424-450

Saatchi S. S., Houghton R. A., Dos Santos Alvala R. C., Soares J. V., and **Yu Y.**, 2007 Distribution of aboveground live biomass in the Amazon basin, *Global Change Biology*, vol. 13, no. 4, p 816-837

CHAPTER 1

Introduction

1.1 Motivation

Forests covers roughly 40 million square km of area, 30% of the total land surface area on Earth, and contain 80% of the Earth's total plant biomass[Kindermann et al., 2008]. Savanna and shrubland biomes cover another 15 million square km. They create the base for most of the terrestrial ecosystems. Additionally, the bio-diversity in these ecosystems is highly correlated with tree species richness and structure of forests and forested landscapes[Perry et al., 2008, chap. 10]. The terrestrial plants are also responsible for removing approximately a quarter of the anthropogenic carbon dioxide emissions, and is one of the most uncertain part of the global carbon cycle[Sarmiento and Gruber, 2002, Ballantyne et al., 2012, Canadell et al., 2007]. Much of this uncertainty comes from emissions from deforestation and land-use change[Pan et al., 2011, Houghton et al., 2009], the estimation of which require knowledge of the fine scale spatial patterns of forest carbon content.

Our knowledge of the spatial patterns of forests is limited on the global scale due to the sheer size of forest area and the costs and difficulties associated with conducting field inventory[Brown et al., 1989, Houghton et al., 2009]. As an example, the United States has one of the most extensive ground-based forest inventory program in the world. Phase 2 of the US Forest Inventory and Analysis (FIA) program, where forest plot measurements are taken, consists of 1 field

sample site for every 6000 acres ($\sim$24 km^2)[FIA, 2005]. The actual area measured in a phase 2 plot is $\sim$700 m^2. This equates to sampling roughly 0.003% of the total area. Over a large enough area, these samples can provide a good estimate of the mean[Heath and Smith, 2000], but they cannot capture the fine scale spatial patterns.

Of the three main categories of tropical, temperate, and boreal forests, the temperate forests are relatively much better sampled with field measurements than the other two. Tropical forests contain over half of the total live biomass in global forests, yet is the least sampled in terms of field measurements[Corlett and Primack, 2006, Grainger, 2008]. It is also where most of the emissions from deforestation is coming from. The lack of field data is partly due to the dense nature of these forests making field measurements difficult and partly due to the fact that these forests are located in the poorer nations who do not have a sophisticated forestry program.

Remote sensing techniques are ideal for providing cost-effective measurements over large areas. Many regional mapping of forest biomass have been conducted using remote sensing data[Saatchi et al., 2011b, Simard et al., 2011, Baccini et al., 2008, Yu et al., 2010, Mitchard et al., 2009]. However, at the global scale, only inventory based estimates exist[Kindermann et al., 2008, Pan et al., 2012] for biomass and carbon stock, or forest coverage using remote sensing[Hansen et al., 2013], but there is no spatially explicit map of biomass or carbon density at the global scale. Mapping forest biomass at the global scale faces several challenges: 1. large heterogeneity of vegetation structure and wood density within and across biomes due to environmental (climate and edaphic) and species variations [Jenkins et al., 2003, Baraloto et al., 2011]; 2. lack of sufficient, well distributed ground samples at the scale of remote sensing image resolutions [Houghton et al., 2009]; 3. limitation of sensitivity of existing satellite observations to the large range of aboveground biomass found across the globe[Patenaude et al., 2005]. The

work in this dissertation address these challenges and creates the first global-scale spatially explicit biomass and carbon map of living woody vegetation at 1km resolution using remote sensing and ground data. A globally consistent biomass and carbon stock map will help reduce the uncertainties in the terrestrial portion of the carbon cycle, as well as providing a resource for national green house gas inventory reporting[Gibbs et al., 2007], such as for the United Nations Framework Convention on Climate Change (UNFCCC).

1.2 Overview of Dissertation

The topic of this dissertation touches a wide area of knowledge. As such, some background information on ecology and remote sensing is provided in Chapter 2 for readers who may not be familiar with the subjects. The reader can feel free to move ahead to a specific subject background or skip the chapter, if already familiar with the subject matters, without any issue. Chapter 3 covers the processing and preparations performed on the remote sensing data sets before they are used in the model. Chapter 4 contains the analyses on ground data, development of allometric equations, and combining the results of those analyses with LiDAR from the Geoscience Laser Altimeter System (GLAS) to create the global sample data set.

Chapter 5 covers the statistical modeling performed using the Maximum Entropy method. The results of the model along with model validation and uncertainty analysis are discussed in the remainder of this chapter before moving on to analyses of the results in terms of carbon stocks and comparison with other ground inventory in Chapter 6. Finally, I'll summarize the work contained in this dissertation in Chapter 7.

CHAPTER 2

Background

This chapter briefly covers some of the background information on ecology and remote sensing. Readers who are not familiar with these subjects may find it useful to go over the following sections before proceeding to the subsequent chapters.

2.1 Forest and other Woody Plant Biomes of the World

What is a forest? This may seem like a simple question with the answer being a grouping of individual trees. However, the specific definition of a forest can have effects on the quantitative values one might calculate involving forests. In the GlobCover landcover mapping effort[Bicheron et al., 2008], forest is defined as greater than 15% cover (at the 300 m native GlobCover resolution) and canopy height of greater than 5 m. The US FIA defined a forest as 10% cover by forest trees of any size with a minimum area of 1 hectare and minimum width of 120 feet[Bechtold and Patterson, 2005]. In the United Nations Food and Agriculture Organization's (FAO) Global Forest Resource Assessment 2010 (FRA2010) [Food and Agriculture Orgnization, 2010], forest is defined as "Land spanning more than 0.5 hectares with trees higher than 5 meters and a canopy cover of more than 10 percent, or trees able to reach these thresholds in situ." This difference in forest definition will be encountered again in Chapter 6 when calculating global total values. The major forest biomes of the world can be grouped into three main categories (tropical, temperate, and boreal) of forests based on climate plus the mangrove forests. Other non-forest biomes that still contain woody vegetation

are described in section 2.1.4.

2.1.1 Tropical Forests

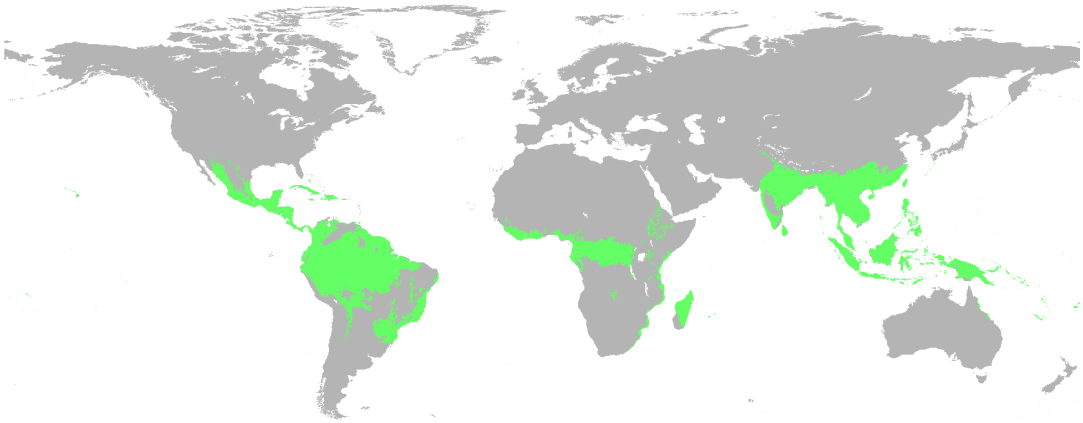

Figure 2.1: Tropical forests of the world. Based on biome map of the world by Olson et al. [2001]

Tropical forests are the most dense forests in the world with the highest species diversity, generally located between 30°N and 30°S latitude (Figure 2.1). Most of these areas are tropical moist broadleaf evergreen forest along with small areas of tropical dry forest and tropical conifer. More than half of the total global biomass in living woody vegetation is contained in the tropical forests.

These regions are mainly located in the poorer nations of the world. Combined with the fact that the density of the forest also makes field inventory difficult, this means the tropical forests are also the most uncertain in terms of total and spatial distribution of biomass[Losos and Leigh, 2004]. This is also where most of the carbon emissions from deforestation is coming from[Achard et al., 2002, Hansen et al., 2008, Asner et al., 2005].

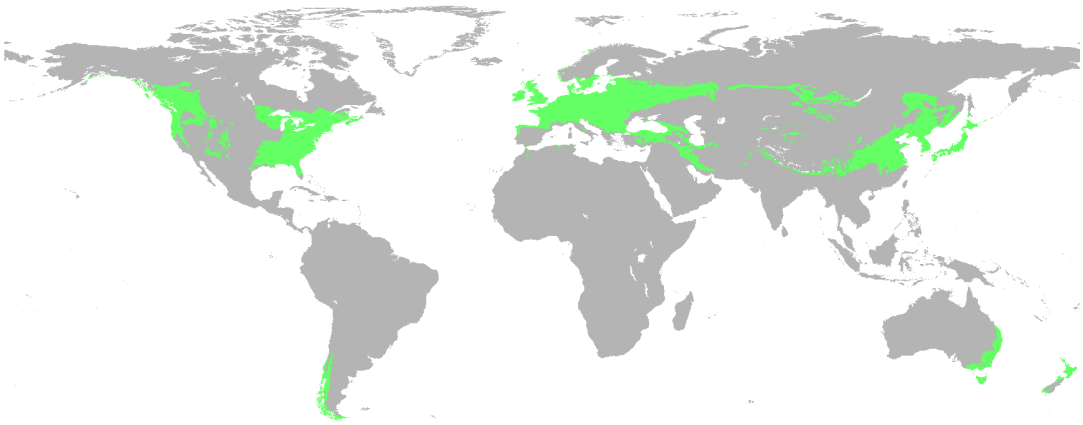

Figure 2.2: Temperate forests of the world. Based on biome map of the world by Olson et al. [2001]

2.1.2 Temperate Forests

Temperate forests consist of deciduous broadleaf forest and needleleaf evergreen forest. Most of these forests are located in the mid-latitudes of the northern hemisphere (Figure 2.2). Biomass density is generally lower than that of tropical forests, but some regions such as the Pacific Northwest of North America can contain very high biomass density[Busing and Fujimori, 2005] (>5000 Mg/ha aboveground biomass for small plots, ∼1.4 ha, >300 Mg/ha over larger area ∼1km) due to the massive redwoods. The temperate forest tends to have the most amount of field inventory.

2.1.3 Boreal Forests

The boreal forest (also known as taiga, from Russian) is dominated by conifers. Due to the harsh environmental conditions of this northern region, the biomass density is much lower than the other two forest groups, generally less than 100 Mg/ha[Botkin and Simpson, 1990]. However, because of the large area of coverage, this biome does contain a significant portion of the global woody biomass. Additionally, there is massive amount of carbon stored in the frozen soils here[Davidson

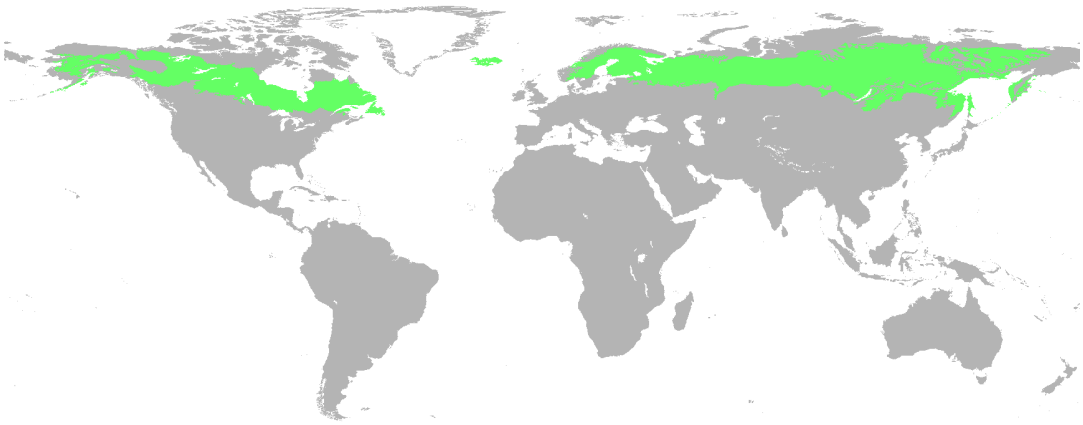

Figure 2.3: Boreal forests of the world. Based on biome map of the world by Olson et al. [2001]

and Janssens, 2006]. However, soil carbon is outside the scope of this dissertation. The sensitivity of this region to climate change also makes it one of interest for study.

2.1.4 Savannas, Shrubland, and Woodland

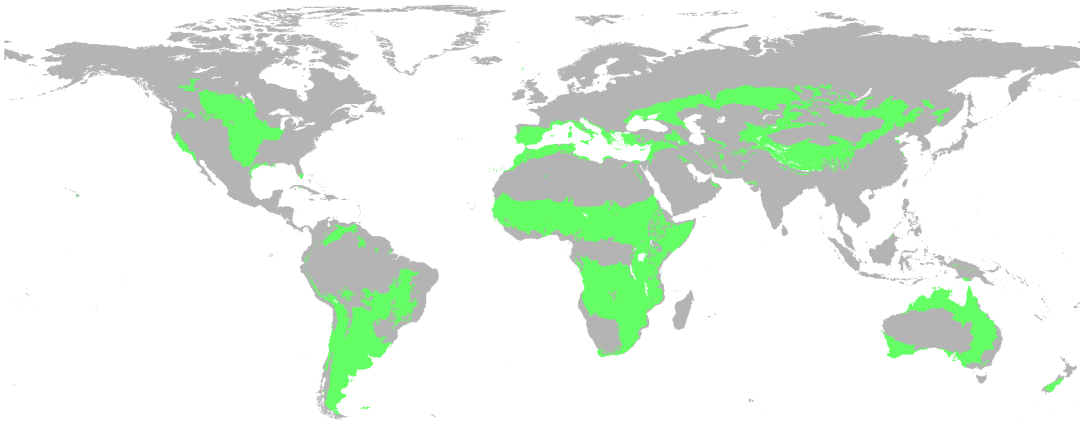

Figure 2.4: Savanna/shrublands/woodlands. Based on biome map of the world by Olson et al. [2001]

The savannas, shrublands, and woodland types span vast areas of the tropics and temperate regions. These biome types contain largely herbaceous vegetation,

and have woody vegetation as shrubs or low number density of trees that do not meet the requirement to be considered forest. This is largely due to the limited precipitation[Dallman, 1998, Archer et al., 1995], but can also be controlled by other factors such as herbivory and fire[Van Langevelde et al., 2003, Roques et al., 2001]. While the biomass density is low in these biomes, their large area of coverage means the total amount of carbon in woody vegetation contained in these biomes globally is significant.

2.1.5 Mangrove

Mangroves dot the coastlines of the tropics. These are trees that are adapted to live in regions that are permanently flooded with salt water. Due to the nature of the mangrove biome, the area is small and do not lend itself well to the spatial resolution of this study. However, some areas of mangrove are captured at the 1 km resolution. This biome is mentioned separately here because it is very different from the other forest types. Even though it contains very small amounts of total biomass compared to the other biomes due to the small total area, it does serve some very important ecological functions[Valiela et al., 2001].

2.2 Remote Sensing

This section contains background information for those readers who may not be familiar with remote sensing data. The actual processing and preparations of specific remote sensing data used as part of this dissertation is covered in Chapter 3. Here, I'll go over the general concepts behind the broad groups of remote sensing techniques used.

2.2.1 Optical

Optical remote sensing uses the visible and near-visible spectrum of the electromagnetic radiation. The satellite-based Moderate Resolution Imagine Spectroradiometer (MODIS)[Justice et al., 2002] and Medium Resolution Imagining Spectrometer (MERIS)[Arino et al., 2008] take advantage of the strong source of light, the sun, and capture the reflected light intensities. When looking at the land-surface, one issue with optical data is that light at this frequency does not penetrate clouds. As a result, any cloud cover will hinder the ability of optical-based satellites to observe the land-surface.

One of the most commonly used metrics for vegetation based on optical data is the Normalized Difference Vegetation Index (NDVI), defined as

$$\text{NDVI} = \frac{a_{\text{NIR}} - a_{\text{VIS}}}{a_{\text{NIR}} + a_{\text{VIS}}} \tag{2.1}$$

where a_{NIR} is the reflectance in the near infra-red band, and a_{VIS} is the reflectance in the visible band. This exploits the difference in absorption characteristics of chlorophyll in the visible and near infrared spectrum[Carlson and Ripley, 1997, Huete et al., 2002] to correlate the remote sensing data with live green vegetation. In the case of MODIS NDVI, the visible band used is red (620-670 nm). Leaf Area Index (LAI) is another commonly used metric derived from optical remote sensing[Myneni et al., 1997]. This derived quantity specifies the ratio of the area of the one-side of all the leaves in an unit area to the unit area.

2.2.2 Radar

Radar instruments work in a much longer wavelength range of the electromagnetic wave spectrum than optical instruments (microwave). As such, these instruments are much better at penetrating clouds. The Quick Scatterometer (QuikSCAT) data [Tsai et al., 2000] and Shuttle Radar Topography Mission (SRTM) data [Van Zyl, 2001] used in this dissertation are based on radar. Over forested areas,

the radar signal is affected by the scattering of the stem, branch, and leaves of the forest[Saatchi and McDonald, 1997]. Because of this effect on the scattering, the backscatter from the radar, such as those measured by QuikSCAT, is correlated with forest structure, and thus, biomass. SRTM uses interferometry to infer surface elevation. While vegetation structure also interacts with SRTM[Yu et al., 2010, Simard et al., 2006], here, SRTM is only used to provide elevation information and surface roughness.

2.2.3 LiDAR

Light Detection and Ranging (LiDAR) uses a laser pulse to measure the distance from the sensor to the target by using the time it takes for the laser pulse to reflect off the target and return. The LiDAR data used in this dissertation is from a space-borne instrument: the Geoscience Laser Altimeter System (GLAS) onboard the Ice, Cloud, and Elevation Satellite (IceSAT). GLAS orbits around the Earth and sends out LiDAR pulses (sometimes referred to as "shots") to the surface at regular intervals. When the LiDAR pulse is over an surface area with vertical structure, such as a forest canopy, information on the vertical structure can be retrieved by looking at the waveform of the return pulse using photon counting[Harding, 2005, Lefsky et al., 2006].

CHAPTER 3

Remote Sensing Data

The remote sensing data used in this dissertation that have wall-to-wall coverage are from the Quick Scatterometer (QuikSCAT), Moderate Resolution Imaging Spectroradiometer (MODIS), GlobCover landcover map based on the Medium Resolution Imaging Spectrometer (MERIS), and the Shuttle Radar Topography Mission (SRTM). While the data products used are already higher level processed products, large amounts of additional processing is required before they can be used as model inputs. This chapter goes over the processing that were performed with each of the remote sensing data.

The MODIS global sinusoidal 1km projection (Figure 3.1, actual pixel size is 926.6m) was chosen as the native projection and resolution for the model runs. All wall-to-wall remote sensing layers are converted to the MODIS sinusoidal 1km grid after processing. This was chosen because MODIS products has the largest number of layers used in the model, and its native projection is an equal area

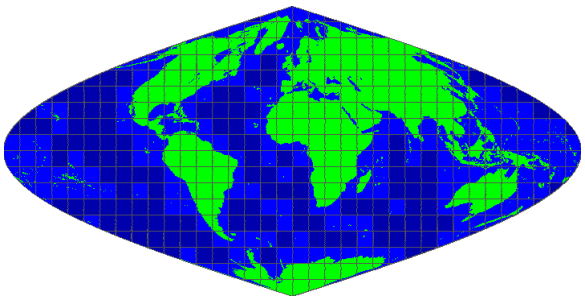

Figure 3.1: MODIS sinusoidal projection with 10 degree tiles. Source: MODIS Land Team website (*modis-land.gsfc.nasa.gov*)

projection, which is necessary to avoid weighting pixels differently at different latitudes in non-equal area projections. A total of 22 remote sensing data layers (12 MODIS, 8 QuikSCAT, 2 SRTM) plus 1 landcover layer are produced and used in the Maximum Entropy model. The following sections describe how each of the layers are produced.

3.1 QuikSCAT

The QuikSCAT data used is the enhanced resolution QuikSCAT "slice" images for 2005 from Brigham Young University's Center for Remote Sensing. These are enhanced resolution images by combining multiple passes of the satellite [Early and Long, 2001]. Data is available as ascending and descending passes, and in H and V polarization. Both the ascending and descending passes for H and V polarization are averaged to create four seasonal averages for each polarization, consisting of December January February (DJA), March April May (MAM), June July August (JJA), and September October November (SON). This creates a total of eight image layers from QuickSCAT (two polarizations per seasonal average). The data is mosaicked into global images and then re-projected into the MODIS sinusoidal projection.

3.2 MODIS

The data products used from MODIS include the Normalized Difference Vegetation Index (NDVI) and infrared reflectance from MOD13A2, and Leaf Area Index (LAI) from MOD15A2. These data are available from the United States Geological Survey's (USGS) Land Processes Distributed Active Archive Center (*lpdaac.usgs.gov*). Cloud cover can be a significant issue, especially in the tropics where cloud-free days can be very difficult to find. To help reduce the effect of

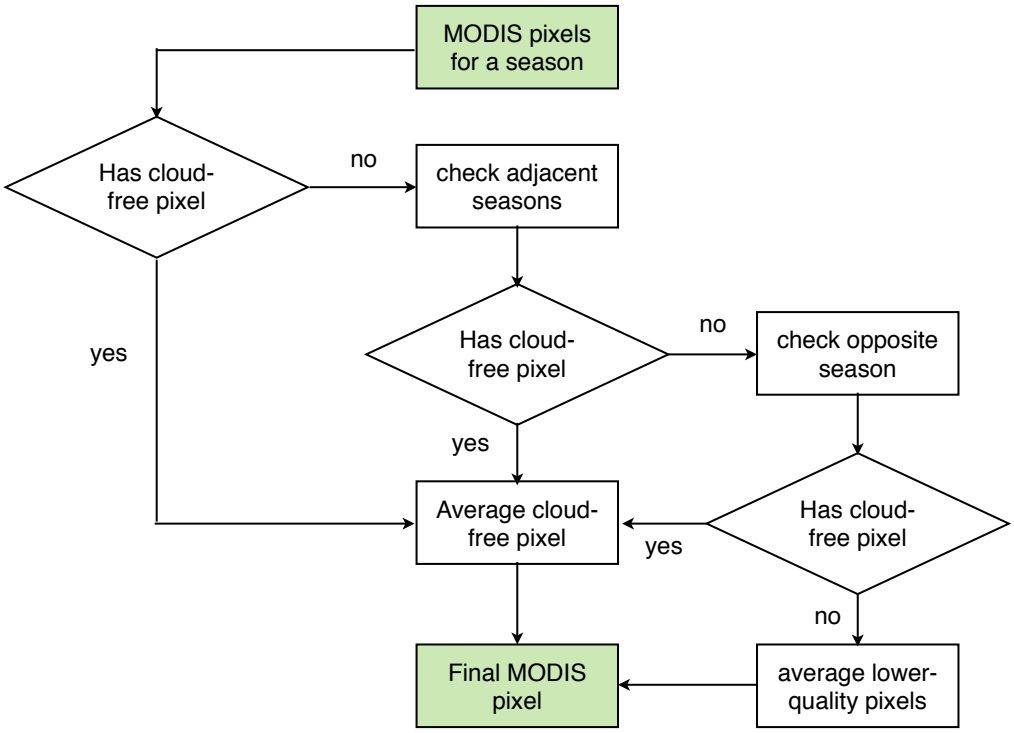

Figure 3.2: MODIS cloud processing algorithm. Cloud check is done using the quality flag of each pixel within the MODIS product. This process is repeated for each pixel location globally for all MODIS image layers

clouds, MODIS image layers are obtained for years 2004-2006, and an algorithm is developed to process the images.

The monthly MODIS images are collected into 4 groups by seasons DJA, MAM, JJA, and SON. Each group contains 9 image layers (3 months $\times$ 3 years). The image groups are then processed using decision algorithm shown in Figure 3.2 by going through the algorithm with each pixel location. All land pixels globally are processed through this algorithm. While some error is introduced due to the time difference through the inclusion of three years, this error is small compared to the the error caused by cloud cover. The inclusion of three years is necessary for acquiring enough cloud-free pixels to create clean seasonal averages.

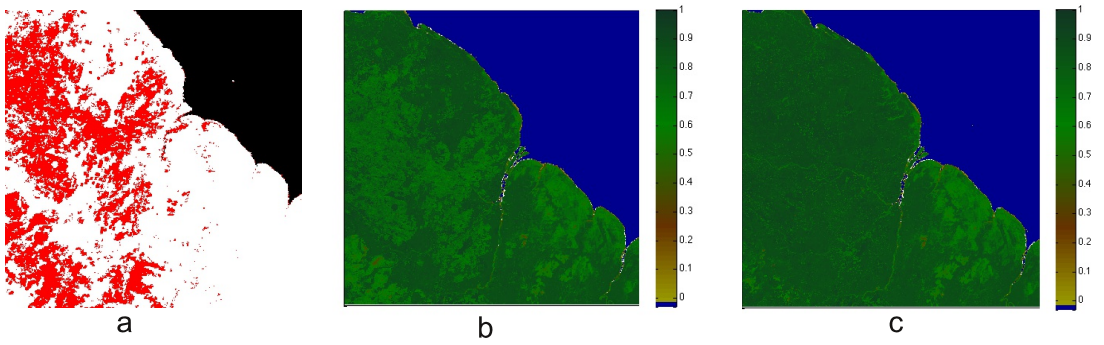

Figure 3.3: Removing cloud-cover effects from MODIS images. Location shown is in the northeast border of the Amazon rain forest. Data is from JJA group of images. a) Red marks areas where no cloud-free pixels exist in the JJA group for that pixel for the entire date range from 2004-2006 b) Average NDVI value by taking a simple average of all pixels within the JJA group c) NDVI value produced by using algorithm shown in Figure 3.2.

The effect of this cloud processing algorithm is shown in Figure 3.3. In panel 3.3a, the red area marks where there are no cloud-free pixels in the JJA group for this area. The second panel 3.3b shows the straight-forward averaging of NDVI values for this area for this season. It is remarkable that the pattern of lower NDVI values on the left portion of the region matches very well with the pattern of cloud contamination. Cloud cover acts to reduce NDVI because it reflects relatively equally between the red and near infrared bands. After processing the seasonal group through the algorithm, panel c shows that the lower NDVI patterns on the left side of the region has disappeared, while the pattern on the right (where there is no cloud contamination) remains, showing actual vegetation pattern on the ground. After the processing, we are left with 4 seasonal averages for each MODIS product (NDVI, LAI, and near infrared reflectance), making it a total of 12 image layers from MODIS.

3.3 GlobCover

The European Space Agency's GlobCover product (2005-2006) version 2.2 is used as landcover map for the model. The native resolution of this product is 300m. In order to use the landcover, it must be reprojected and scaled to the MODIS 1km sinusoidal projection. Because landcover type is categorical, an decision rule algorithm must be developed to scale the image. This process is shown in figure 3.4. This algorithm treats the forest/non-forest classes more intelligently than a simple majority-rule algorithm. By taking the information of the various forest class types into account, it allows certain classes to change, such as a mixture of small forest stands of different types at high resolution to become a mixed forest class pixel at low resolution. In addition to creating the output landcover map, the program also keeps track of the heterogeneity of each final pixel by calculating a the ratio of the dominant class pixels to the total number of pixels that fall into a final output pixel. This information is used later when filtering data samples for the Maximum Entropy model.

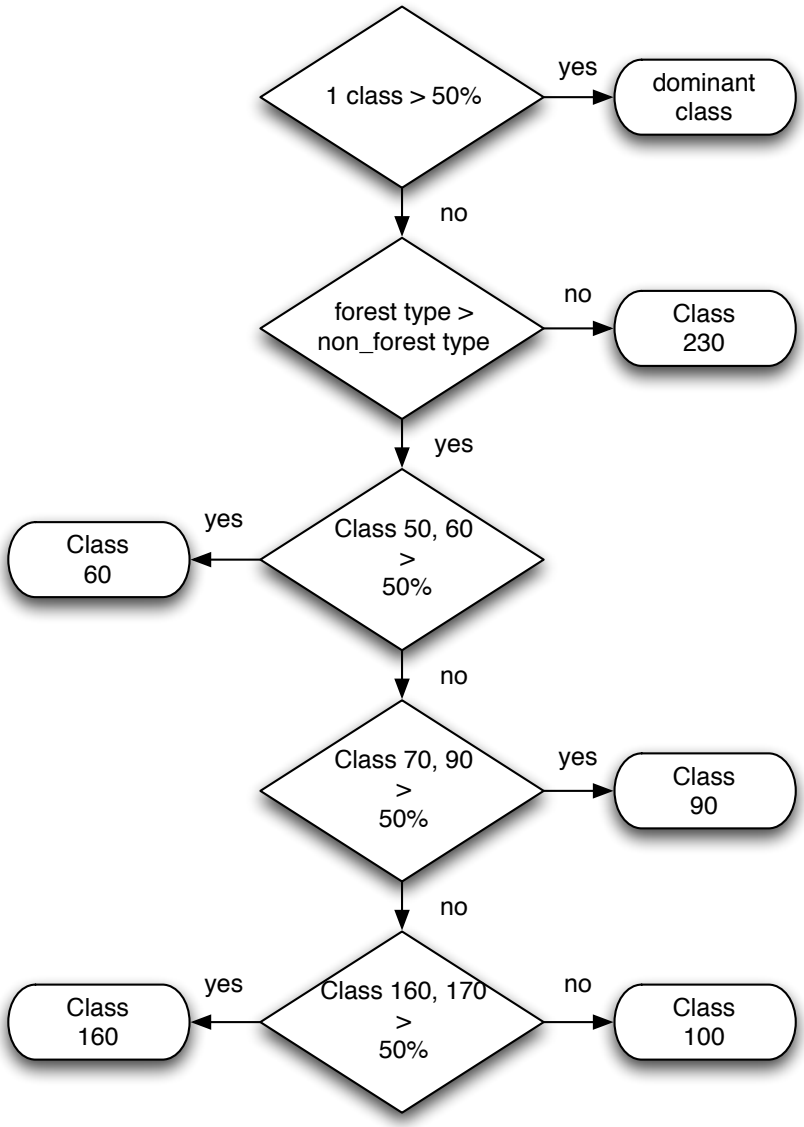

Figure 3.4: Flowchart for algorithm on scaling 300m GlobCover data to 1km. Class numbers corresponds to the class numbering used in GlobCover product.

3.4 SRTM

The elevation data used is the Shuttle Radar Topography Mission (SRTM) digital elevation map (DEM) enhanced with USGS' GTOPO30 DEM. This dataset is referred to as SRTM30 version 2.1, and can be downloaded from the USGS website (*dds.cr.usgs.gov/srtm*). The use of GTOPO30 in this dataset is due to the fact that SRTM coverage ends at around 60°N and 56°S. A surface roughness map is calculated using the standard deviation of SRTM DEM based on higher resolution (3-arcsec, 90m) SRTM DEM. Additionally, a global percent slope map is created using the 3-arcsec SRTM DEM. While the slope map is not used in the Maximum Entropy model, it is used to help correct the effect of slope when calculating Lorey's height from GLAS waveform, as well as filtering GLAS shots based on slope threshold (refer to section 5.1).

CHAPTER 4

LiDAR Based Aboveground Biomass

GLAS LiDAR data has been used in numerous studies on forest structure[Lefsky et al., 2006, Lefsky, 2010, Simard et al., 2011, Neigh et al., 2013, Popescu et al., 2011, Los et al., 2012]. The large number of GLAS LiDAR shots globally make it the ideal source of biomass samples for the global scale study. Figure 4.1 shows the coverage of the GLAS LiDAR shots globally. The actual number and coverage of GLAS LiDAR data is much larger. Only ones that provide a return on vertical vegetation structure are included here. Therefore, the pattern roughly follows that of woody vegetation cover.

The GLAS level 1A waveform from operational periods 3A through 3J, which corresponds to October 2004 through March 2008, are used to derive Lorey's height by Michael Lefsky (personal communication) using techniques similar to those in [Lefsky et al., 2007, Lefsky, 2010]. Metrics of percentile return height from the waveforms are fitted empirically to Lorey's height, defined below, using co-located GLAS shots and field plots. Lorey's height is the basal area weighted mean height of a forest plot, defined as:

$$H_l = \frac{\sum_{i=1}^{N} BA_i h_i}{\sum_{i=1}^{N} BA_i} \tag{4.1}$$

where BA_i is the basal area, defined as the cross-sectional area of the trunk at breast height (typically 1.3m above ground), N is the number of trees in the plot, and h_i is the height of the i^{th} tree. Empirical equations for H_l as a function of GLAS waveform are in the form of

$$H_l = \alpha + \beta_1 extent + \beta_2 lead_{10} + \beta_3 trail_{10} \tag{4.2}$$

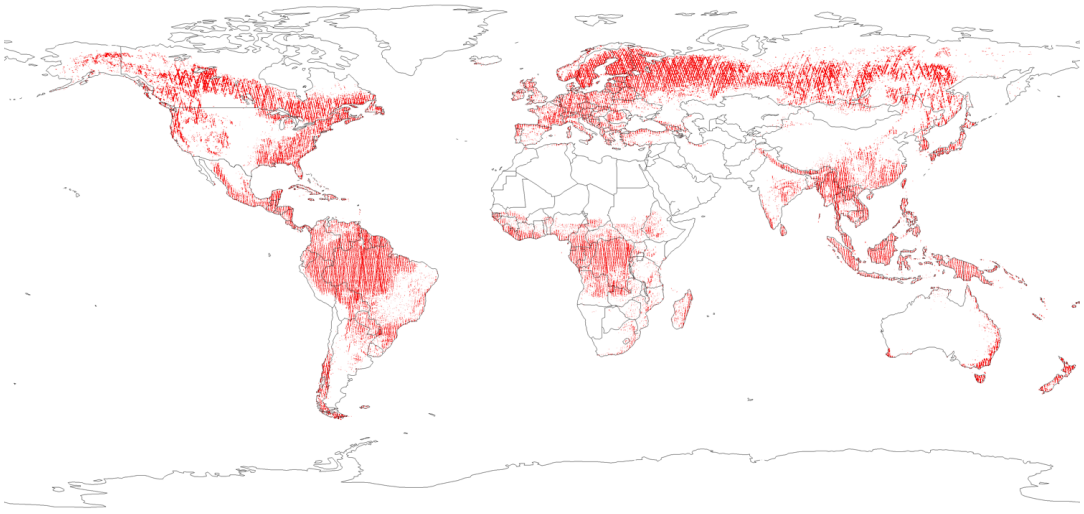

Figure 4.1: Global coverage of GLAS LiDAR shots. Only shots that have vertical structural return over vegetation are included.

where *extent* is the distance from the first to the last wave energy return, $lead_{10}$ and $trail_{10}$ are the heights of the 10^{th} and 90^{th} percentile of waveform energy. Three sets of coefficients for equation 4.2 are fitted for broadleaf, needleleaf, and mixed forest types with root mean squared error (RMSE) of 3.3 m, 4.9 m, and 6.9 m respectively. More details of GLAS and ground datasets used can be found in Lefsky et al. [2007], and details on the fitting of equation 4.2 can be found in Lefsky [2010]. A total of 7 million individual GLAS shots are processed for this study.

Lorey's height is chosen as the measure on the plot level over simple average height because it exhibits better correlation with the total aboveground biomass (AGB) of the plot. This is due to the fact that the AGB of a forest plot is dominated by the largest trees, as the AGB of an individual tree scales with the height of that tree with a power higher than 1[West et al., 1997]. Allometric equations can then be used to convert Lorey's height into AGB.

Mass is equal to density times volume. Therefore, a general allometric equation between Lorey's height and AGB will take on the form of $\text{AGB} = \alpha H_l^{\beta} \rho$ where α

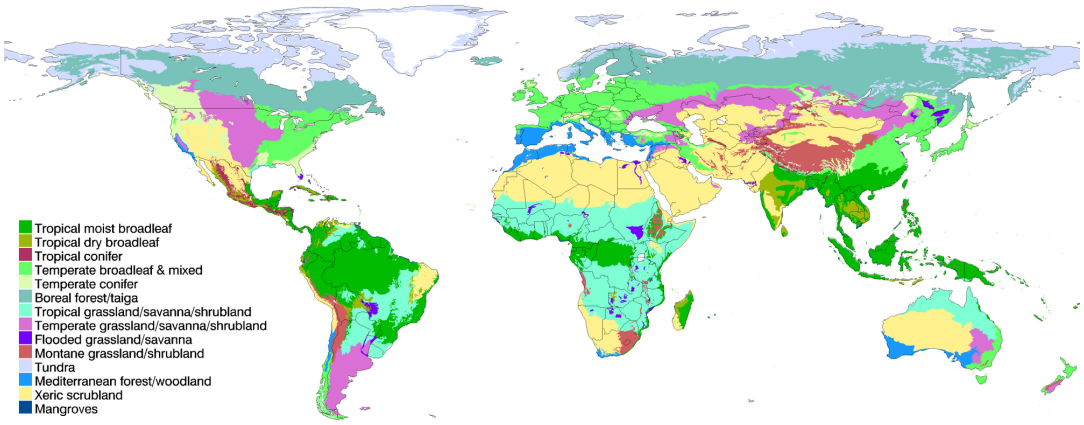

Figure 4.2: Major terrestrial biomes of the world. Map is based on the division of biomes from [Olson et al., 2001].

and β are fitting coefficients, and ρ is the wood density. Since wood density data is generally not available, ρ is absorbed into the fitting coefficient α:

$$\text{AGB} = \alpha H_l^{\beta} \tag{4.3}$$

However, there are a few cases in the pan-tropics where wood density come into play. These are discussed in more detail in sections 4.2 and 4.3.

How H_l scales with volume depend on the growth characteristics of individual trees, which depend on the species of the tree and environmental conditions[West et al., 1997, Chave et al., 2005, Komiyama et al., 2008]. Because of the footprint size of GLAS being roughly 50m across, it is necessary to develop allometric equations at similar plot size. To account for the variation in allometry of forests across the globe, the entire global land area is divided by continents as well as biomes based on the World Wide Fund for Nature (WWF) major terrestrial biomes[Olson et al., 2001]. There are 14 major terrestrial biomes based on this division (Figure 4.2). Allometric equations are developed for each biome/continent combination where ground-based inventory data is available. The following sections of this chapter detail this process for the various regions.

4.1 United States Inventory Data

The US Forest Inventory and Analysis (FIA) provide extensive forest plot samples across the contiguous 48 states. This data is available to the public at the FIA website (*http://apps.fs.fed.us/fiadb-downloads/datamart.html*). Plot level data from phase 2 of the FIA inventory was used. Figure 4.3 shows the design of the FIA field plot. In each plot, trees with diameter greater than or equal to 5 inches are measured within the 4 circular subplots with 24 ft radius. This makes the total area measured for each plot $\sim 700\text{m}^2$. For each plot, FIA provides tree-level basal area measurement, height measurement, and AGB value based on species-specific allometry. From these data, one can calculate a Lorey's height and total AGB for each plot[Jenkins et al., 2003].

The individual plots are grouped based on which biome (Figure 4.2) they fall in. For the temperate conifer biome, the east and west coast regions are treated as separate biomes, although, it was later found that the difference in allometric coefficients between these two regions are minimal. The temperate broadleaf/mixed forest (WWF biome 4) and temperate coniferous forest (WWF biome 5) are further divided into broadleaf, needleleaf, and mixed forests using GlobCover landcover map. Each group is fitted to equation 4.3 to find α and β. These relationships are shown in figure 4.4 a-i. GLAS-based H_l values are then used in equation 4.3 along with these coefficients to calculate AGB values in North America. Due to the lack of field inventory in other continents compared to North America, some of the allometric equations developed using FIA plot data are used for the same biome in other continents.

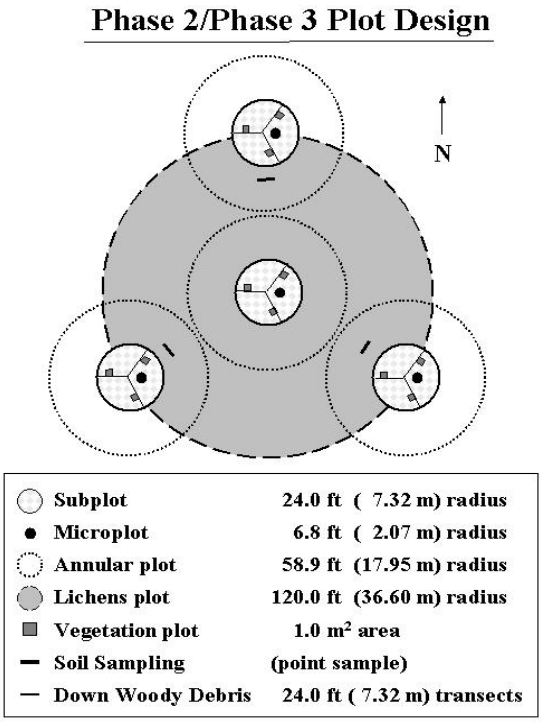

Figure 4.3: FIA plot design. In a phase 2 inventory, which were used for this dissertation, trees 5in in diameter or larger inside the 4 subplots (24 ft radius) were measured. Plot level values are then calculated based on all the trees measured inside these subplots. Figure is from FIA website

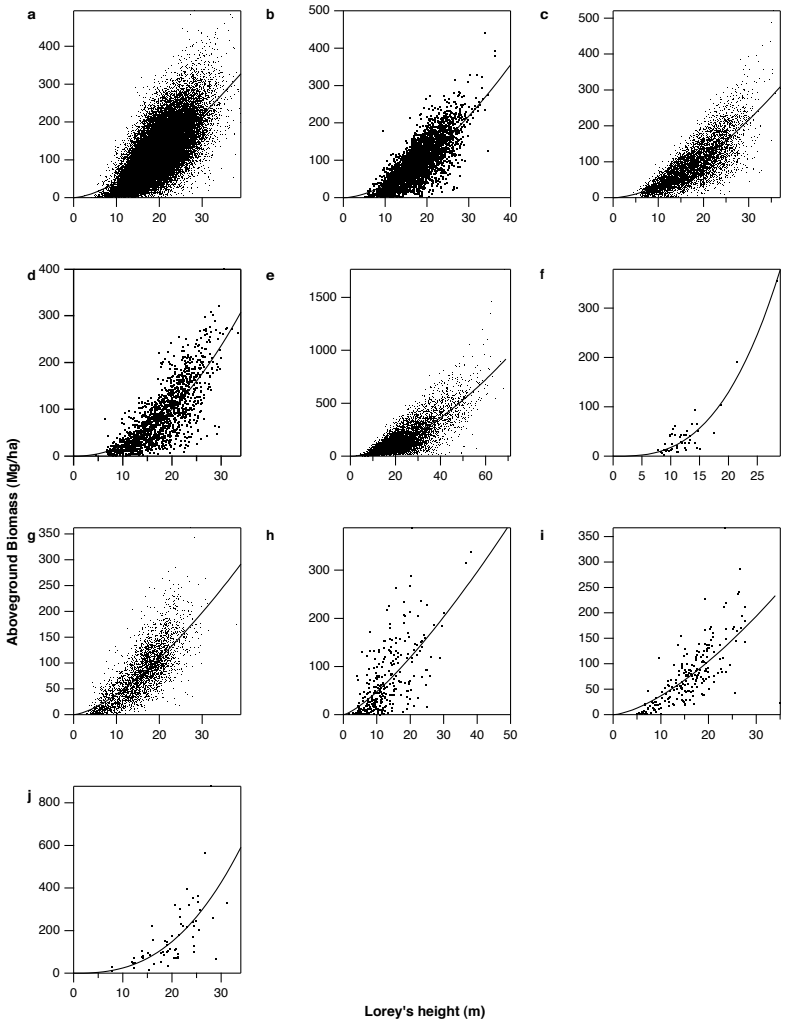

Figure 4.4: Scatterplots showing relationship between Lorey's height and AGB based on field inventory. a) North America temperate broadleaf forest (WWF biome 4). b) North America temperate mixed forest (WWF biome 4). c) North America east coast coniferous forest (WWF biome 5). d) North America east coast mixed forest (WWF biome 5). e) North America west coast coniferous forest (WWF biome 5). f) North America boreal forest (WWF biome 6). g) North America temperate savanna and shrublands (WWF biome 8). h) North America Mediterranean shrublands (WWF biome 12 and 13). i) North America tropical savanna and shrublands (WWF biome 7). j) China broadleaf/mixed forest (WWF biome 4).

4.2 Pan-Tropics

Plot-level allometric equations were developed by Saatchi et al. [2011b] for the pan-tropical regions of South America, Africa, and Asia. These equations are AGB = $0.6011H_l^{1.894}$, AGB = $0.2788H_l^{2.12}$, AGB = $0.06328H_l^{2.4814}$ for America, Africa, and Asia respectively. In the case of tropical moist broadleaf forests in Asia, it was found later that the plots used to develop the allometric equation are dominated by plantation plots, thus not a good representation of the biome as a whole (S. Saatchi, personal communication). As a result, South America and Africa moist broadleaf forest equations are based on Saatchi et al. [2011b], while Asia uses the Africa allometric equation of the same biome.

These allometric equations were developed with a certain set of field plots. When comparing these field plots with a more substantial set of wood density measurements in the region, it was found that the plots used to develop the allometric equations have a slightly different average wood density than the more extensively sampled wood density of the area. For Africa and Asia, where wood density variation is not as large, the AGB derived from allometric equations based on Saatchi et al. [2011b] are scaled by the ratio of the average wood density values, which are 1.047 and 1.017 for Africa and Asia respectively. The following section 4.3 will go into detail on the treatment of wood density in the tropical moist forest of the Americas.

4.3 Wood Density in the Amazon

The Amazon rainforest is treated differently from Africa and Asia when dealing with wood density because the area is much larger and the variation in wood density is also larger. It has been shown that wood density plays an important role in the regional variation of AGB in this region[Baker et al., 2004]. In this

case, a wood density map over the biome was developed using Maximum Entropy approach similar to what is used for the estimation of AGB in this dissertation. The remote sensing layers used for this model run includes the L-band synthetic aperture radar backscatter from the Japanese Advanced Land Observing Satellite (ALOS), mean and standard deviation of surface temperature based on MODIS MOD11C3 product, as well as elevation and standard deviation of elevation from SRTM. Ground-based samples (3468 total samples) of wood-density values (Figure 4.5) are used as input to the model. Only model predictions over broadleaf evergreen forest as classified by GlobCover are used to scale the GLAS-based AGB values.

The mean wood density for the entire region, $\bar{\rho}$, is calculated by taking the mean wood density of all the ground plots. For each GLAS-based AGB sample within the region, the AGB value is then scaled using $\rho/\bar{\rho}$ where ρ is the model predicted wood density at the location of the GLAS shot.

4.4 Mexico, Russia, and China Inventory Data

Mexico contains large areas of tropical conifer and tropical dry broadleaf forests. Inventory data from the Mexican Forestry Commission (*www.conafor.gob.mx*) are used to develop allometric equations for these biomes. Russian forest inventory data is obtained from the Russian Forests and Forestry website (*webarchive.iiasa.ac.at*). Both the Mexico and Russia inventory data only contain mean canopy heights for the plots instead of Lorey's height. The data are fitted using the same functional form as equation 4.3 using mean height in place of Lorey's height.

Using the FIA plot data, relationships are then developed between mean canopy height and Lorey's height over all FIA plots and over only the Boreal plots, shown in figure 4.6. The equation based on all plots (Figure 4.6a) is used to

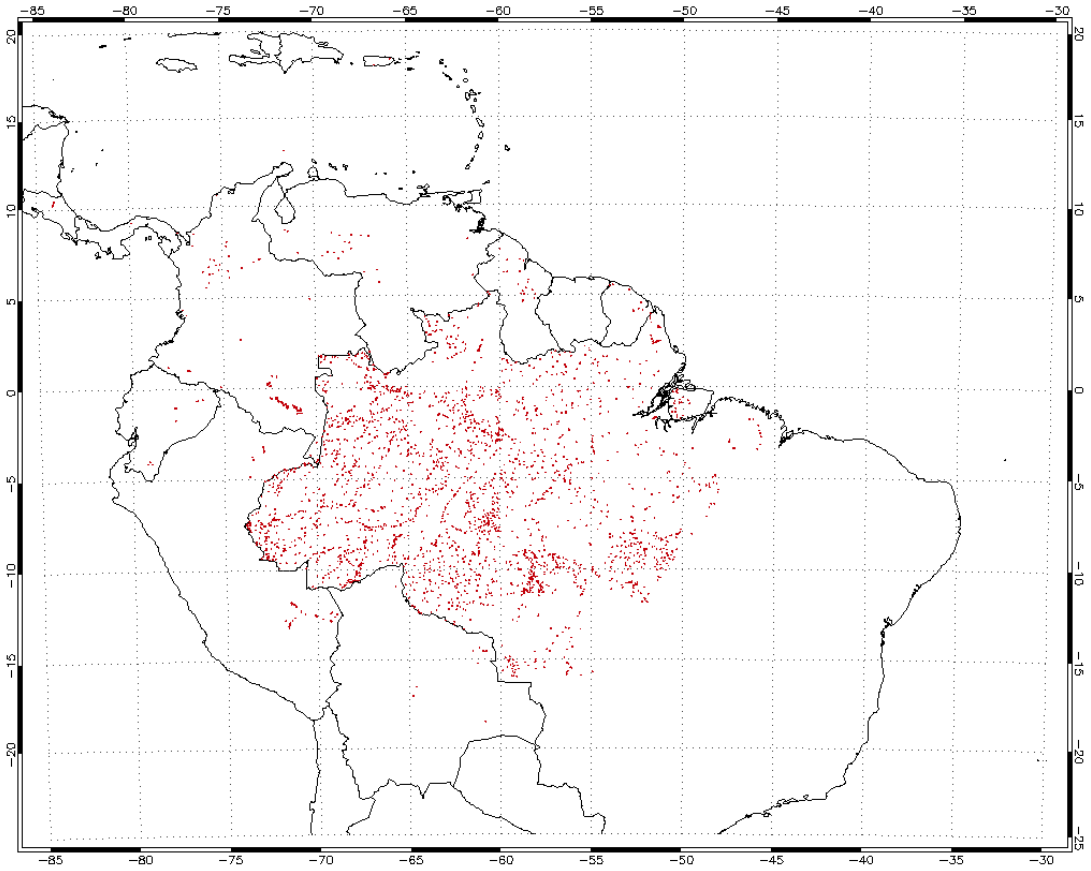

Figure 4.5: Locaitons of ground-based wood density plots in South America. Only those that are classified as broadleaf evergreen forest by GlobCover were used in the wood density model.

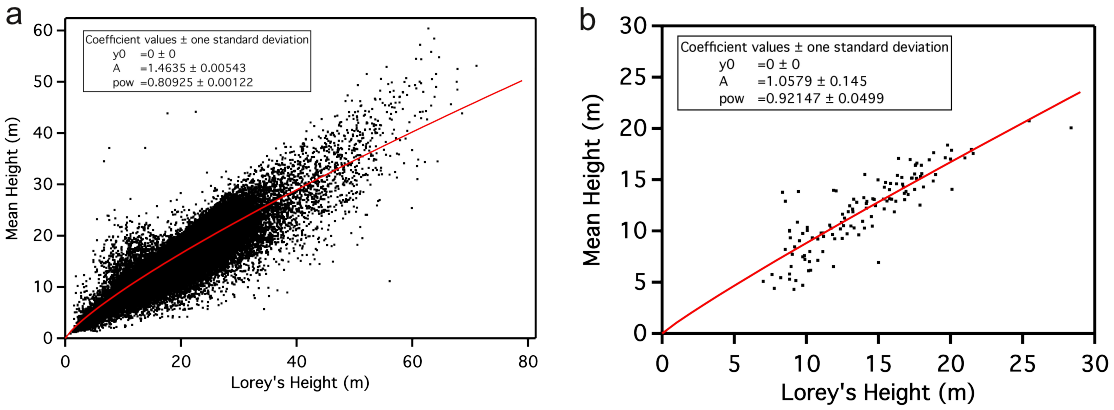

Figure 4.6: Scatterplot between mean canopy height and Lorey's height. a) Relationship using all FIA plots. b) Relationship using only FIA plots within the Boreal biome using the WWF biome map

convert GLAS Lorey's height into mean canopy height for tropical dry broadleaf and tropical conifer biomes; equation based on Boreal plots (Figure 4.6b) is used to convert GLAS Lorey's height into mean canopy height for the Russian taiga biome. The allometric equations developed are then used to calculate AGB from the mean canopy height values.

For the temperate broadleaf/mixed biome in Asia, allometric equation is developed using field data from China (Guoqing Sun, personal communication). These plots do include Lorey's height, and equation 4.3 is used in this case with relationship shown in figure 4.7.

4.5 Summary of Biome-Level Allometric Equations

Due to the limited availability of ground based inventory plots, not all biome/continent combinations have their own allometric equations. For the regions that do not have ground data, allometric equations from another continent of the same biome is used. Pedro Rodriguez-Veiga (University of Leicester) also provided allometric equation for the Mediterranean biome of Europe based on forestry data from Spain

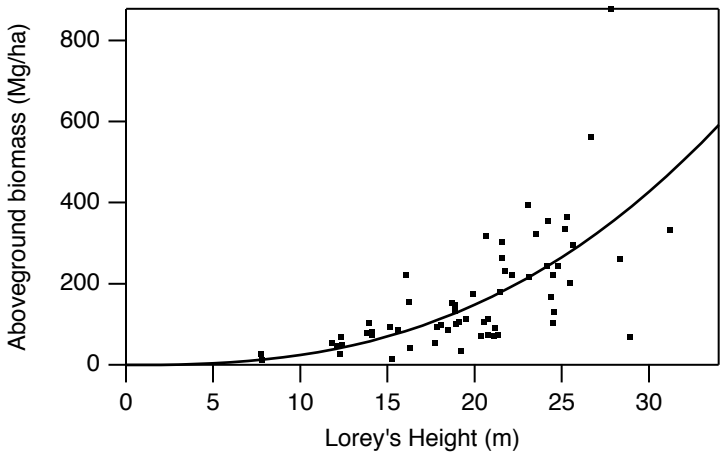

Figure 4.7: Scatterplot between Lorey's height and AGB for temperate broadleaf and mixed forests in China.

(personal communication). All the coefficients for allometric equations across the globe are summarized in table 4.1.

Table 4.1: Summary of allometric equations between Lorey's height and AGB for different biomes of the world. $*$ Only mean heights of plots were available. Coefficients are for mean height, and GLAS based Lorey's heights were converted to mean heights first before applying allometric equations. † Saatchi et al. 2011 ‡ Equation provided by Pedro Rodriguez-Veiga (personal communication)

	North America	South America	Africa	Eurasia	Southeast Asia	Australia
Tropical/subtropical moist broadleaf	α=0.6011 β=1.894	α=0.6011 β=1.894 †	α=0.2788 β=2.12 †	– –	α=0.2788 β=2.12 †	α=0.06328 β=2.4814 †
Tropical/subtropical dry broadleaf	α=0.73696 β=2.0062 $*$	α=0.73696 β=2.0062 $*$	α=0.73696 β=2.0062 $*$	– –	α=0.73696 β=2.0062 $*$	α=0.73696 β=2.0062 $*$
Tropical/subtropical conifer	α=6.4389 β=1.0556 $*$	– –	– –	– –	α=6.4389 β=1.0556 $*$	– –
Temperate broadleaf / mixed	α=1.1799 β=1.536 α=0.689 (mixed) β=1.6932	– –	– –	α=1.1799 (W) β=1.536 α=0.061015 (E) β=2.6032	α=0.061015 β=2.6032	α=1.1799 β=1.536
Temperate conifer	α=0.68255 (East) β=1.6939 α=0.18321 (Mixed E) β=2.1059 α=0.71774 (West) β=1.6892	α=0.71774 β=1.6892	α=0.68255 β=1.6939	α=0.68255 β=1.6939	α=0.68255 β=1.6939	– –
Boreal / taiga	α=0.023409 β=2.8782	– –	– –	α=4.5925 β=1.1627 $*$	– –	– –
Tropical/subtropical savanna,shrubland	α=1.1633 β=1.504	α=1.1633 β=1.504	α=1.1633 β=1.504	α=1.1633 β=1.504	α=1.1633 β=1.504	α=1.1633 β=1.504
Temperate savanna,shrubland	α=1.3403 β=1.4694	α=1.3403 β=1.4694	α=1.3403 β=1.4694	α=1.3403 β=1.4694	– –	α=1.3403 β=1.4694
Mediterranean forest,woodlands	α=2.3053 β=1.3171	α=2.3053 β=1.3171	α=1.4243 β=1.595 ‡	α=1.4243 β=1.5953 ‡	– –	α=2.3053 β=1.3171

CHAPTER 5

Maximum Entropy modelling of Aboveground Biomass

This chapter covers the statistical modeling of aboveground biomass (AGB) using the Maximum Entropy model MaxEnt[Phillips and Dudík, 2004, Phillips et al., 2006, Phillips and Dudík, 2008]. The global land areas are divided into 6 regions based on continents as shown in figure 5.1. The regions are labeled North America, South America, Africa, Eurasia, Southeast Asia, and Australia. For the remainder of this dissertation, reference to these continent names will be referring to the divisions shown in figure 5.1. Sections 5.1 and 5.2 describe the preparation of the AGB samples and the statistical model itself. The subsequent sections will discuss the specific steps taken for the modeling of each of the continental regions. Section 5.3 contains analysis of model uncertainty at the pixel level.

5.1 GLAS AGB Sample Preparation

In chapter 4, it was shown how GLAS shots were converted to AGB values. Further processing is performed on these GLAS-based AGB values before being used for the statistical model. The footprint of a single GLAS shot is an oval of roughly 70m along the long side. Additionally, the Gaussian pattern of the GLAS laser energy means the effective foot-print size is even slightly smaller[Popescu et al., 2011]. Along the orbital track, the distance between adjacent GLAS shots is 200m. The relative size of GLAS foot-print and shot spacing when compared to a

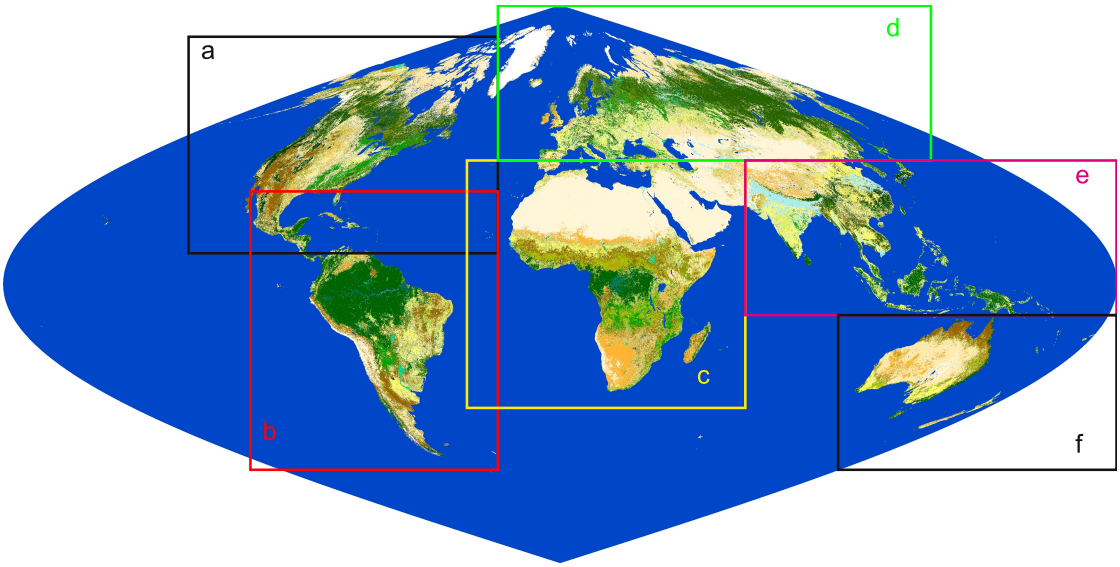

Figure 5.1: Division of global land area into 6 regions for model run. a)North America, b)South America, c)Africa, d)Eurasia, e)Southeast Asia, f)Australia. Base map shown is the scaled and reprojected GlobCover landcover map described in section 3.3

1km square area is shown in figure 5.2. It is easy to see that a single GLAS shot would be a poor representation of a native pixel in this case because any heterogeneity in the forest and landcover will introduce noise. To help reduce this effect, GLAS shots that fall within the same pixel are aggregated to produce an average AGB value for the pixel. However, due to the spacing between GLAS shots being approximately 200m, it becomes much less likely to find pixels with more than 5 GLAS shots (Figure 5.3), as that will generally require having either two orbits crossing or two nearby orbits. Therefore, a minimum of 5 shots is chosen as the threshold for aggregating GLAS AGB values to represent pixel-level AGB values.

Another source of error for using GLAS-waveform to infer AGB is the underlying topography within the GLAS footprint[Lefsky et al., 2007]. Since the LiDAR waveform returns distance from the instrument to the reflecting surface, the height information from vegetation will be mixed with the change in height of

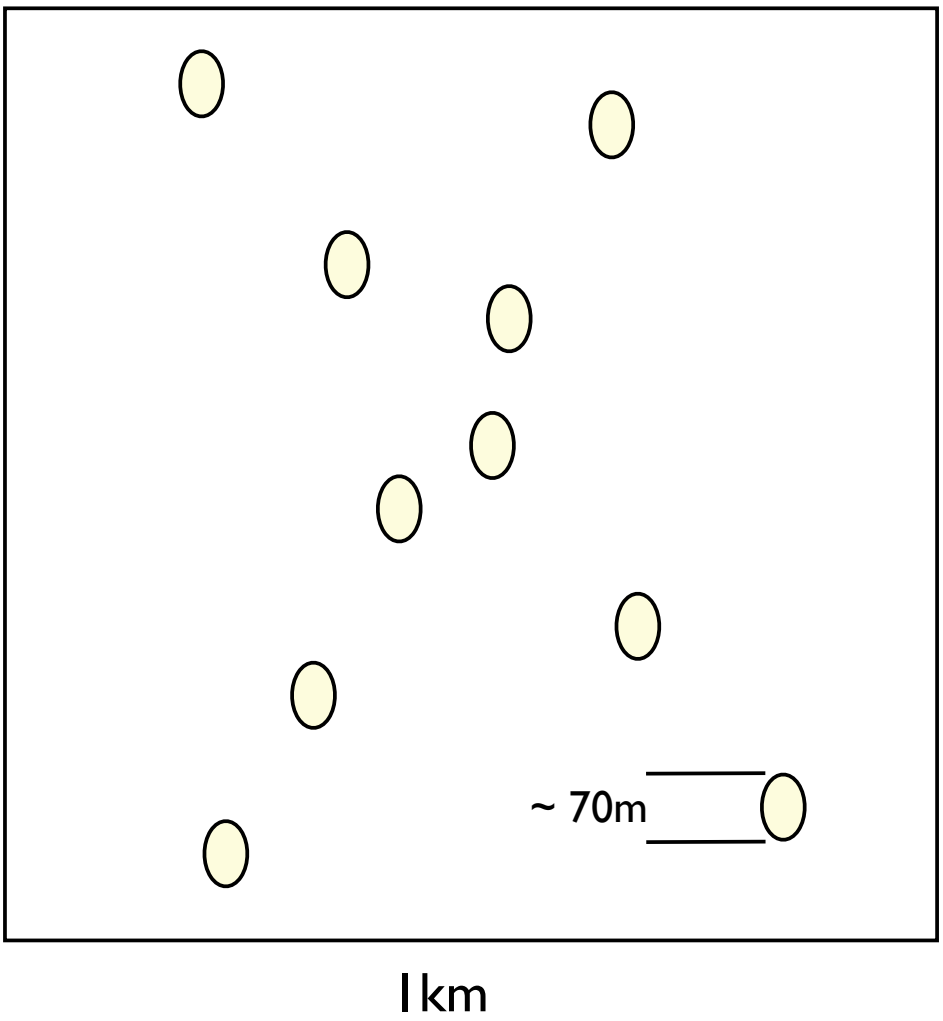

Figure 5.2: Comparison, to scale, of GLAS shot foot-print size within an 1km area. Two hypothetical crossing orbits are shown with average distance between shots of 200m

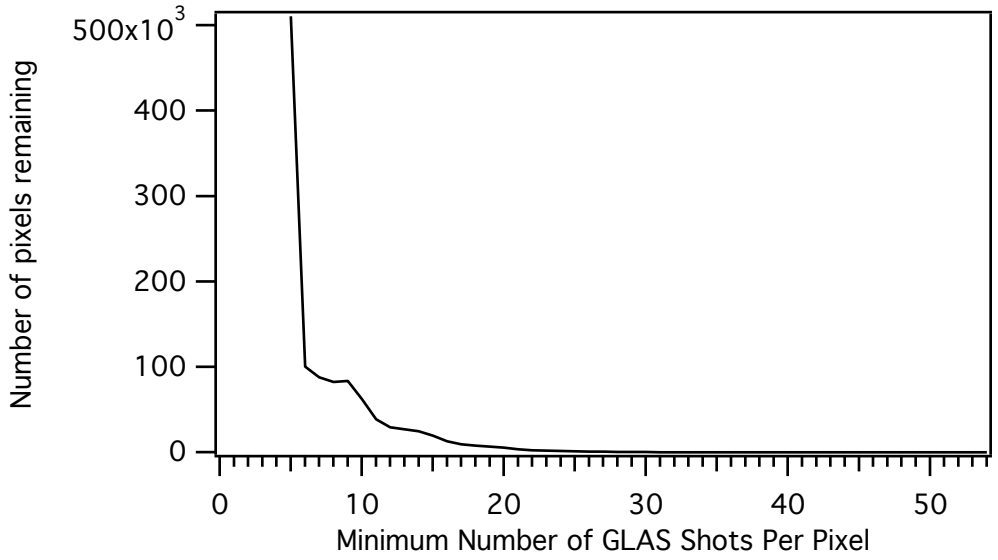

Figure 5.3: Distribution of number of pixels with 5 or more GLAS shots per pixel. The number shows significant drop after 5

the underlying topography within the LiDAR foot-print. This is not an issue with small-footprint LiDAR, but the larger foot-print size of GLAS LiDAR means steep topography within the foot-print will introduce more error. A threshold of 20 percent slope, calculated from 90m SRTM (Section 3.4), is used to filter out LiDAR shots over steep topography. After all the filtering and aggregation, ∼400,000 pixel-level AGB samples are available for the statistical modeling.

5.2 Maximum Entropy Model

The model chosen for this study is a statistical model based on the Maximum Entropy concept called MaxEnt[Phillips et al., 2006, Phillips and Dudík, 2008]. There are several factors in choosing this model over others. MaxEnt has been successfully used in the modeling of AGB in the US as well as the pan-tropics[Saatchi et al., 2011b]. Because each remote sensing layer generally has poor correlation with AGB with high levels of noise, typical linear regression models do not work

well in this case.

The Maximum Entropy method approaches the problem in the following manner. There is an unknown actual probability distribution $\pi(i,j)$ of a quantity we are interested in being positive at any given pixel location (i,j), for example, the presence of a certain species (what MaxEnt was originally developed for). We have a set of observed samples X in the area, as well as remote sensing image layers covering the same area. We try to construct a distribution $\hat{\pi}(i,j)$ that approximates $\pi(i,j)$. There are many choices for $\hat{\pi}$, but they can be constrained using information from the samples and values from the remote sensing layers at the locations X.

We can calculate a set of statistics on the remote sensing data using the values from the locations of the observed samples at (i,j). Assuming that these statistics are close to the true values of all the positive locations, we can then constrain our choices of $\hat{\pi}$ using this information. For example, one such constraint can be that the expectation value, using $\hat{\pi}$, of NDVI, defined in equation 5.1

$$\langle \text{NDVI} \rangle \equiv \frac{\sum_{(i,j)} \text{NDVI}_{(i,j)} \hat{\pi}_{(i,j)}}{\sum_{(i,j)} \hat{\pi}_{(i,j)}} \tag{5.1}$$

has to be close to the mean value calculated from the samples X. We cannot set the constraint to be exactly equal because we do not expect the mean value calculated from samples X to be exactly equal to the true meal value.

Given this constraint, we can then construct a set of $\hat{\pi}$ that all give expectation values of NDVI within a pre-set threshold of the value calculated from X. The Maximum Entropy theory then tellls us which of this set of $\hat{\pi}$ is the best approximation of π. The theory states that the best choice of $\hat{\pi}$ here, out of all the ones that satisfy the given constraints, is the one that maximizes the entropy where the entropy of a probability distribution p is defined as $H(p) \equiv -\sum_{x \in X} p(x) ln[p(x)]$.

This statement can be interpreted as saying that the best approximate to the distribution π is the estimate $\hat{\pi}$ that satisfies all the known constraints based on

the observed samples without introducing any other artificial constraints. Since entropy can also be interpreted as information or randomness, a distribution that has a higher entropy is more random and contains more information, meaning less constraints. If we have a set of approximate distributions $\hat{\pi}$ that all satisfy the observed constraints, then the one with the highest entropy has the least amount of constraints other than the ones from the observed samples.

The software implementation of the Maximum Entropy method used in this study is MaxEnt. It is designed for the modeling of animal species distribution using sampling of presence data with gridded remote sensing environmental layers. The MaxEnt implementation is a binomial model that estimate the probability of the presence of the given species at each location[Elith et al., 2010]. As such, some adaptation is required for the modeling of AGB, which is a continuous variable.

To adapt MaxEnt for the estimation of a continuous variable, AGB values are broken down into bins. For example, one possible set of AGB bins might look like 0-20 Mg/ha, 20-40 Mg/ha, 40-60 Mg/ha, and >60 Mg/ha. Each AGB sample is then placed into one of the bins and used to calculate the mean AGB of each bin. The MaxEnt model is then used independently for each of the bin over a region. Each individual MaxEnt run will estimate a probability distribution $\hat{\pi}(x)$ over the area for the probability of a pixel x being inside that bin. Using the variable B (biomass) to represent AGB, just to make the equations easier to read, we can write this as $P(B_{min} \leq B_{i,j} \leq B_{max}|A)$: the probability of B at pixel i, j being inside the bin (with B_{min} and B_{max} being the end values of the bin) given condition A. In this case, condition A refers to the specific MaxEnt run for this particular bin. Generalizing this over all MaxEnt runs for the bins, we get the expectation value over a pixel i, j as

$$\langle B_{i,j} \rangle = \frac{\sum_{k=1}^{N} P(B_{min} \leq B_{i,j} \leq B_{max}|A_k)P(A_k)\bar{B}_k}{\sum_{k=1}^{N} P(B_{min} \leq B_{i,j} \leq B_{max}|A_k)P(A_k)} \tag{5.2}$$

where N is the total number of bins, $P(A_k)$ is the probability of any pixel in the

domain being inside the k^{th} bin, and $\bar{B}_k$ is the mean AGB of the k^{th} bin.

We can estimate $P(A_k)$ by using the observed samples as $P(A_k) = \frac{N_k}{N_{total}}$ where N_k is the number of samples in the k^{th} bin and N_{total} is the total samples across all bins. This can also be interpreted as the prior probability, or prior knowledge, based on our observed samples. $P(B_{min} \leq B_{i,j} \leq B_{max}|A)$ is then the modeled probability. It was found through empirical tests that the model performance is increased when the modeled probability across the bins is weighted by using

$$\langle B_{i,j} \rangle = \frac{\sum_{k=1}^{N} P(B_{min} \leq B_{i,j} \leq B_{max}|A_k)^m P(A_k) \bar{B}_k}{\sum_{k=1}^{N} P(B_{min} \leq B_{i,j} \leq B_{max}|A_k)^m P(A_k)} \tag{5.3}$$

where m can be used to adjust the weight of the model probability. Different values of m were tested and the results for m=3 is chosen for giving the best predictor of AGB (for results of comparison between different values, see section 5.3).

In their usage of MaxEnt model for the pan-tropic biomass study, Saatchi et al. [2011b] only separated the model domains by continent. Here, to further increase the model's ability to differentiate between AGB ranges, landcover map is included in the form of GlobCover classification (Section 3.3). This can be thought of in terms of the constraints on sample data statistics. The constraints, referred to as "features" in Phillips and Dudík [2008], are statistical quantities calculated from the observed samples. The features implemented in MaxEnt are: linear, quadratic, product, threshold, hinge, and category indicator. The linear, quadratic, and product features constrain the means, variances, and covariances respectively. It is easy to see then, that these features will be dependent on the distribution of the values of the different remote sensing layers for the sample pixels.

Different forest types tend to have different distribution of corresponding remote sensing values. For example, radar backscatter is dependent on the shape and structure of the water-containing leaves and branches of the trees [Imhoff,

1995, Saatchi and Moghaddam, 2000]. This growth pattern is different between broadleaf trees and conifers. Therefore, a 50 Mg/ha broadleaf forest will have a slightly different radar backscatter profile than a 50 Mg/ha conifer forest, all other things being equal. Another effect is the phenology of deciduous and evergreen forests. The NDVI value, which depends on the chlorophyll content of the leaves, will be different between these forests. Additionally, different forest types tend to have different AGB distributions [Perry et al., 2008]. Therefore, it would be more precise to divide the bins differently for different forest types such that their unique distributions may be captured as various features in MaxEnt. To this effect, the GlobCover landcover map is used as an ancillary data to divide the maxent runs, determine AGB binning, and as an input to MaxEnt model as categorical layer for certain runs.

The GlobCover classes 40, 50, 60, 70, 90, 100, 110, 120, 130, 160, 170, and 180 are modeled in this study. These correspond to, in the order above: closed to open (>15%) broadleaf evergreen or semi-deciduous forest (>5 m); closed (>40%) broadleaved deciduous forest (>5m); open (15-40%) broadleaved deciduous forest/woodland (>5m); closed (>40%) needleleaved deciduous or evergreen forest (>5m); open (15-40%) needleleaved deciduous or evergreen forest (>5m); closed to open (>15%) mixed broadleaved and needleleaved forest (>5m); mosaic forest or shrubland (50-70%) / grassland (20-50%); mosaic grassland (50-70%) / forest or shrublnd (20-50%); closed to open (>15%) (broadleaved or needleaved, evergreen or deciduous) shrubland (<5m); closed to open (>15%) broadleaved forest regularly flooded (semi-permanently or temporarily) - fresh or brackish water; closed (>40%) broadleaved forest or shrubland permanently flooded - saline or brackish water; closed to open (>15%) grassland or woody vegetation on regularly flooded or waterlogged soil - fresh, brackish or saline water[Bicheron et al., 2008]. Classes 40 - 100, 160, and 170 are considered forest classes. The rest are considered shrubland/savanna classes.

A special class is created, in the tropical regions, for forested areas that may be misclassified by GlobCover. This tends to be an issue especially in the tropical forests due to cloud cover. Dong et al. [2012] found that GlobCover forest area in Southeast Asia tropical forests to be significantly lower than other forest cover estimates. A random sample of mean NDVI value across all 3 years is taken for the GlobCover non-forest classes to represent the global NDVI distribution for these classes. The NDVI value of all GLAS shots that fall within these same non-forest classes are also extracted. The distribution of NDVI values for each class is compared with the distribution of NDVI values of the GLAS shot locations within those classes in figure 5.4. It is clear that the distribution of NDVI for a given

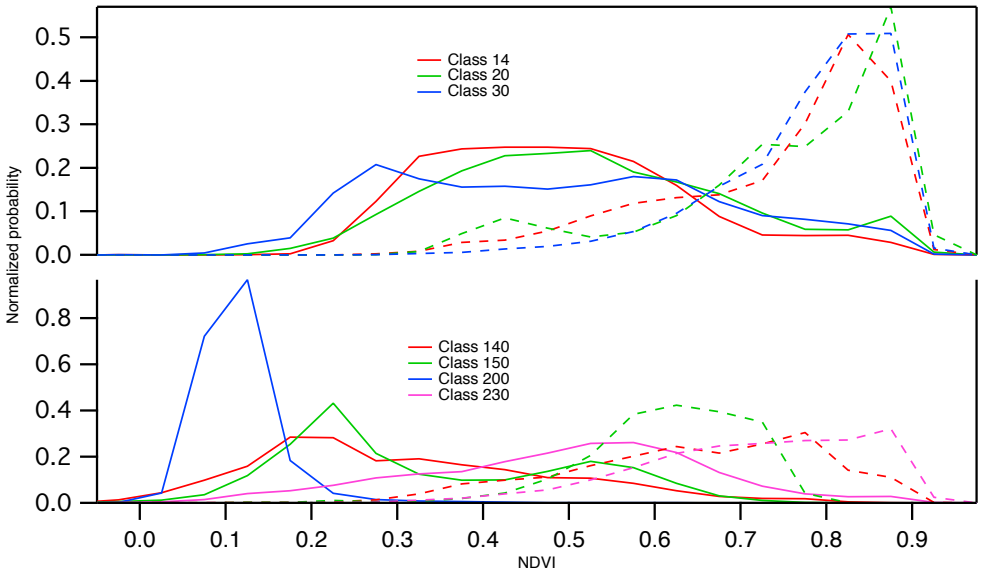

Figure 5.4: NDVI distribution for GlobCover non-forest class types (solid lines) compared with NDVI distribution of all pixels in the same landcover classes where GLAS-shot based AGB exist (dashed lines). The distribution of pixel locations with GLAS AGB values represent areas with vertical vegetation structure that GlobCover misclassified as non-forest.

GlobCover non-forest class in areas with GLAS shots is very different from the overall distribution of that non-forest class itself.

A threshold at NDVI of 0.75 is chosen to distinguish the areas that are most likely forested but misclassified as non-forest by GlobCover. Almost all of the areas that qualify using this threshold are within the tropical regions with persistent cloud cover. For areas between the latitudes of 20°N and 15°S, the pixels of non-forest classes shown in figure 5.4 that also have NDVI values ≥ 0.75 are marked as a separate "misclassed" category that is added as an additional MaxEnt model run domain.

Finally, 80% of the AGB samples (∼320,000) are randomly selected as model input, while the other 20% (∼80,000) are set aside for model validation. Each continental region is handled differently in terms of how the landcover classes are used in the Maximum Entropy model. The details are covered in the following subsections.

5.2.1 North America

Landcover types that exist in the North America domain are classes 40, 50, 60, 70, 90, 100, 110, 120, 130, 160 and 170. Due to the total size of certain landcover types within the domain, some of the smaller landcover types need to be combined with other similar landcover types in order to have enough samples for the MaxEnt model. In this case, classes 50 and 60 are combined; 160 and 170 are combined; 110, 120, and 130 are combined.

Model performance is evaluated using receiver operating characteristic (ROC) curves[Phillips et al., 2006, Fielding and Bell, 1997]. The ROC for a binomial model is the sensitivity of the model (fraction of positive instances predicted) plotted against 1-specificity (false positive rate) for all threshold values. The area under the curve (AUC) of the ROC can then be used to test model performance by comparing against the AUC of a random prediction, which is 0.5. The maximum achievable AUC will always be less than 1. The ROC curve for the North America

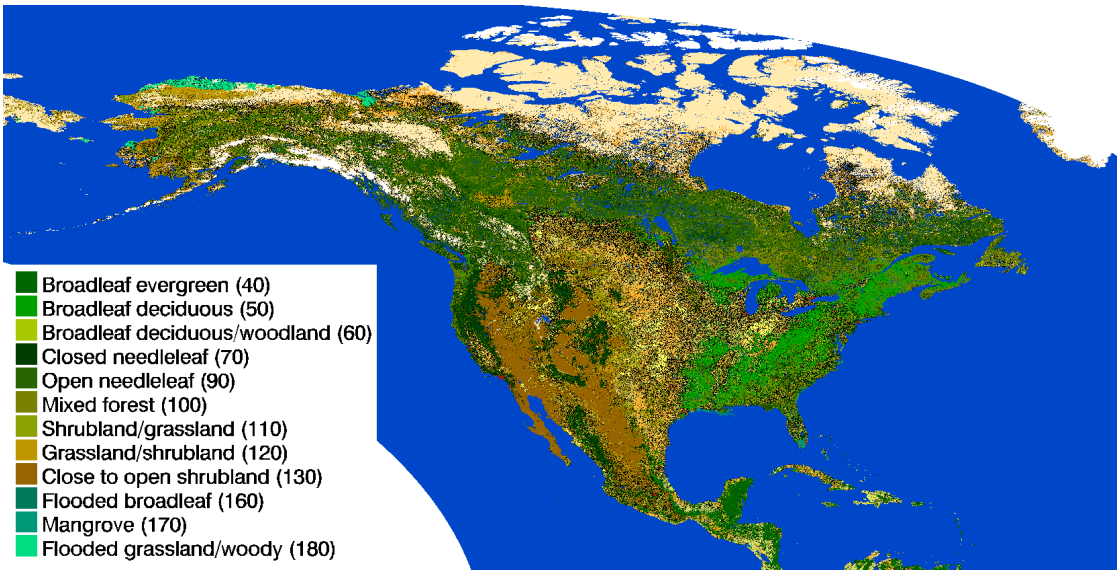

Figure 5.5: GlobCover map of North America model domain reprojected to geographic lat/lon projection. Curved white areas are outside of model domain, since native model projection is sinusoidal, straight lines become curved in this reprojection.

deciduous broadleaf class (50,60) AGB bin of 91-104 Mg/ha is shown in figure 5.6. This figure shows strong model performance as the AUC is much higher than random prediction of 0.5, and is very close to the maximum possible value. The performance of all the MaxEnt instances for North America is summarized in table 5.1.

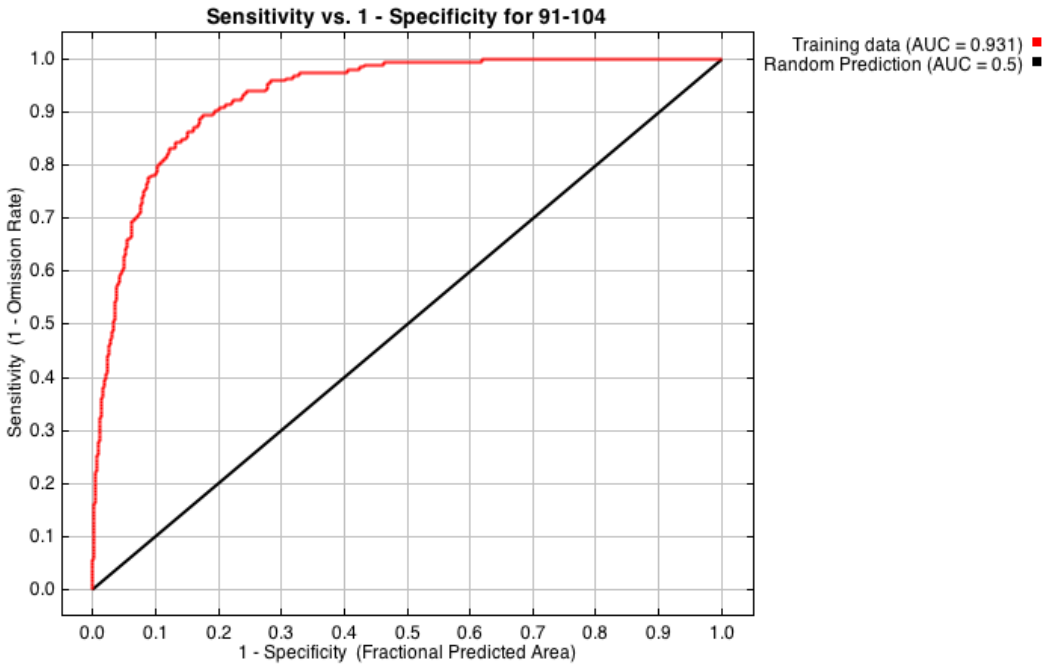

Figure 5.6: Receiver operating characteristic curve for North America MaxEnt run over deciduous broadleaf forest class for the AGB bin of 91-104 Mg/ha.

Table 5.1: MaxEnt model performance statistics for North America domain runs. Each row represents a separate domain with its own bins for AGB and area for model prediction. A random prediction will have an AUC of 0.5.

GlobCover class	# of bins	min AUC	median AUC	max AUC
110, 120	3	0.928	0.969	0.974
130	3	0.854	0.931	0.981
160	9	0.827	0.902	0.952
170, 180	2	0.926	0.932	0.932
40, 70, 90, 100	18	0.784	0.886	0.977
50	11	0.880	0.939	0.978
60	5	0.867	0.943	0.990
misclass	9	0.768	0.887	0.966

5.2.2 South America

South America (domain shown in Figure 5.7) contains the largest area of tropical moist broadleaf forests as well as the largest amount of aboveground biomass in a single biome. In addition to the wood density map used to help distinguish AGB patterns (Section 4.3), another technique is introduced when interpreting model output probabilities. In equation 5.3, one prior probability distribution $P(A)$ is calculated for each landcover type. If the same approach is used for the Amazon, one $P(A)$ would be calculated for the entire region. Since the area is very large with strong spatial patterns of AGB [Slik et al., 2013, Baker et al., 2004, Losos and Leigh, 2004], it is important to try to capture this spatial variation without having too much of it being over-ridden by the use of one single prior probability distribution.

Luckily, this region also contain the largest amount of GLAS samples (over 160,000 samples globally are located here). The spatial patterns of AGB probability distribution can be incorporated by breaking the region into smaller areas, each with its own local prior distribution $P(A)$. This is facilitated by the dense coverage of GLAS samples, which allows enough samples in each local region to develop its own $P(A)$. The soil map developed by Saatchi et al. [2009] is used as an independent dataset for separating the Amazon into local regions (Figure 5.8). For the "young alluvial deposits", the eastern segments and the western segment is further differentiated. The AGB samples in each soil type is counted to create a local $P(A)$ for the area of that particular soil type. This is then used when calculating $\langle AGB \rangle$ from the model probabilities for each area in equation 5.3. The actual types of soil do not matter in this case because it is only used as an independent way of subdividing the Amazon. Six of the soil types did not have sufficient samples to calcultae $P(A)$. The default probability distribution that was calculated for the entire Amazon is used for these areas.

There is a small region of overlap between the North America domain and the South America domain (Figure 5.1). This is by design so that the regions of tropical moist broadleaf forests in Central America can be modeled together with the rest of this forest type within South America. The "misclass" category is included here for areas that pass the threshold value of NDVI 0.75. Summary of South America model performance is included in table 5.2.

Table 5.2: MaxEnt model performance statistics for South America domain runs. Each row represents a separate domain with its own bins for AGB and area for model prediction. A random prediction will have an AUC of 0.5.

GlobCover class	# of bins	min AUC	median AUC	max AUC
110, 120, 130	7	0.933	0.973	0.990
160, 170	9	0.830	0.876	0.952
40	24	0.741	0.881	0.970
50, 60, 100	5	0.873	0.971	0.985
misclass	11	0.898	0.940	0.975

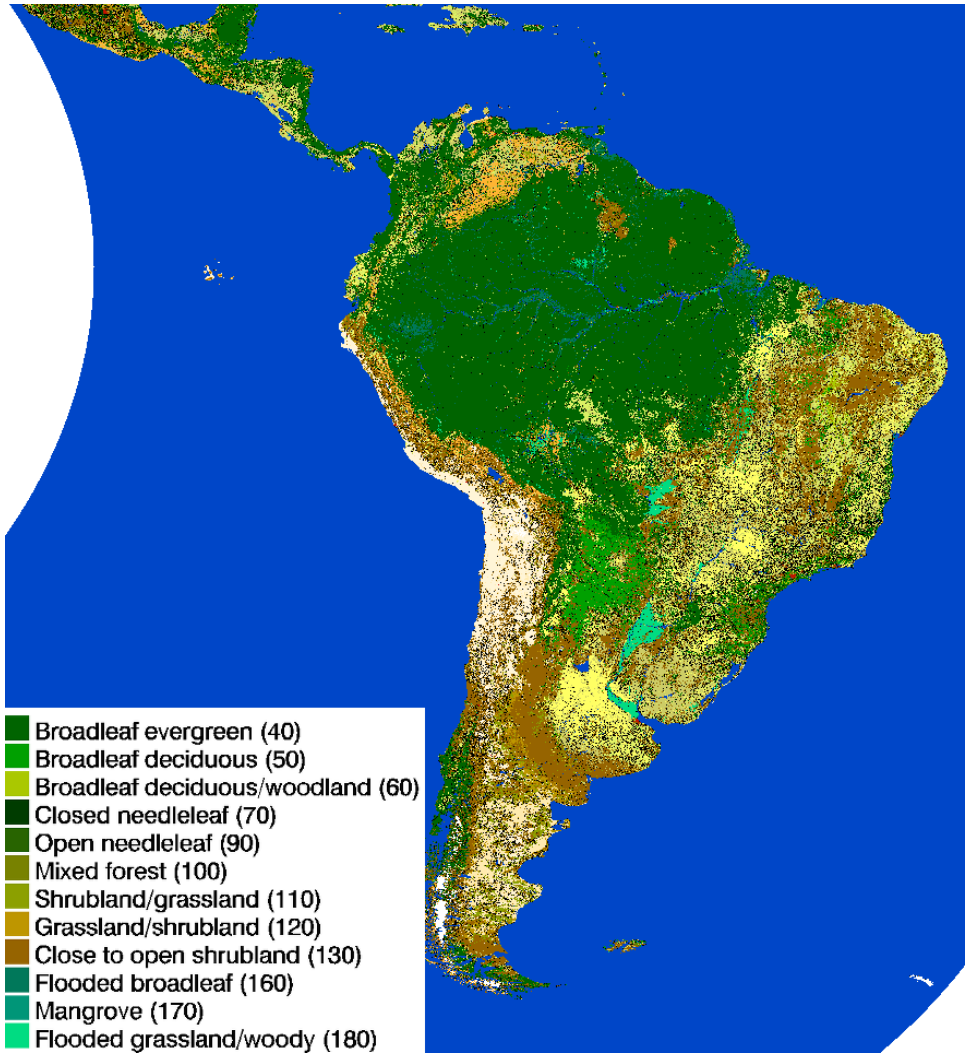

Figure 5.7: GlobCover map of South America model domain reprojected to geographic lat/lon projection. Curved white areas are outside of model domain, since native model projection is sinusoidal, straight lines become curved in this reprojection.

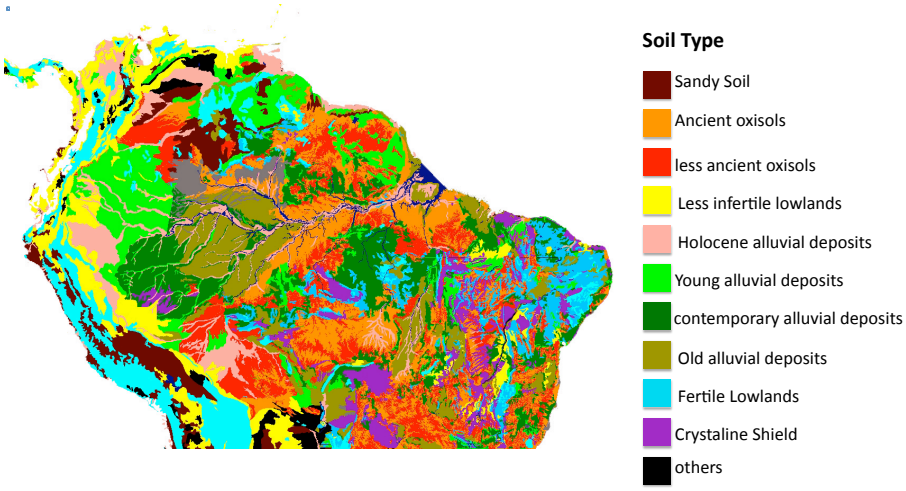

Figure 5.8: Soil map of the Amazon. The specific classes of soil do not matter in this case because they are only used as an independent way of subdividing the Amazon into smaller regions. Source: [Saatchi et al., 2009]

5.2.3 Africa

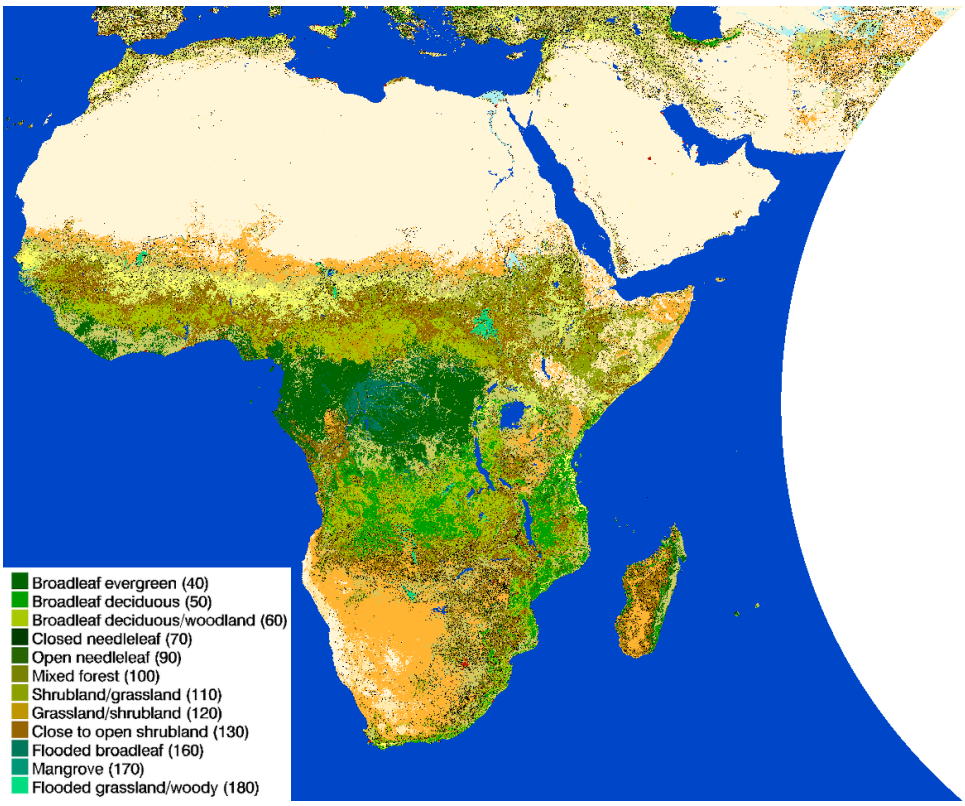

Figure 5.9: GlobCover map of Africa model domain reprojected to geographic lat/lon projection. Curved white areas are outside of model domain, since native model projection is sinusoidal, straight lines become curved in this reprojection.

The GlobCover class types within the Africa domain are 40, 50, 60, 70, 90, 100, 110, 120, 130, 160, 170, and 180. Africa contains large areas of woodlands and savannas/shrublands compared with the other continents. Here, the savanna/shrubland class of 130 and woodland class of 60 have enough AGB samples to be modeled independently. Classes 110 and 120 are combined; 170 and 180 are combined; 40, 70, 90, and 100 are combined; "misclass" category is also included here. Model performance evaluation statistics are shown in table 5.3.

Table 5.3: MaxEnt model performance statistics for Africa domain runs. Each row represents a separate domain with its own bins for AGB and area for model prediction. A random prediction will have an AUC of 0.5.

GlobCover class	# of bins	min AUC	median AUC	max AUC
110, 120	3	0.928	0.969	0.974
130	3	0.854	0.931	0.981
160	9	0.827	0.902	0.952
170, 180	2	0.926	0.932	0.932
40, 70, 90, 100	18	0.784	0.886	0.977
50	11	0.880	0.939	0.978
60	5	0.867	0.943	0.990
misclass	9	0.768	0.887	0.966

5.2.4 Eurasia

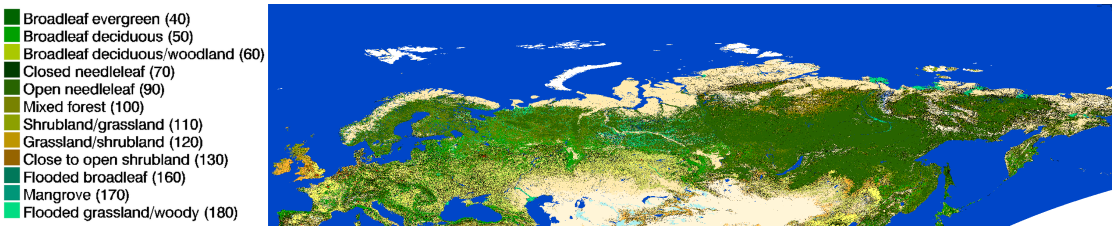

Figure 5.10: GlobCover map of Eurasia model domain reprojected to geographic lat/lon projection. Curved white areas are outside of model domain, since native model projection is sinusoidal, straight lines become curved in this reprojection.

The Eurasia domain covers Europe as well as portions of northern Asia (Figure 5.10). Being located in the northern latitudes, there are no tropical landcover types in this region. Majority of the region are needleleaf forest types, and as such, the open and closed needleleaf classes (70 and 90) are each modeled independently. There is also no "misclass" category in this domain because cloud contamination is

minimal at higher latitudes. Summary of model performance evaluation is shown in table 5.4

Table 5.4: MaxEnt model performance statistics for Eurasia domain runs. Each row represents a separate domain with its own bins for AGB and area for model prediction. A random prediction will have an AUC of 0.5.

GlobCover class	# of bins	min AUC	median AUC	max AUC
100	9	0.844	0.887	0.967
110, 120, 130	2	0.950	0.960	0.960
160, 170, 180	2	0.890	0.906	0.906
50, 60	9	0.801	0.882	0.944
70	8	0.926	0.940	0.959
90	6	0.811	0.880	0.935

5.2.5 Southeast Asia

The Southeast Asia domain contains the tropical forests of Asia. Due to the extensive cloud cover in this region, it is also the most problematic area in terms of GlobCover misclassification. The "misclass" category is included here to improve the forest cover estimation. Model performance evaluation is summarized in table 5.5.

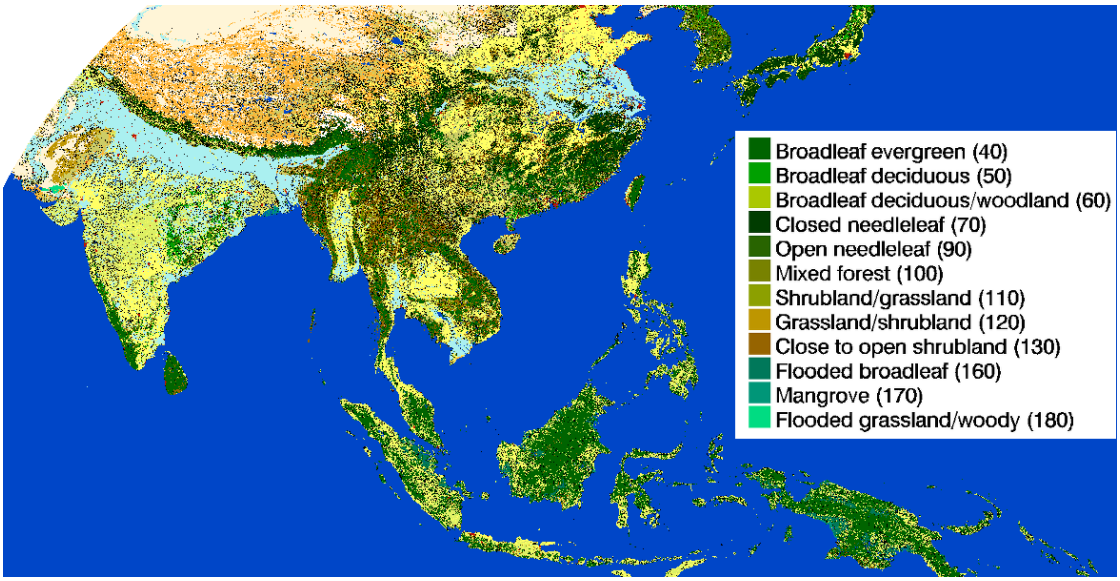

Figure 5.11: GlobCover map of Southeast Asia model domain reprojected to geographic lat/lon projection. Curved white areas are outside of model domain, since native model projection is sinusoidal, straight lines become curved in this reprojection.

Table 5.5: MaxEnt model performance statistics for Southeast Asia domain runs. Each row represents a separate domain with its own bins for AGB and area for model prediction. A random prediction will have an AUC of 0.5.

GlobCover class	# of bins	min AUC	median AUC	max AUC
110, 120, 130	10	0.925	0.950	0.972
160, 170, 180	7	0.833	0.891	0.928
40	17	0.860	0.908	0.976
50, 60	3	0.956	0.958	0.959
70, 90, 100	2	0.965	0.965	0.965
misclass	9	0.885	0.927	0.955

5.2.6 Australia

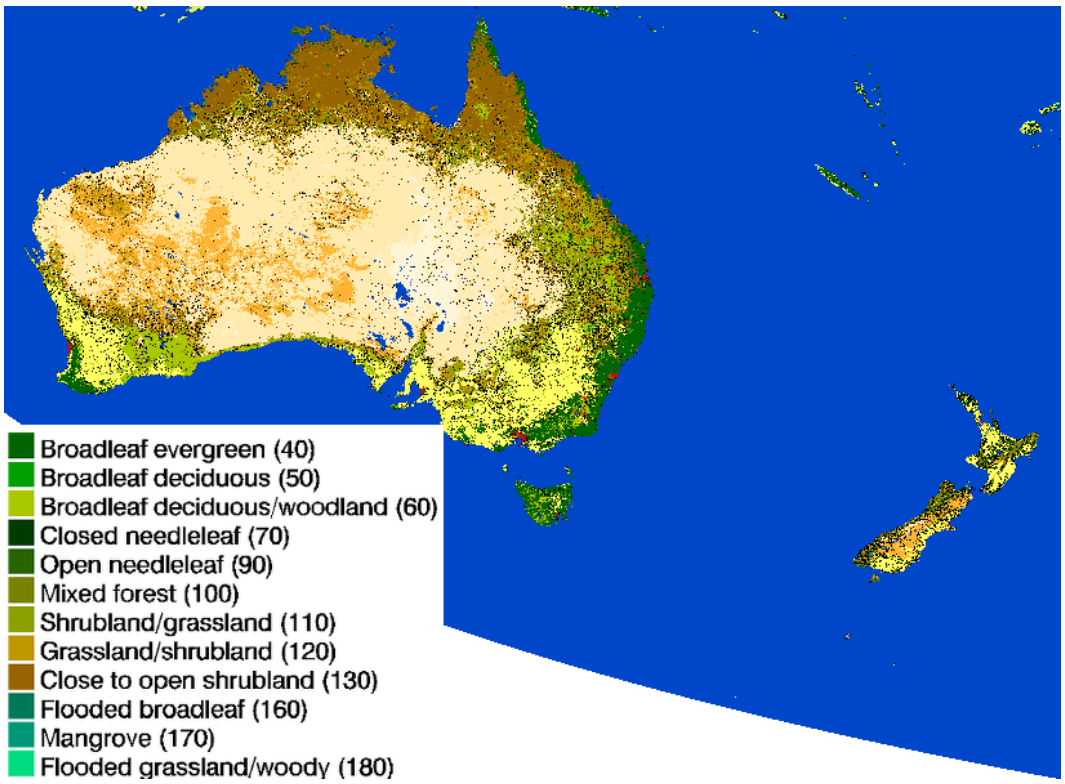

Figure 5.12: GlobCover map of Australia model domain reprojected to geographic lat/lon projection. Curved white areas are outside of model domain, since native model projection is sinusoidal, straight lines become curved in this reprojection.

The Australia model domain contains Australia and some of the larger islands in the region such as New Zealand. This domain is also close enough to the tropics to warrant the "misclass" category, although the total area is small and AGB values are not as high as the ones in the other tropical regions. Model performance evaluation is summarized in table 5.6.

Table 5.6: MaxEnt model performance statistics for Australia domain runs. Each row represents a separate domain with its own bins for AGB and area for model prediction. A random prediction will have an AUC of 0.5.

GlobCover class	# of bins	min AUC	median AUC	max AUC
120, 130	2	0.922	0.954	0.954
40	14	0.870	0.919	0.960
50, 60, 160, 170, 180	2	0.916	0.938	0.938
70, 90, 100, 110	2	0.960	0.985	0.985
misclass	4	0.878	0.931	0.989

5.2.7 Sapling Biomass

One more adjustment to AGB is needed after calculating expectation values of AGB from the model output using equation 5.3: to take into account the biomass of the saplings. Generally, when trees are measured in an inventory plot in the field, only trees above a certain diameter are measured. This is due to the fact that measuring the small saplings are prohibitive because of the typically large number of saplings within a forest. In the US, FIA measures trees that have a diameter at breast height (DBH) greater than or equal to 5 inches[FIA, 2005]. Similar methods are used elsewhere with slightly varying DBH thresholds. The saplings represent a small (generally around 10%) but significant amount of total forest AGB[Makana et al., 2011, Smith et al., 2013, Losos and Leigh, 2004].

Since the allometric equations are developed using field plots that do not include sapling biomass, the AGB estimated by the model is also the AGB of the larger trees excluding sapling biomass. To take the sapling AGB into account, methods of estimating sapling AGB from model predicted AGB is developed. There are typically a small subset of forest inventory plots that do measure saplings. These plots are used to develop a relationship between larger-tree AGB

and sapling AGB.

Data from FIA is used to develop this relationship for the temperate and boreal forests. The FIA plots are separated into hardwood, softwood, and mixed types, and the AGB of saplings (DBH < 12.7 cm) is plotted against AGB of larger trees (DBH ≥ 12.7 cm) in figure 5.13. While the maximum range of sapling AGB exhibits a decreasing trend with increasing large-tree AGB, the overall correlation is insignificant. Therefore, for the temperate and boreal regions, three simple ratios are calculated from FIA field data and used to calculate sapling AGB. Ratios of 9.8%, 10.6%, and 13.5% are used for deciduous, conifers, and mixed forests respectively.

In the tropics, field plot samples from Southeast Asia and Barro Colorado Island (BCI) in South America are used to evaluate sapling AGB (Sassan Saatchi, personal communication). Here, the sapling measurements are for trees with DBH $<$ 10 cm. Figure 5.14 shows sapling AGB versus large tree AGB as well as the distribution of AGB in the rainforest landcover types (class 40) from model output. Simple linear regression is used to develop a relationship between sapling AGB and larger tree AGB. The fitted equations are $AGB_{sap} = 16.8 - 0.01072AGB$ and $AGB_{sap} = 24.263 - 0.034396AGB$ for BCI and Southeast Asia respectively, where AGB_{sap} is the sapling AGB and AGB is the AGB of trees with DBH $\geq$ 10cm. The distribution of AGB from model output for landcover class 40 is also included in figure 5.14. This is to show that the AGB ranges sampled in the field inventory cover the large ranges of AGB found in the forest class. No sapling plot data was available for the Africa tropical forests. The AGB distributions in figure 5.14 show that the Africa tropical forest AGB distribution is closer to that of South America than Southeast Asia. Therefore, the sapling equation developed using BCI plots is used for the Africa tropical rain forest.

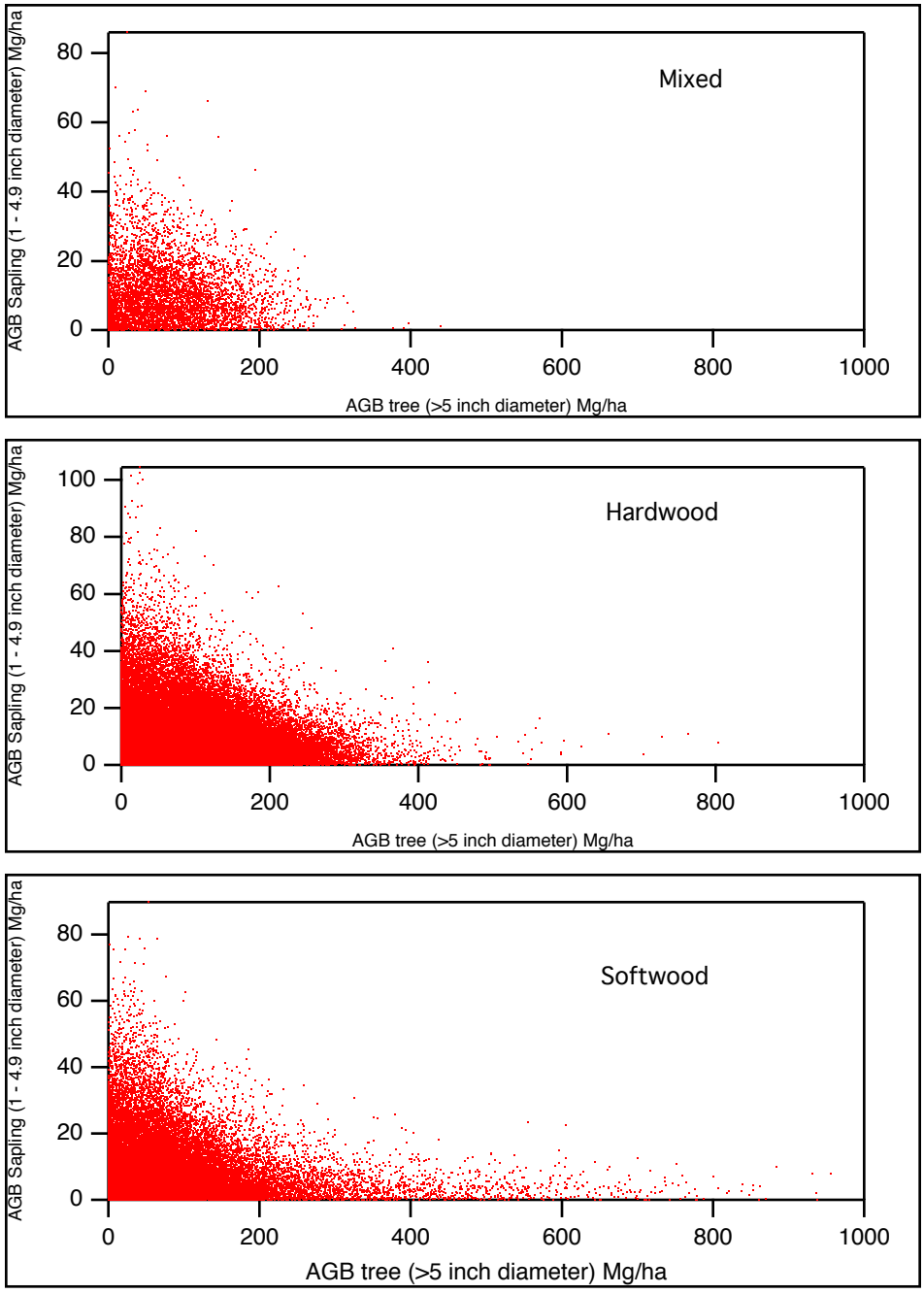

Figure 5.13: Scatterplot of sapling (DBH $<$ 12.7 cm) AGB versus AGB of trees with DBH $\geq$ 12.7 cm in using FIA plot data. The forest plots are separated by mixed (top panel), hardwood (middle panel), and softwood (bottom panel).

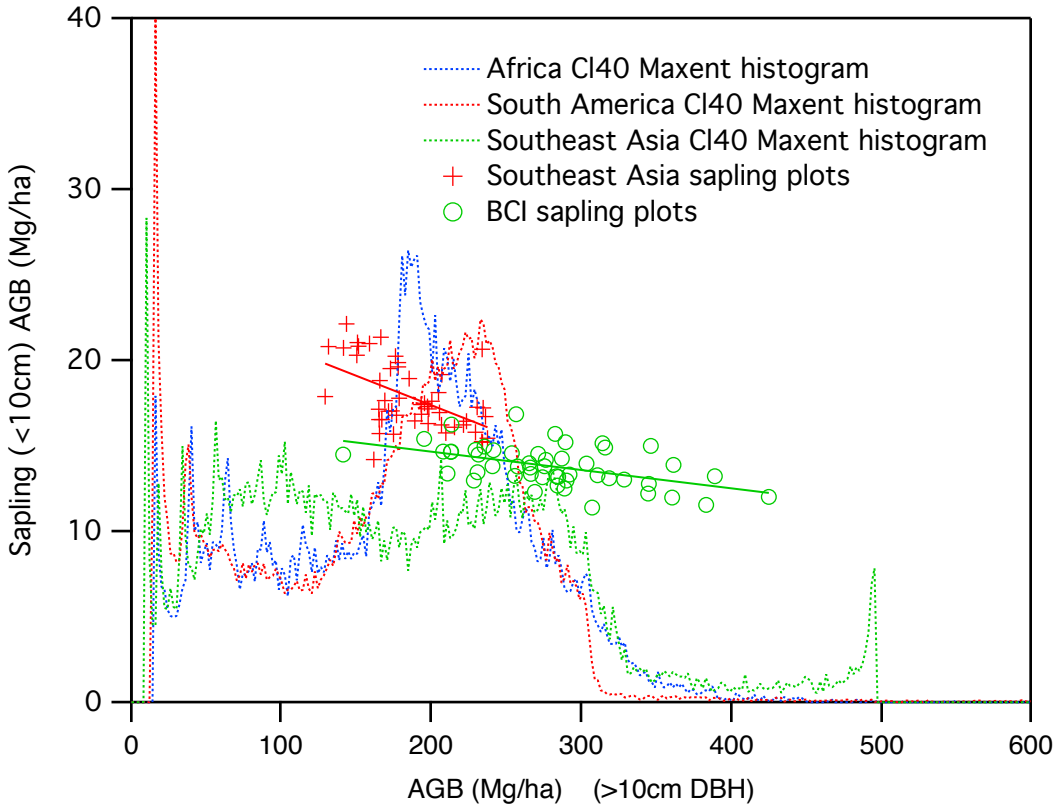

Figure 5.14: Tropical sapling (DBH $<$ 10 cm) AGB versus larger tree (DBH $\geq$ 10cm) AGB from plots in Southeast Asia and Barro Colorado Island. Solid lines show the fitted linear regression equations for sapling AGB. Dotted lines show normalized probability density of model predicted AGB for GlobCover class 40 (tropical moist broadleaf forest). Vertical axis for the normalized probability is not shown.

5.2.8 Global Aboveground Biomass Distribution

The map of global distribution of aboveground biomass can now be assembled from the 6 model domains after adjusting for sapling AGB. The results are shown in figure 5.15. Because of resolution limitations, the global map at 1km resolution cannot be shown here. Instead, the values are aggregated to 10km resolution for display. A more detailed view of the AGB over South America is shown in figure 5.17 with the inset showing detailed patterns of biomass and deforested areas.

The areas with the highest density of AGB are found in Pacific coast of North America; the Guiana Shields and western end of the Amazon and coastal regions of Columbia in South America; Gabon, small portions of Libera, and eastern Democratic Republic of Congo in Africa; Indonesia (especially central Borneo), central region of New Guinea island, southeastern border of the Himalayas, and central region of Taiwan. These regions all have AGB values of over 300 Mg/ha.

The distribution of AGB across four major forest types based on GlobCover is analyzed globally with the histograms shown in figure 5.16. The four categories consist of broadleaf evergreen (GlobCover class 40), broadleaf deciduous and mixed (GlobCover 50 and 100), needleleaf (GlobCover class 70 and 90), and woodlands (GlobCover 60). These forest show distinct AGB distribution patterns with the tropical forest group of broadleaf evergreen containing the highest AGB density, peaking around 220 Mg/ha. Broadleaf deciduous and mixed forests have much lower AGB in comparison with most values lower than 150 Mg/ha. Needleleaf forests mostly contain similar lower AGB values but have a smaller peak in the 350 Mg/ha range, which correspond to the massive red-woods of the Pacific coast of North America. Woodlands contain the lowest AGB density with most values being below 100 Mg/ha.

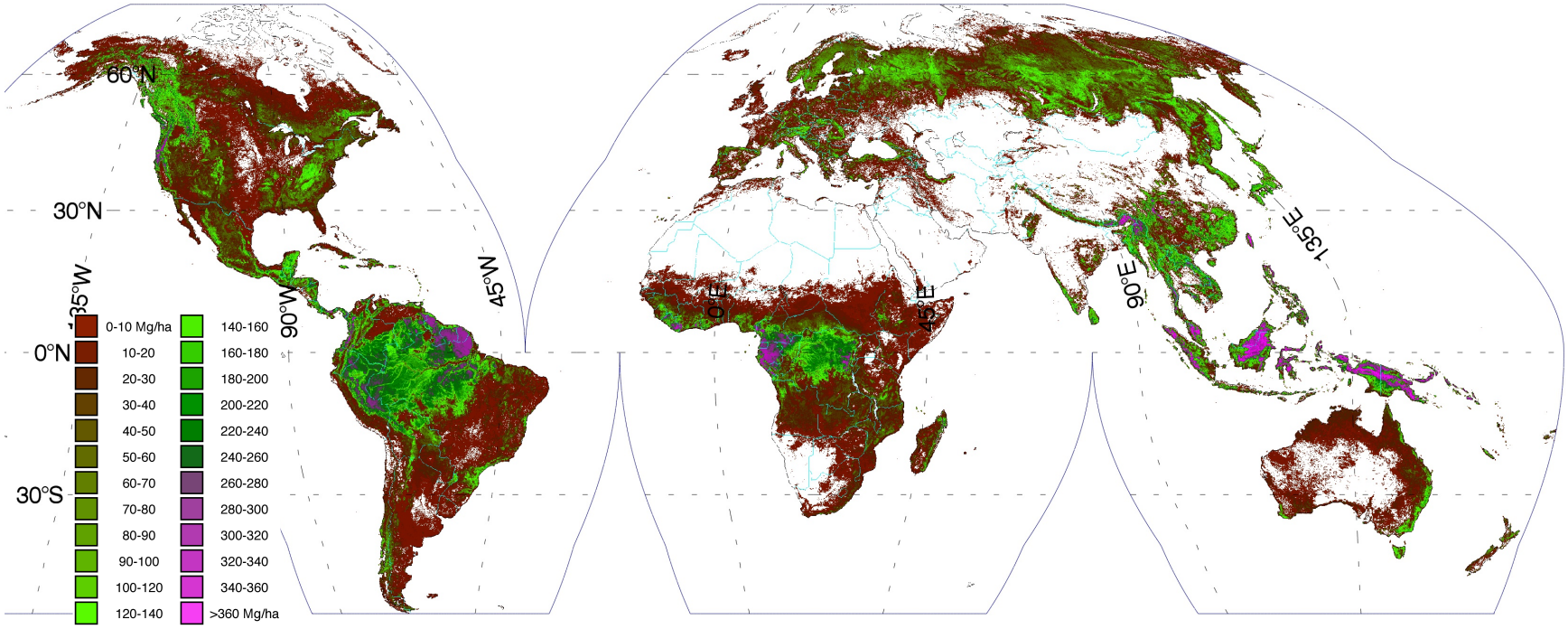

Figure 5.15: Global aboveground biomass distribution. AGB values are continuous, but colored by bins for display. Values are adjusted to include sapling using methods discussed in section 5.2.7. Map is shown in interrupted Goode homolosine projection.

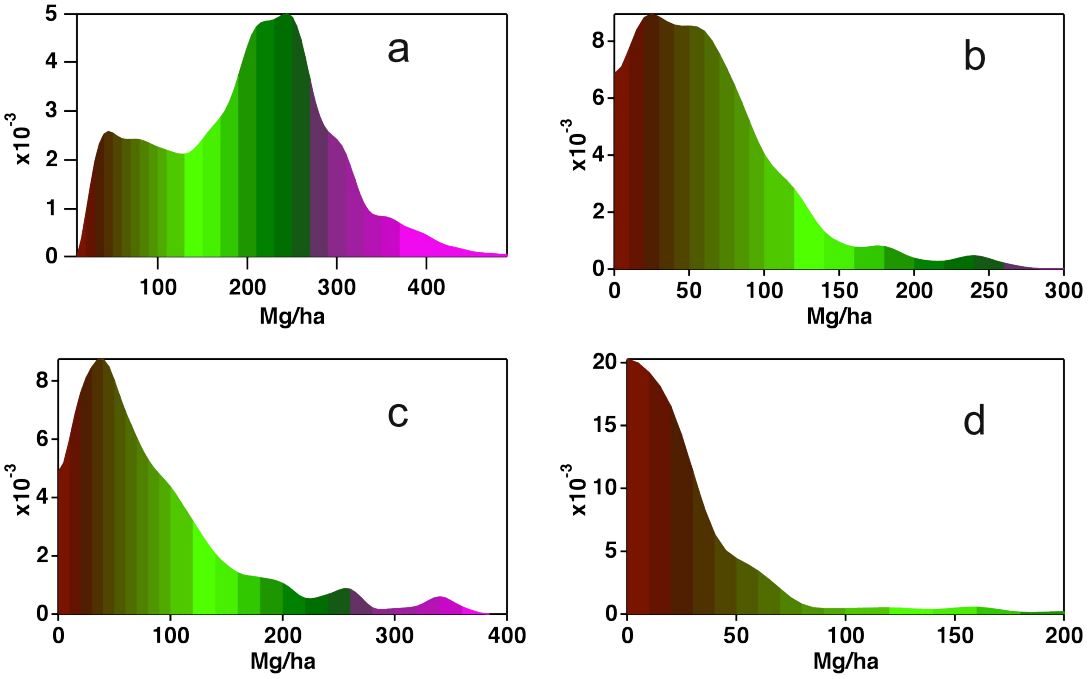

Figure 5.16: Histogram of global forest AGB for a) tropical broadleaf evergreen, b) broadleaf deciduous and mixed, c) needleleaf, and d) woodland forest classes. Forest classification here is based on GlobCover with a) class 40; b) class 50 and 100; c) class 70 and 90; d) class 60. Coloring uses the same AGB coloring bin as figure 5.15.

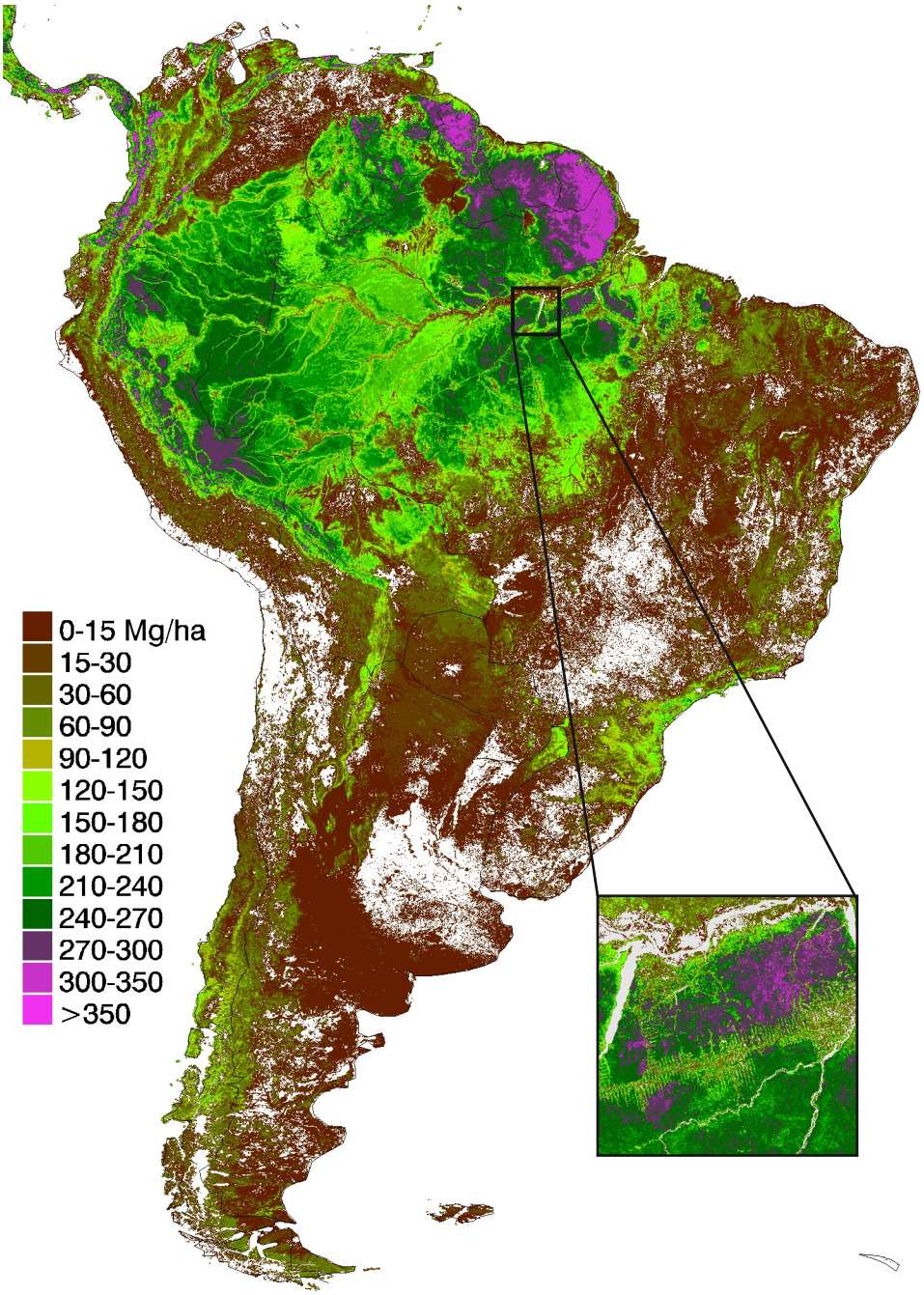

Figure 5.17: Detailed view of model results for aboveground biomass over South America. Inset is at actual resolution, showing detailed variation in AGB and deforested areas.

5.3 Model Evaluation and Uncertainty Analysis

Model uncertainty at the pixel level is evaluated by using the 20% AGB samples (∼80,000) that were set aside for validation. The GLAS based AGB samples are plotted against model predicted AGB values at those pixels in figure 5.18. Three values of m=1, 2, and 3 in equation 5.3 are shown with R^2 values of 0.667, 0.665, and 0.642 respectively. The root mean squared error (RMSE) at the pixel level is calculated to be 51.1, 51.5 55.6 Mg/ha. Average relative error at the pixel level is 36%, 30%, and 29% respectively.

The values of R^2, RMSE, and average percent relative error cannot definitively decide which value of m gives the best predictor of AGB. A more prominent way of comparing the relative performance of the three weighting values of m is through analysis of the density scatterplot shown in figure 5.18. In panel a) of figure 5.18, three regions of high density is visible around 220 Mg/ha, 50-100 Mg/ha, and <50 Mg/ha. These three regions correspond to the peak densities of tropical broadleaf evergreen forests (Figure 5.16a); temperate forests (Figure 5.16b and c); woodlands (Figure 5.16d) and shrubs/savanna. In panel a) of figure 5.18, we can see the three main density clusters are estimated more towards the mean of each respective cluster (visually as the distribution turning more horizontal). As we increase m from 1 to 2 and then 3, the three density clusters become more aligned with the 1-to-1 line, meaning that the model does a better job at predicting values away from the mean. After testing different values of m, m=3 is found to give the best predictor for AGB.

The probability distribution of AGB density is tested against the validation points for each of the GlobCover landcover type, shown in Figures 5.19 and 5.20. The forested landcover types of broadleaf evergreen (40), closed broadleaf deciduous (50), open broadleaf deciduous (60), closed needleleaf (70), open needleleaf (90), and mixed (100) are shown in figure 5.19. The other landcover types of

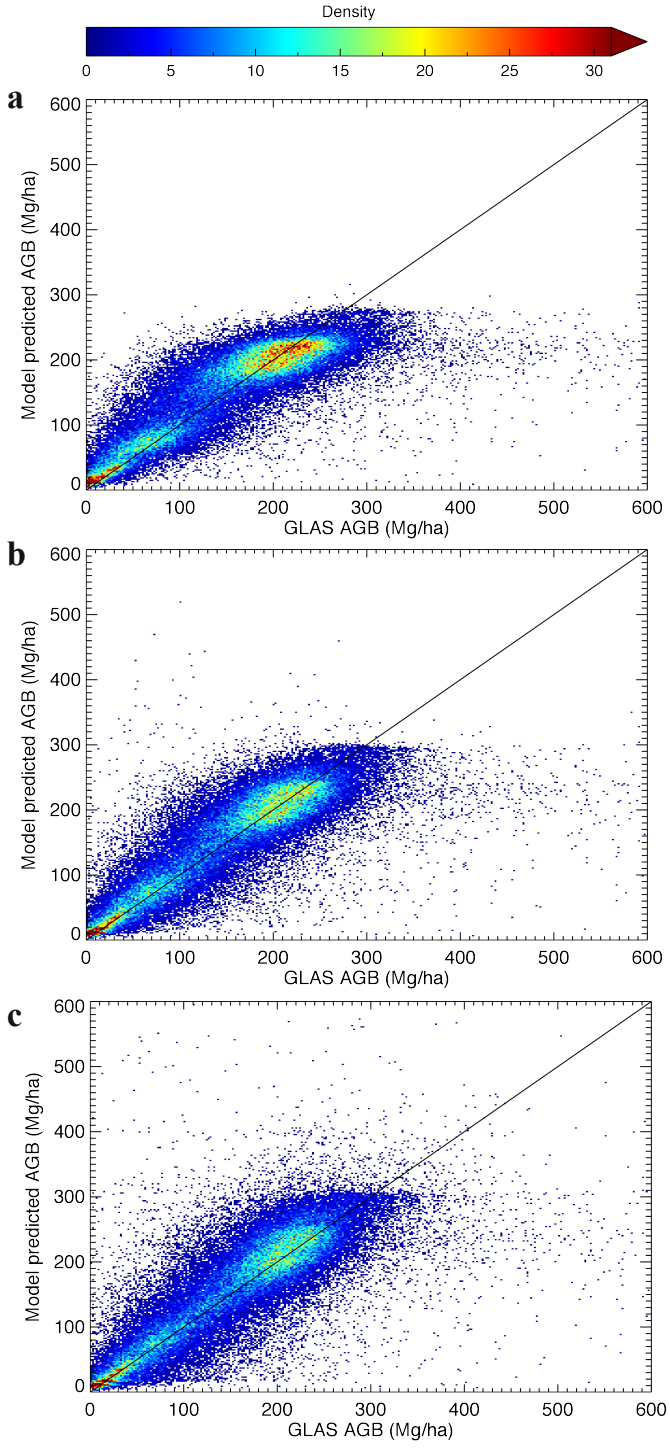

Figure 5.18: Sample test of using different weighting values of m in equation 5.3 in the tropical moist broadleaf region of South America for a) m=1, b)m=2, c)m=3. 80% of AGB samples were used for model run and 20% were used for validation to create the density scatter plot. One-to-one line is drawn in for reference.

mosaic forest/shrubland with grassland (110), mosaic grassland with forest or shrubland (120), closed to open shrubland (130), closed to open flooded broadleaf (160), mangroves (170), and closed to open flooded woody vegetation (180) are shown in figure 5.20. All landcover types show good agreement between input sample probability distribution of AGB and model-predicted AGB probability distribution.

Spatially explicit pixel-level model uncertainty is also calculated. For a given pixel, the model uncertainty is calculated as

$$\epsilon_B = \frac{\sum_{k=1}^{N} |\bar{B}_k - \langle B \rangle| P_k P(A_k)}{\sum_{k=1}^{N} P_k P(A_k)} \tag{5.4}$$

where k is the AGB bin number, $\bar{B}_k$ is the mean AGB for k^{th} bin, $\langle B \rangle$ is the model predicted expectation value of AGB for the pixel, P_k is the model predicted probability at the pixel for the k^{th} bin, and $P(A_k)$ is the prior probability. Here, the expectation value of the absolute error is used instead of the typical expectation of squared error as variance and then the square root of variance as standard deviation.

The variance definition is commonly used because the algebra is generally easier with squares than with absolute values, leading to the typical definition of variance and then taking the square root for standard deviation to get a measure with the same unit as the quantity being examined [Pitman, 1993, chap 3.]. The issue with using standard deviation is that when taking the square root, due to the non-linear nature of the function, a bias is introduced. This leads to the use of approximations in trying to remove this bias such as using Bessel's correction for normal distributions. However, in this case, the AGB value distribution is not normal, and no good approximation is known to remove the bias. Instead, by working with the expectation of the absolute error, no bias is introduced, and since the values are directly computed here, the ease of working with squared function is a moot point.

Using equation 5.4, an accompanying pixel-level model uncertainty map is generated at 1km resolution, shown in figure 5.21. Similar to figure 5.15, for display purposes, the 1km error pixels are aggregated to 10km pixels and then colored by bin. As expected, the areas with higher AGB values tend to have higher absolute error, meaning the relative error is more constant. In terms of the high biomass density tropical rain forests, the absolute model uncertainty over the Amazon is less than that over Gabon or Southeast Asia. This is likely partly due to the more detailed treatment over the Amazon using local prior probability distributions as well as the higher density of AGB samples in the area.

There are additional sources of error other than model prediction error (ϵ_B in equation 5.4, here now referred to as $\epsilon_{\text{prediction}}$). These are listed here in the order they appear in the methodology. These are: measurement error associated with estimation of Lorey's height from GLAS ($\epsilon_{\text{measure}}$), allometric error when converting Lorey's height to AGB ($\epsilon_{\text{allometry}}$), and sampling error associated with representativeness of GLAS-derived AGB on the true AGB of GLAS footprint as well as heterogeneity of forest biomass in the 1-km pixel ($\epsilon_{\text{sampling}}$). RMSE for Lorey's height prediction from GLAS is estimated at 3.3 m, 4.9 m, and 6.9 m for broadleaf, needleaf, and mixed forests [Lefsky, 2010]; which are 13.7%, 20.3%, and 28.6% relative errors respectively. Allometric errors for individual allometric equations can be estimated from the relationships in figure 4.4. The total uncertainty taking all the errors into account can now be calculated, assuming all errors are independent and random, by using

$$\epsilon_{\text{AGB}} = \sqrt{\epsilon^2_{\text{measure}} + \epsilon^2_{\text{allometry}} + \epsilon^2_{\text{sampling}} + \epsilon^2_{\text{prediction}}} \tag{5.5}$$

This equation, when applied on the pixel level, will increase the error terms to take into account the other sources of error. But since the other terms are relatively constant spatially, the spatial pattern of error in figure 5.21 is preserved.

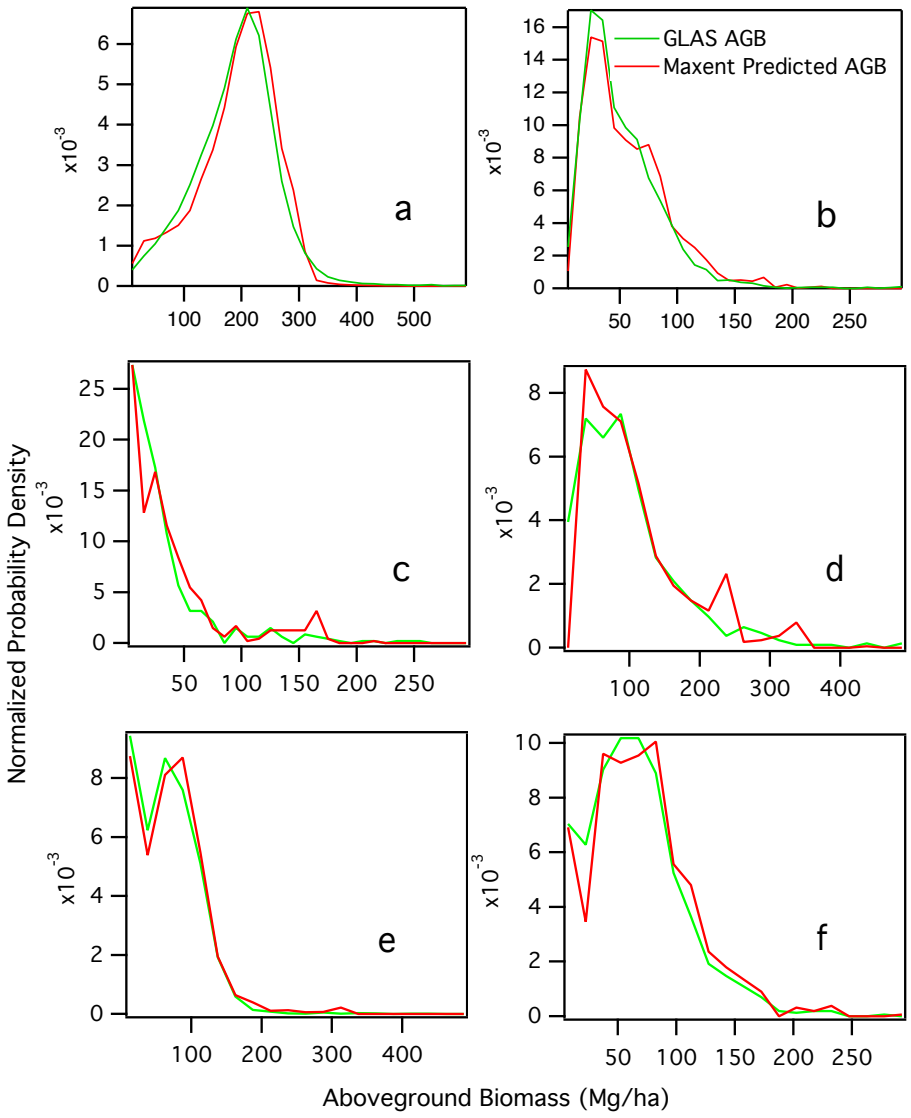

Figure 5.19: Histogram of normalized probability distribution of aboveground biomass for validation samples in the forested landcover types. Green lines are probability distribution of AGB of the GLAS-based samples that were set aside and not used in the model. Red lines are the probability distribution of model predicted AGB at the same pixel locations of the validation samples. Landcover types are based on GlobCover for classes a) 40, b) 50, c) 60, d) 70, e) 90, f) 100

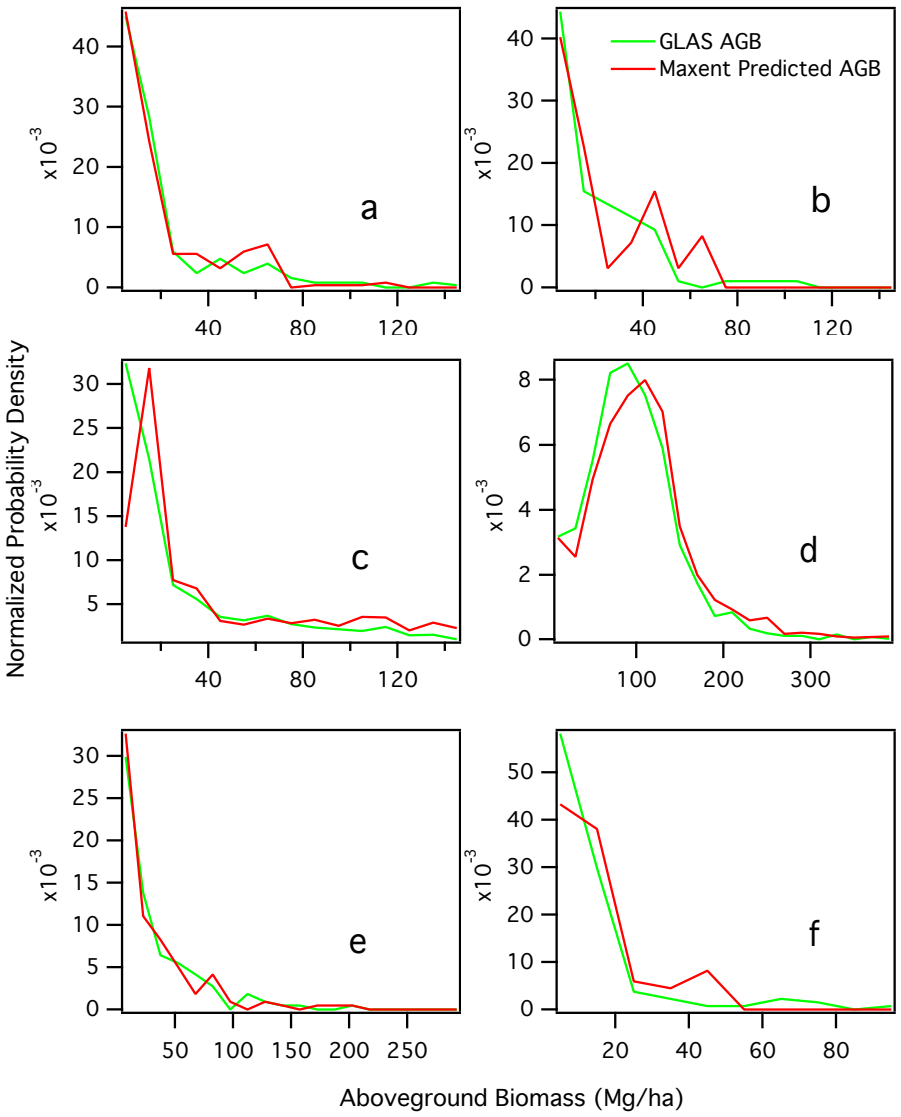

Figure 5.20: Histogram of normalized probability distribution of aboveground biomass for validation samples in the nonforest landcover types and mangrove. Green lines are probability distribution of AGB of the GLAS-based samples that were set aside and not used in the model. Red lines are the probability distribution of model predicted AGB at the same pixel locations of the validation samples. Landcover types are based on GlobCover for classes a) 110, b) 120, c) 130, d) 160, e) 170, f) 180

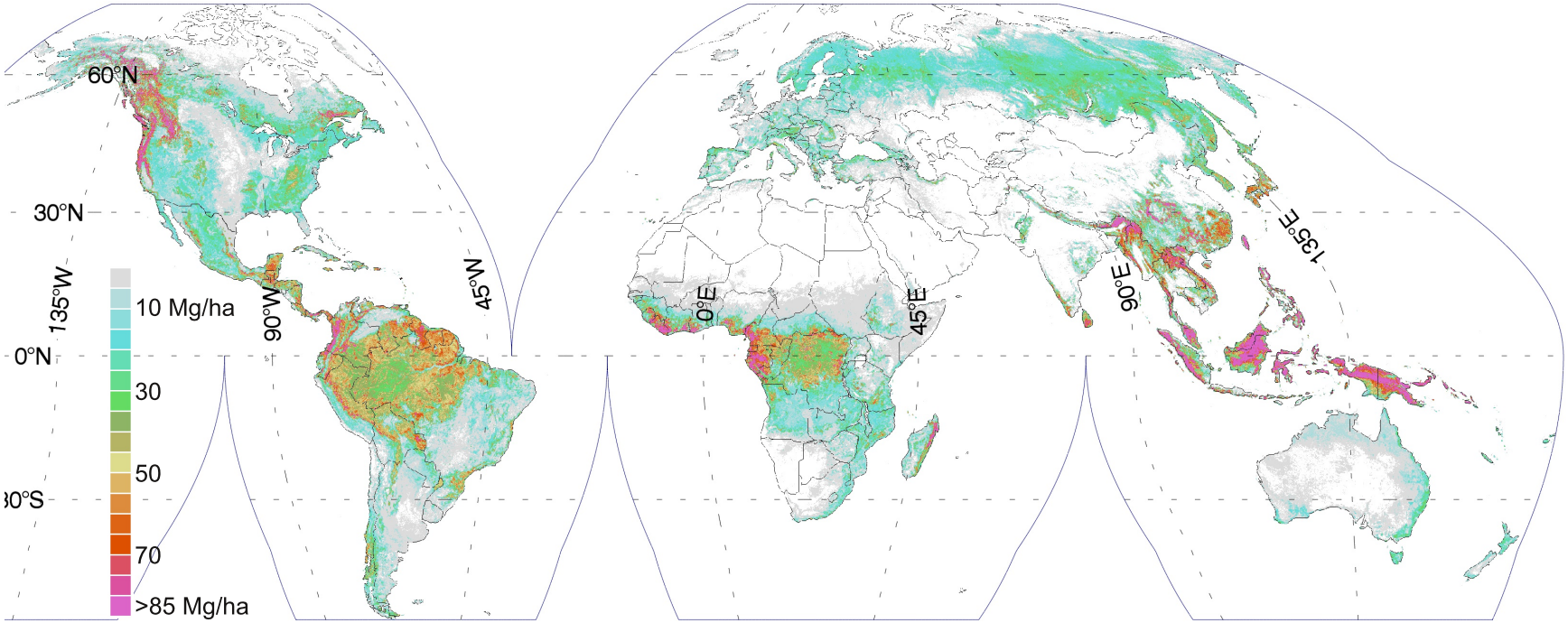

Figure 5.21: Global model error uncertainty. Values are continuous but colored by bin, with each bin being 5 Mg/ha in width (i.e., first bin is 0 - 5 Mg/ha). Map is shown in interrupted Goode homolosine projection.

5.4 Summary

The entire process in the modeling of aboveground biomass is presented in this chapter. GLAS-derived AGB values are used as samples in the Maximum Entropy model MaxEnt, along with 22 wall-to-wall remote sensing image layers and land-cover map as ancillary input, to predict global spatial distribution of aboveground biomass at ∼1km (926.6 m) resolution. Associated pixel-level model uncertainty is also calculated. Other sources of error are discussed and quantified and can be included to account for errors outside of the Maximum Entropy model. The aboveground biomass and associated uncertainty map presented here are the first of its kind on the global scale. This spatially explicit dataset can help to greatly reduce the uncertainties in the terrestrial portion of the global carbon cycle by locating and improving calculations of carbon emissions from land-use change and forest regrowth. It will also help with the national reporting efforts on greenhouse gas inventory. The next chapter will now go over the calculation of carbon stocks that can be used for carobn emission calculations and reporting purposes.

CHAPTER 6

Carbon Stocks and Comparison with Existing Inventory

The carbon content of woody biomass is typically around 50% by weight [McKendry, 2002]. The generally accepted convention is to multiply biomass by 0.5 to get mass of carbon[Saatchi et al., 2011b, Baccini et al., 2012], and that is used here as well to calculate carbon content. The calculation of carbon, therefore, is straightforward. However, for inventory reports, the carbon pools of live woody vegetation typically include both aboveground and belowground portions. This chapter will first go over the calculation of the belowground biomass. Then, the carbon stocks based on AGB+BGB is analyzed for spatial patterns and compared with other existing inventory data.

6.1 Belowground Biomass

Belowground biomass is extremely difficult and time consuming to measure in the field, typically involving careful excavation of the roots by hand [Ryan et al., 2011, Kajimoto et al., 1999, Aerts et al., 1991]. Therefore, field plots are very limited. Additionally, due to the physical location of the root system, it is practically impossible for remote sensing methods to detect this portion of the plant. Here, relationships between aboveground biomass and belowground biomass, generally known as root:shoot ratio are compiled from exiting literature that is based on field study, and BGB is then calculated from AGB.

Table 6.1: Equations used for calculation of BGB. Bold fonts are default equations for that landcover type while regular fonts are equations for specific regions where available. $*$ Brown S. (personal communication via Saatchi S.) † FIA field plots ‡ [Saatchi et al., 2011b] § [Mokany et al., 2006] ‖ [Ryan et al., 2011] ¶ [Komiyama et al., 2008]

Temperate/Boreal forest $*$	$BGB = 4.0165 + 0.204AGB$
deciduous (NAm) †	$BGB = 0.196631AGB$
evergreen (NAm) †	$BGB = 0.221198AGB$
mixed (NAm) †	$BGB = 0.20634AGB$
flooded (NAm) †	$BGB = 0.203549AGB$
Tropical forest ‡	$BGB = 0.489AGB^{0.89}$
Shrubs & savanna §	$BGB = 7.83AGB^{0.32}$
Africa ‖	$BGB = 0.4933AGB$
Mangrove ¶	$BGB = 0.4AGB$

All the BGB equations used are shown in table 6.1. The general equation for temperate and boreal forests is based on simple linear regression model using ∼1000 plots located in US, Asia, and Europe (S. Saatchi, personal communication, data from S. Brown). North America equations are calculated using FIA plot data by fitting BGB to AGB using linear regression with intercept set at 0 for deciduous, evergreen, mixed, and flooded forests (A. Fore, personal communication). Tropical forest relationship is from Saatchi et al. [2011b]. General equation for shrubs and savannas are based on Mokany et al. [2006]. For Africa, shrub and savanna equations are from Ryan et al. [2011]. When calculating BGB, if an equation for a specific region exist, then that equation is used. If no regional equation exist, then the default equation for the given landcover type is used (shown in bold in the table). GlobCover landcover classification is used to determine which equation to apply.

6.2 National and Biome Level Comparison

It is difficult to compare the model output with field plots at the pixel level due to the mismatch in size. A typical ground plot, such as from the FIA, is less than 0.1 ha while one pixel is roughly 100 ha, which is 3 orders of magnitude larger. Any heterogeneity in the AGB within the pixel will cause mismatch between field value and model predicted value even if both are correct. Instead, the model predicted carbon stock using $0.5(\mathrm{AGB} + \mathrm{BGB})$ is compared with national and biome levels as independent validation.

In order to only select national inventories that are relatively reliable, 26 of the 35 nations listed under the International Monetary Fund's "advanced economies", excluding ones that do not have appreciable forest area, are selected to compare the reported national carbon stocks with those calculated from model prediction. The national reports are from the Food and Agriculture Organization (FAO) of

the United Nations' 2010 report[Food and Agriculture Orgnization, 2010]. This comparison is shown in figure 6.1. When comparing the reported total carbon stock directly with the model predicted total stock, the correlation is high but there are some discrepancies in the larger countries where the difference should be smaller. This is due to the difference in estimation of forest area between the reported inventory and remote sensing based estimates.

In conducting field inventory, since the area of coverage is sparse, the goal is to design a good sampling scheme such as that of the US FIA [Bechtold and Patterson, 2005] so that over a large enough area, the samples can approximate the mean carbon density well. To report a national carbon stock, this mean value is then multiplied by forest area. In order to correct for this mismatch in forest area, in panel b) of figure 6.1, the national carbon density from the report is used. This value is multiplied by the forest area based on the remote sensing data of this study to create a national total carbon stock value. When scaled by the forest area, the agreement improves significantly with 99.5% of the variance explained at this national level. Model estimated total carbon stock for the US is within 0.03% of the FAO reported total. The model estimated total for Canada is higher than reported, which is to be expected due to the fact that Canada's reported values only included "managed forests", which would have lower carbon density than undisturbed forests.

At the biome level, the total carbon stock is calculated for each of the WWF major terrestrial biome on each continent. Their total values are shown in figure 6.2. The tropical moist broadleaf forests of Americas contain the largest carbon stock of any biome at 70.5 PgC aboveground and 19.2 PgC belowground. The next highest biome, tropical broadleaf forests of Asia, is approximately half of that with 35.5 PgC aboveground and 9.49 PgC belowground. The taiga forests of Eurasia comes in third at 29.9 PgC aboveground and 7.89 PgC belowground. Even though this biome has relatively lower carbon density, the large extend of

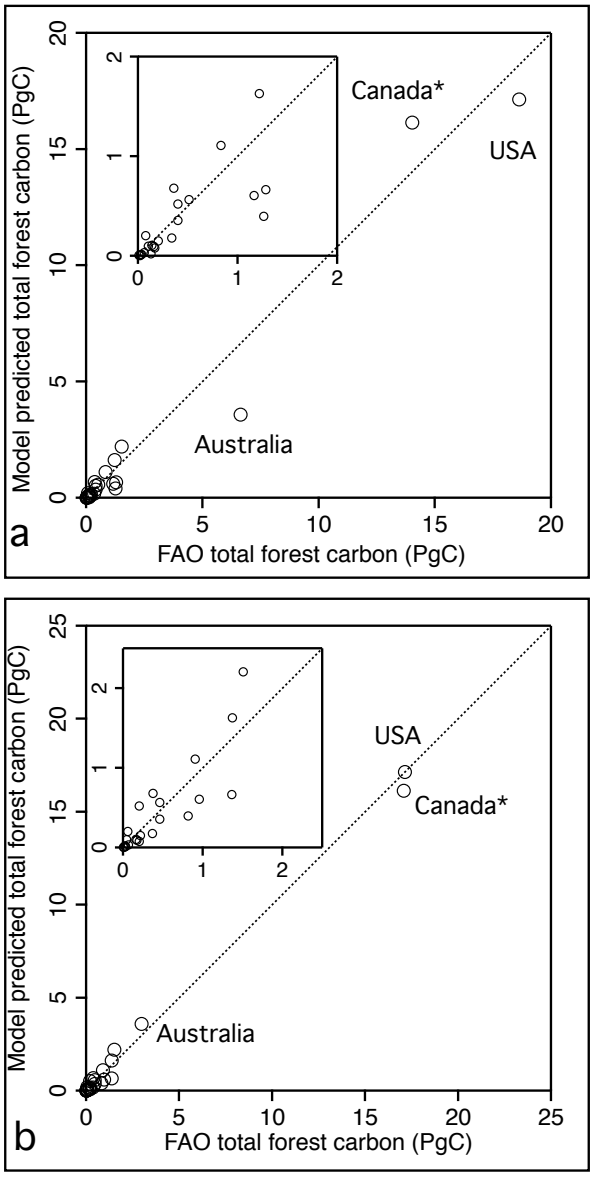

Figure 6.1: Comparison of model predicted national forest carbon stock (AGB + BGB) with reported forest stock in the FAO 2010 report [Food and Agriculture Orgnization, 2010], table 11, 2005 column. One-to-one line is drawn in. a) National carbon stock from the report is directly compared with model calculated total. b) Mean reported carbon density is used to calculate total using forest area based on remote sensing data in this study. Inset is an expanded view of the lower carbon ranges. ∗Canada report only includes "managed" forests.

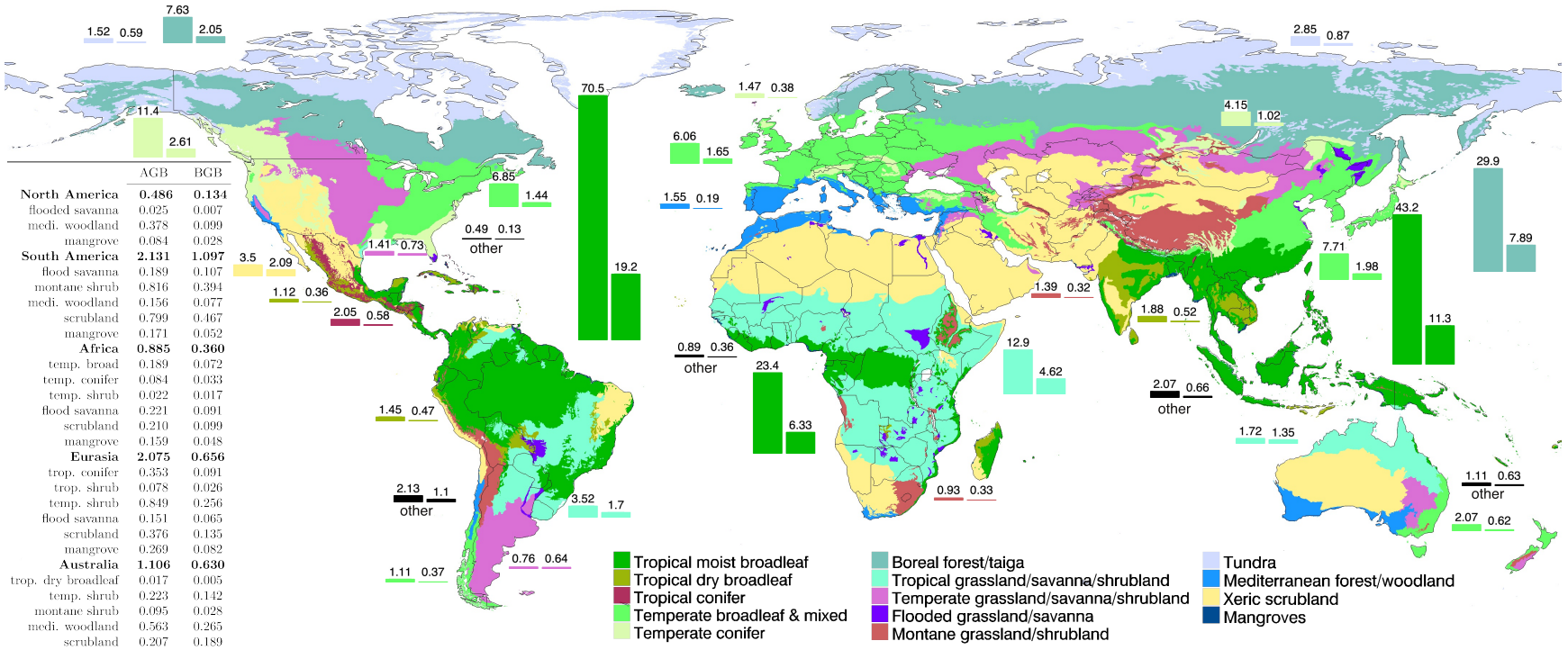

	AGB	BGB
North America	**0.486**	**0.134**
flooded savanna	0.025	0.007
medi. woodland	0.378	0.099
mangrove	0.084	0.028
South America	**2.131**	**1.097**
flood savanna	0.189	0.107
montane shrub	0.816	0.394
medi. woodland	0.156	0.077
scrubland	0.799	0.467
mangrove	0.171	0.052
Africa	**0.885**	**0.360**
temp. broad	0.189	0.072
temp. conifer	0.084	0.033
temp. shrub	0.022	0.017
flood savanna	0.221	0.091
scrubland	0.210	0.099
mangrove	0.159	0.048
Eurasia	**2.075**	**0.656**
trop. conifer	0.353	0.091
trop. shrub	0.078	0.026
temp. shrub	0.849	0.256
flood savanna	0.151	0.065
scrubland	0.376	0.135
mangrove	0.269	0.082
Australia	**1.106**	**0.630**
trop. dry broadleaf	0.017	0.005
temp. shrub	0.223	0.142
montane shrub	0.095	0.028
medi. woodland	0.563	0.265
scrubland	0.207	0.189

Figure 6.2: Aboveground and belowground carbon stock of live woody vegetation in the world's biomes. Biomes with very small carbon totals are shown in the table with their total for each continent shown as "other" with black bars.

forest cover makes the total carbon stored in this biome significant. The tropical broadleaf forest and savannas of Africa comes in third and fourth. In the global boreal forests, the model estimation of total aboveground carbon from this study is also compared with recently published results by Neigh et al. [2013]. Neigh et al. [2013] estimates the total aboveground carbon in the boreal biome globally to be 38 PgC. The model estimate from this study puts the boreal biome total aboveground carbon at 37.5 PgC, 2% less than Neigh's estimate, but well within their margin of error of 3.1 PgC.

The distribution of carbon is also calculated using GlobCover classes and latitude bands, shown in figure 6.3. Roughly half of the total global carbon in live woody vegetation is contained in the broadleaf evergreen forests. Needleleaf forests contains just under a quarter, while shrubland also contain a significant amount of the global live carbon stock at 11.7%. Latitudinally, over 65% (212 PgC) is located in the tropics (30°N - 30°S), 26% (85 PgC) in the mid-latitudes (30-60 latitude), and 9% (29PgC) in the polar regions (>60° latitude). The total global carbon stock in live woody vegetation is estimated at 337 PgC, with 311.4 PgC being in the forests. This is within 3% of the reported global forest carbon number (302.8 PgC for the year 2005) in the United Nations Food and Agriculture Organization's (FAO) Forest Resources Assessment 2010 (FRA 2010)[Food and Agriculture Orgnization, 2010, table 2.19]. The reported biomass value is used with conversion factor of 0.5 instead of the reported total carbon stock number because for that value (288.8 PgC), different countries used different conversion factors ranging from 0.47 to 0.5. By using total biomass and a conversion factor of 0.5, it is consistent with the conversion factor used in this dissertation.

National carbon inventories are also calculated using political boundaries from Esri's (*www.esri.com*) world boundaries 2010 edition. As demonstrated earlier, a big factor in discrepancy between inventories is the disagreement in forest area. Taking this factor into account, carbon stock numbers are calculated using Glob-

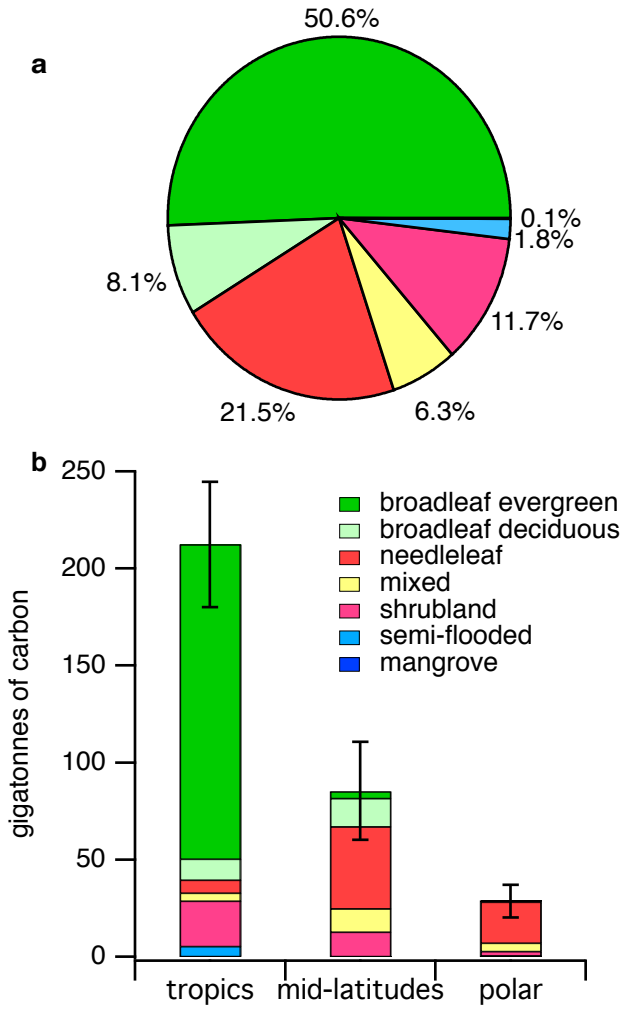

Figure 6.3: Global distribution of carbon stock (AGB + BGB) divided by a) GlobCover classes and b) latitude bands. Tropics here is between 30°N and 30°S. Mid-latitudes is between 30° and 60°. Polar is above 60°.

Cover, and MODIS vegetation continuous field (VCF) [DiMiceli et al., 2011] values of 10%, 25%, and 30% forest cover. MODIS VCF value of 10% comes closest to the forest definition in FRA 2010. The national inventory values are included in tables 6.2 - 6.8.

Table 6.2: National inventory of total live carbon (AGB+BGB) in woody vegetation. Calculation is performed using political boundaries from Esri (*www.esri.com*) world boundaries 2010 edition. All carbon numbers are in units of million tonnes of carbon (TgC). All area numbers are in units of million hectares. MODIS columns use VCF as thresholds.

	GlobCover						MODIS					
	forest		shrub/savanna		total		VCF 10%		VCF 25%		VCF 30%	
Country	carbon	area	carbon	area	carbon	area	carbon	area	carbon	area	carbon	area
Afghanistan	47.072	0.1370	5.8803	0.3112	52.952	0.4482	45.336	0.1483	31.674	0.1022	25.649	0.0831
Albania	31.115	0.5610	3.4228	0.1023	34.538	0.6633	33.756	0.6364	23.788	0.4002	19.241	0.3076
Algeria	19.477	0.2561	57.756	1.4161	77.233	1.6723	47.060	0.6978	28.435	0.3817	24.678	0.3228
American Samoa	0.0049	0.0004	–	–	0.0049	0.0004	0.0049	0.0004	0.0049	0.0004	0.0049	0.0004
Andorra	1.7454	0.0186	–	–	1.7454	0.0186	1.7454	0.0186	1.7198	0.0183	1.6628	0.0174
Angola	1618.9	65.384	642.02	29.182	2260.9	94.566	1811.4	68.017	1126.5	34.170	964.05	27.219
Anguilla	–	–	0.0008	0.0001	0.0008	0.0001	–	–	–	–	–	–
Antigua and Barbuda	1.0637	0.0179	0.0022	0.0003	1.0660	0.0182	1.0629	0.0180	1.0384	0.0171	1.0184	0.0165
Argentina	999.89	29.673	2262.1	108.36	3262.0	138.03	1489.0	57.453	874.15	22.867	763.93	17.454
Armenia	22.157	0.4508	3.3778	0.1467	25.535	0.5974	20.600	0.3836	15.727	0.2569	14.214	0.2268
Aruba	–	–	0.0094	0.0003	0.0094	0.0003	–	–	–	–	–	–
Australia	3584.9	69.140	3620.1	173.14	7205.0	242.28	4065.5	92.849	2779.0	43.250	2569.8	37.164
Austria	355.24	4.4634	4.6365	0.1307	359.88	4.5941	359.46	4.5867	349.50	4.3755	340.71	4.1987
Azerbaijan	47.081	0.8718	21.177	0.8738	68.258	1.7456	49.079	0.9353	40.365	0.6869	37.371	0.6083
Bahamas	4.6635	0.1519	0.9944	0.0893	5.6579	0.2412	5.3456	0.2101	4.1319	0.1298	3.6087	0.1060
Bahrain	–	–	0.0025	0.0003	0.0025	0.0003	–	–	–	–	–	–
Bangladesh	61.877	0.9524	49.353	0.8066	111.23	1.7590	111.02	1.7497	105.72	1.5473	102.87	1.4418
Barbados	0.7872	0.0140	–	–	0.7872	0.0140	0.6862	0.0118	0.3212	0.0043	0.3047	0.0039
Belarus	336.65	9.2550	3.6683	0.2722	340.31	9.5272	339.45	9.4543	327.34	8.5839	317.26	7.9821
Belgium	33.663	0.7013	0.8916	0.0312	34.554	0.7325	34.542	0.7320	33.463	0.6873	32.374	0.6457
Belize	197.07	1.9096	0.9196	0.0567	197.99	1.9663	197.85	1.9581	195.24	1.8421	193.45	1.7753
Benin	52.710	3.3337	64.851	5.3660	117.56	8.6997	35.964	2.2942	0.1360	0.0039	0.0613	0.0013
Bhutan	485.39	2.8961	7.8038	0.0686	493.19	2.9647	490.75	2.9461	482.02	2.8839	476.14	2.8404
Bolivia	5068.3	62.590	428.82	13.029	5497.1	75.620	5130.1	65.322	4935.1	57.020	4838.1	53.495
Bosnia and Herzegovina	131.20	2.0736	14.878	0.3345	146.07	2.4081	146.07	2.4079	145.00	2.3691	143.06	2.3092
Botswana	4.6282	0.4197	47.136	4.3250	51.764	4.7447	12.000	1.1712	0.6953	0.0718	0.2066	0.0208
Brazil	47917	429.14	3108.7	123.91	51026	553.05	50095	499.64	47694	417.22	46964	399.74
Brunei Darussalam	78.562	0.5231	0.0495	0.0007	78.611	0.5238	78.610	0.5236	78.587	0.5224	78.492	0.5188
Bulgaria	244.19	4.5115	5.2998	0.1499	249.49	4.6614	242.19	4.3952	222.67	3.7797	213.96	3.5285
Burkina Faso	4.4957	0.4224	47.806	5.4263	52.302	5.8487	1.9948	0.1966	–	–	–	–
Burundi	57.978	1.4559	5.6503	0.1643	63.628	1.6202	25.443	0.5556	8.7580	0.1096	7.0025	0.0790
Cambodia	625.75	5.3204	200.49	2.8785	826.24	8.1989	825.62	8.1755	795.47	7.3011	768.71	6.6524
Cameroon	3893.9	33.762	160.05	7.4312	4054.0	41.193	3987.3	37.189	3472.6	23.368	3327.3	21.755
Canada	16138	377.80	964.41	59.362	17102	437.16	16742	419.99	15219	346.77	14323	309.72
Cape Verde	0.0059	0.0005	–	–	0.0059	0.0005	0.0020	0.0002	–	–	–	–

Table 6.3: National inventory of total live carbon (AGB+BGB) in woody vegetation. Continued - part 2

	GlobCover						MODIS					
	forest		shrub/savanna		total		VCF 10%		VCF 25%		VCF 30%	
Country	carbon	area	carbon	area	carbon	area	carbon	area	carbon	area	carbon	area
Cayman Islands	0.1962	0.0058	0.0102	0.0004	0.2063	0.0062	0.1966	0.0058	0.1380	0.0039	0.1066	0.0031
Central African Republic	1699.3	37.808	574.62	22.155	2273.9	59.963	2160.9	53.225	1129.4	13.904	978.17	10.445
Chad	55.657	4.9663	168.14	18.957	223.79	23.923	61.004	5.5237	0.5197	0.0392	0.1929	0.0146
Chile	931.57	14.928	674.98	16.874	1606.5	31.802	1325.3	25.055	1134.0	19.121	1078.4	17.657
China	12686	122.51	1839.9	31.881	14526	154.39	14160	149.48	13278	133.00	12761	124.90
Christmas Island	0.1231	0.0022	–	–	0.1231	0.0022	0.1231	0.0022	0.1231	0.0022	0.1231	0.0022
Colombia	9516.8	85.529	157.66	5.1664	9674.5	90.696	9441.2	87.801	8783.0	75.434	8530.7	71.027
Comoros	10.632	0.1294	0.5895	0.0087	11.222	0.1381	11.014	0.1364	9.6759	0.1130	9.1059	0.1037
Congo	2952.2	24.729	239.36	6.6639	3191.5	31.393	3019.9	27.796	2698.9	22.455	2619.9	21.471
Congo DRC	16372	198.12	379.31	11.235	16751	209.36	16581	200.76	15653	165.14	15275	152.91
Costa Rica	370.31	3.8664	1.3509	0.0297	371.66	3.8961	370.62	3.8811	354.06	3.6264	342.25	3.4147
Cote d'Ivoire	1206.6	21.338	113.46	5.8835	1320.0	27.221	1251.7	22.399	793.07	8.1990	700.09	6.6426
Croatia	100.75	1.8261	9.7701	0.2109	110.52	2.0370	110.51	2.0367	109.73	2.0067	108.08	1.9501
Cuba	197.02	2.8647	13.788	0.9424	210.80	3.8072	208.92	3.6255	197.52	2.9303	191.76	2.7093
Cyprus	14.770	0.1207	5.8310	0.1370	20.601	0.2577	17.447	0.1698	5.4628	0.0673	3.2469	0.0428
Czech Republic	178.22	2.8693	1.4887	0.0431	179.70	2.9124	179.65	2.9085	176.85	2.7888	173.41	2.6605
Denmark	13.792	0.4357	1.9216	0.1229	15.714	0.5585	15.140	0.5197	13.331	0.4042	12.566	0.3650
Djibouti	0.0006	0.0001	0.2581	0.0174	0.2588	0.0175	0.0563	0.0032	–	–	–	–
Dominica	6.8115	0.0504	1.4625	0.0161	8.2741	0.0665	7.9595	0.0633	7.5450	0.0596	7.3178	0.0577
Dominican Republic	168.37	2.4039	2.3824	0.0762	170.75	2.4801	170.62	2.4748	162.80	2.2952	155.96	2.1393
Ecuador	2103.4	17.996	84.437	1.8927	2187.8	19.889	2100.2	18.277	1879.8	14.646	1816.7	13.775
Egypt	–	–	0.8164	0.0629	0.8164	0.0629	0.0578	0.0069	–	–	–	–
El Salvador	37.977	0.4260	1.9024	0.0522	39.880	0.4782	39.787	0.4743	38.828	0.4483	37.917	0.4308
Equatorial Guinea	439.78	2.6403	0.0568	0.0012	439.84	2.6415	433.09	2.5819	425.94	2.5204	421.01	2.4798
Eritrea	0.0054	0.0003	19.124	1.1821	19.130	1.1823	2.2045	0.1140	–	–	–	–
Estonia	78.892	2.7111	3.3908	0.2117	82.283	2.9228	82.213	2.9168	79.582	2.6997	76.617	2.4864
Ethiopia	457.41	8.6193	699.68	39.656	1157.1	48.275	804.15	23.596	333.54	4.5187	305.15	4.0320
Falkland Islands (Malvinas)	3.9981	0.1493	9.8345	0.5429	13.833	0.6922	10.123	0.4611	2.5752	0.0955	1.7120	0.0606
Faroe Islands	0.1571	0.0017	0.5924	0.0276	0.7495	0.0294	0.6154	0.0230	0.1359	0.0035	0.0520	0.0009
Fiji	40.814	0.3553	1.0157	0.0143	41.830	0.3696	41.703	0.3684	41.591	0.3659	41.447	0.3634
Finland	1109.7	24.088	23.204	0.8891	1132.9	24.977	1129.3	24.866	1077.0	23.228	1017.4	21.511
France	605.65	12.882	12.133	0.3421	617.79	13.224	617.11	13.192	584.96	11.653	558.65	10.698
French Guiana	1489.9	8.2074	1.2357	0.0216	1491.2	8.2290	1491.1	8.2251	1487.8	8.1752	1479.8	8.1184

Table 6.4: National inventory of total live carbon (AGB+BGB) in woody vegetation. Continued - part 3

	GlobCover						MODIS					
	forest		shrub/savanna		total		VCF 10%		VCF 25%		VCF 30%	
Country	carbon	area	carbon	area	carbon	area	carbon	area	carbon	area	carbon	area
Gabon	4129.7	23.794	65.047	1.1397	4194.8	24.933	4174.2	24.609	4092.0	23.571	4028.1	23.061
Gambia	2.0058	0.1813	1.4537	0.1664	3.4595	0.3477	1.1806	0.1084	0.0448	0.0039	0.0071	0.0006
Georgia	169.47	2.7026	10.581	0.2957	180.05	2.9983	174.27	2.7588	165.77	2.4930	160.41	2.3661
Germany	665.07	11.776	11.759	0.4589	676.83	12.235	676.53	12.217	654.10	11.302	634.57	10.627
Ghana	554.01	11.055	108.87	7.8148	662.88	18.869	535.83	8.6938	261.24	2.7692	212.14	2.1690
Gibraltar	–	–	0.0026	0.0002	0.0026	0.0002	0.0026	0.0002	–	–	–	–
Greece	195.35	2.8536	62.967	1.0504	258.32	3.9040	250.64	3.7112	214.62	3.0254	196.11	2.6962
Greenland	–	–	25.229	1.5097	25.229	1.5097	5.1185	0.3190	0.4784	0.0264	0.1381	0.0077
Grenada	2.6161	0.0264	–	–	2.6161	0.0264	2.6161	0.0264	2.4604	0.0245	2.3081	0.0225
Guadeloupe	9.2537	0.1000	0.0100	0.0002	9.2637	0.1002	9.2560	0.0999	8.7772	0.0902	8.2885	0.0806
Guam	0.0140	0.0009	–	–	0.0140	0.0009	0.0140	0.0009	0.0126	0.0008	0.0098	0.0006
Guatemala	664.44	7.3336	46.928	1.1422	711.37	8.4758	708.69	8.4067	673.53	7.6341	646.34	7.1328
Guernsey	0.0022	0.0001	–	–	0.0022	0.0001	0.0022	0.0001	–	–	–	–
Guinea	489.28	12.587	216.46	7.9371	705.74	20.525	643.49	16.536	162.63	2.4387	110.98	1.4532
Guinea-Bissau	43.181	1.8565	8.5538	0.4220	51.734	2.2786	46.787	1.9369	8.1906	0.2819	3.0853	0.1345
Guyana	3026.5	19.379	13.882	1.1174	3040.4	20.496	3031.5	19.846	3009.6	19.064	2986.2	18.790
Haiti	23.616	0.3830	0.3482	0.0125	23.964	0.3955	23.937	0.3943	23.073	0.3726	22.075	0.3512
Honduras	649.19	7.5199	12.262	0.4073	661.45	7.9273	661.10	7.9043	637.91	7.2100	614.03	6.6870
Hungary	69.308	1.4854	1.2238	0.0337	70.532	1.5192	70.074	1.4815	67.795	1.3908	65.783	1.3138
Iceland	–	–	38.264	2.2609	38.264	2.2609	24.246	1.3408	5.0053	0.2234	2.1993	0.0892
India	3654.9	32.877	647.97	10.551	4302.9	43.428	3999.8	37.688	3602.2	30.099	3411.2	27.093
Indonesia	21901	155.87	70.372	2.5602	21971	158.44	21672	156.77	21142	149.22	20689	143.83
Iran Islamic Republic of	152.10	1.8255	93.531	4.2453	245.63	6.0708	155.11	1.9601	140.71	1.7046	135.40	1.6153
Iraq	0.6918	0.0189	14.556	0.6942	15.247	0.7131	2.6360	0.0907	0.0572	0.0021	–	–
Ireland	3.6250	0.0819	33.152	1.3120	36.777	1.3939	35.641	1.3339	24.641	0.7943	20.965	0.6353
Israel	0.0996	0.0015	1.3001	0.0326	1.3997	0.0342	0.7012	0.0116	0.1444	0.0020	0.0849	0.0011
Italy	565.21	7.8805	22.457	0.4855	587.66	8.3659	583.69	8.2278	550.31	7.3871	522.49	6.8362
Jamaica	75.967	0.7997	0.0601	0.0039	76.027	0.8036	76.007	0.8024	75.148	0.7839	74.222	0.7657
Japan	2210.9	24.652	1.4003	0.0172	2212.3	24.669	2211.4	24.636	2188.6	23.979	2169.0	23.568
Jordan	–	–	0.1745	0.0076	0.1745	0.0076	–	–	–	–	–	–

Table 6.5: National inventory of total live carbon (AGB+BGB) in woody vegetation. Continued - part 4

	GlobCover						MODIS					
	forest		shrub/savanna		total		VCF 10%		VCF 25%		VCF 30%	
Country	carbon	area	carbon	area	carbon	area	carbon	area	carbon	area	carbon	area
Kazakhstan	124.58	2.4523	21.296	1.0671	145.88	3.5194	137.85	3.0565	114.38	2.1608	101.19	1.7796
Kenya	156.47	5.3382	174.20	14.041	330.67	19.379	166.98	5.1011	77.010	1.5147	68.205	1.2685
Korea DPRK	462.27	6.5592	87.910	1.7038	550.18	8.2630	497.55	7.1395	428.89	5.9265	406.60	5.5457
Korea	412.71	5.6697	71.220	1.1753	483.93	6.8450	469.01	6.5245	429.84	5.8121	410.35	5.4809
Republic of												
Kyrgyzstan	9.9963	0.1777	3.4172	0.1481	13.413	0.3258	12.396	0.2925	6.8624	0.1296	4.7595	0.0799
Laos	1562.7	10.478	648.51	7.3462	2211.2	17.824	2210.9	17.816	2196.0	17.390	2177.3	17.014
Latvia	120.40	4.0720	2.6161	0.1484	123.01	4.2204	122.95	4.2146	118.30	3.8060	113.72	3.4553
Lebanon	0.5995	0.0059	1.9641	0.0445	2.5636	0.0504	1.9557	0.0316	1.1164	0.0137	0.8518	0.0094
Lesotho	6.4108	0.2425	8.5997	0.3310	15.010	0.5735	7.6868	0.2212	0.4059	0.0063	0.1606	0.0024
Liberia	1175.9	8.0934	0.3255	0.0125	1176.3	8.1059	1143.0	7.8368	950.06	6.2054	821.22	5.2768
Libyan Arab	–	–	12.678	0.4523	12.678	0.4523	–	–	–	–	–	–
Jamahiriya												
Liechtenstein	0.8693	0.0094	0.0148	0.0003	0.8841	0.0098	0.8841	0.0098	0.8273	0.0087	0.7857	0.0079
Lithuania	83.254	2.5568	0.3690	0.0191	83.623	2.5758	83.410	2.5587	78.623	2.1878	75.345	1.9712
Luxembourg	4.8974	0.0941	0.0076	0.0002	4.9050	0.0943	4.9025	0.0941	4.5077	0.0830	4.1824	0.0751
Macedonia	48.748	0.9933	2.9774	0.0872	51.725	1.0805	50.063	1.0290	41.585	0.7873	37.051	0.6709
Madagascar	942.69	12.218	557.08	17.789	1499.8	30.007	1167.8	17.256	853.95	8.5724	803.94	7.5513
Malawi	96.142	2.9795	74.911	3.1566	171.05	6.1361	122.54	3.7408	44.548	1.0854	29.908	0.6630
Malaysia	4516.5	29.270	8.3275	0.1444	4524.9	29.415	4518.5	29.346	4464.2	28.595	4412.4	27.951
Mali	11.200	0.8746	134.67	13.856	145.87	14.730	24.495	1.5715	0.0228	0.0006	–	–
Martinique	7.4420	0.0820	0.0015	0.0002	7.4435	0.0822	7.4065	0.0817	6.4401	0.0693	5.9792	0.0629
Mauritania	–	–	16.881	1.7356	16.881	1.7356	0.0448	0.0107	–	–	–	–
Mauritius	0.3224	0.0282	–	–	0.3224	0.0282	0.3204	0.0281	0.2616	0.0229	0.2420	0.0212
Mayotte	2.1048	0.0280	–	–	2.1048	0.0280	2.1048	0.0280	2.0800	0.0272	2.0558	0.0268
Mexico	3978.8	48.350	2641.8	84.880	6620.6	133.23	4670.7	67.182	3418.9	40.344	3074.3	34.990
Micronesia	0.0268	0.0003	–	–	0.0268	0.0003	0.0268	0.0003	0.0268	0.0003	0.0268	0.0003
Moldova	6.6619	0.1529	0.2106	0.0097	6.8725	0.1626	6.8190	0.1590	6.6266	0.1499	6.4510	0.1426
Republic of												
Mongolia	150.33	3.7168	4.6919	0.2827	155.02	3.9995	152.59	3.8910	132.35	3.0284	118.61	2.5155
Montenegro	24.473	0.4006	1.5872	0.0391	26.060	0.4396	26.039	0.4388	25.178	0.4140	23.759	0.3805
Montserrat	0.4638	0.0041	0.0301	0.0009	0.4939	0.0050	0.4612	0.0040	0.4313	0.0033	0.4011	0.0032
Morocco	4.6563	0.0568	61.767	1.8679	66.423	1.9246	26.071	0.4534	8.6252	0.1157	6.2293	0.0819
Mozambique	1135.5	45.854	385.17	15.038	1520.7	60.891	1358.6	51.166	566.29	16.833	348.69	9.5441
Myanmar	3307.5	23.257	1350.3	14.745	4657.8	38.001	4653.8	37.950	4590.6	36.512	4526.8	35.319

Table 6.6: National inventory of total live carbon (AGB+BGB) in woody vegetation. Continued - part 5

	GlobCover						MODIS					
	forest		shrub/savanna		total		VCF 10%		VCF 25%		VCF 30%	
Country	carbon	area	carbon	area	carbon	area	carbon	area	carbon	area	carbon	area
Namibia	1.4741	0.1072	15.917	1.9962	17.392	2.1035	4.4144	0.4108	0.2323	0.0160	0.0711	0.0042
Nepal	423.02	3.6311	28.054	0.4627	451.07	4.0938	448.59	4.0636	405.56	3.5071	374.39	3.1367
Netherlands	12.675	0.3720	1.8803	0.1014	14.555	0.4735	14.554	0.4734	13.662	0.4212	12.941	0.3842
Netherlands Antilles	0.0752	0.0019	0.0415	0.0026	0.1168	0.0045	0.0596	0.0019	0.0030	0.0001	0.0030	0.0001
New Caledonia	77.231	0.8804	1.8877	0.0750	79.119	0.9554	79.083	0.9539	75.105	0.8579	72.354	0.8038
New Zealand	397.61	5.3789	61.309	1.7772	458.91	7.1561	458.85	7.1505	455.79	7.0286	453.19	6.9561
Nicaragua	691.15	7.6215	5.2756	0.1976	696.43	7.8191	695.20	7.7683	656.10	6.8613	628.97	6.2853
Niger	0.0038	0.0003	12.600	1.3708	12.604	1.3711	0.0161	0.0025	–	–	–	–
Nigeria	980.45	19.836	398.07	22.177	1378.5	42.013	904.76	17.722	312.74	3.3598	215.27	2.1152
Niue	0.0020	0.0002	–	–	0.0020	0.0002	0.0020	0.0002	0.0020	0.0002	0.0020	0.0002
Northern Mariana Islands	0.0042	0.0003	–	–	0.0042	0.0003	0.0042	0.0003	0.0042	0.0003	0.0028	0.0002
Norway	679.60	10.057	27.050	0.9374	706.65	10.995	666.97	10.285	560.42	8.2405	523.16	7.5447
Oman	0.0013	0.0002	4.3719	0.3392	4.3732	0.3393	0.0075	0.0003	–	–	–	–
Pakistan	75.375	0.4328	129.98	2.6256	205.35	3.0585	75.278	0.4470	60.705	0.3593	54.506	0.3246
Palau	4.2206	0.0295	0.0668	0.0009	4.2874	0.0303	4.2874	0.0303	4.2758	0.0301	4.2522	0.0299
Palestinian Territory	–	–	0.0036	0.0003	0.0036	0.0003	–	–	–	–	–	–
Palestinian Territory	–	–	0.0614	0.0023	0.0614	0.0023	0.0112	0.0002	–	–	–	–
Panama	736.82	5.4417	11.969	0.1661	748.79	5.6077	718.89	5.3876	619.45	4.5330	580.77	4.2107
Papua New Guinea	6852.0	42.031	16.901	0.6160	6868.9	42.647	6747.5	42.002	6529.2	40.213	6366.4	38.925
Paraguay	503.26	20.373	109.29	5.8207	612.55	26.194	591.93	24.837	397.22	14.209	324.63	10.395
Peru	10682	77.619	717.95	20.354	11400	97.973	10682	79.568	10354	73.836	10233	72.417
Philippines	2501.7	17.491	25.222	0.4730	2527.0	17.964	2491.8	17.729	2287.8	15.974	2173.3	14.933
Poland	431.07	9.3719	1.6521	0.0653	432.73	9.4373	432.37	9.4157	420.85	8.8332	408.98	8.3304
Portugal	94.435	1.4350	76.773	1.7006	171.21	3.1356	132.01	2.2116	86.324	1.3035	73.292	1.0633
Puerto Rico	61.338	0.5959	0.0458	0.0037	61.383	0.5996	61.378	0.5990	58.782	0.5604	55.299	0.5148
Qatar	–	–	0.0113	0.0013	0.0113	0.0013	–	–	–	–	–	–
Reunion	1.0994	0.0963	–	–	1.0994	0.0963	1.0475	0.0918	0.9436	0.0827	0.8819	0.0773
Romania	458.65	6.7910	20.362	0.6849	479.01	7.4760	476.48	7.3634	466.13	6.9824	457.56	6.7091
Russia	42708	863.68	2628.2	113.56	45336	977.24	42078	869.92	32698	590.57	29655	508.67
Rwanda	49.077	0.8832	3.2337	0.1680	52.311	1.0512	36.949	0.6148	15.771	0.1683	14.414	0.1386

Table 6.7: National inventory of total live carbon (AGB+BGB) in woody vegetation. Continued - part 6

	GlobCover						MODIS					
	forest		shrub/savanna		total		VCF 10%		VCF 25%		VCF 30%	
Country	carbon	area	carbon	area	carbon	area	carbon	area	carbon	area	carbon	area
Saint Kitts and Nevis	0.8593	0.0074	–	–	0.8593	0.0074	0.8593	0.0074	0.8593	0.0074	0.8593	0.0074
Saint Lucia	5.2994	0.0488	0.0867	0.0017	5.3861	0.0505	5.3861	0.0505	5.2855	0.0493	5.1075	0.0467
Saint Pierre and Miquelon	0.5176	0.0153	0.0419	0.0009	0.5595	0.0162	0.5595	0.0162	0.4671	0.0099	0.3976	0.0079
Saint Vincent and the Grenadines	3.2199	0.0246	0.0088	0.0002	3.2287	0.0247	2.7584	0.0214	1.9291	0.0143	1.6240	0.0121
Samoa	0.2156	0.0189	–	–	0.2156	0.0189	0.2156	0.0189	0.2156	0.0189	0.2126	0.0186
Sao Tome and Principe	10.938	0.0915	–	–	10.938	0.0915	8.4594	0.0747	6.2781	0.0578	5.2741	0.0495
Saudi Arabia	0.0374	0.0037	5.8102	0.2330	5.8476	0.2367	0.0403	0.0020	–	–	–	–
Senegal	29.815	2.3594	44.616	4.4214	74.431	6.7808	13.418	0.9236	0.1342	0.0110	0.0881	0.0073
Serbia	140.42	2.7372	12.211	0.2696	152.63	3.0068	152.31	2.9896	143.47	2.6784	135.20	2.4373
Seychelles	0.0010	0.0001	0.0013	0.0001	0.0023	0.0002	0.0023	0.0002	0.0010	0.0001	0.0010	0.0001
Sierra Leone	351.41	6.0159	6.6397	0.2153	358.05	6.2312	355.73	6.1731	262.60	4.0595	216.17	3.0291
Singapore	0.4819	0.0047	0.0056	0.0002	0.4875	0.0049	0.4565	0.0046	0.3546	0.0033	0.2196	0.0021
Slovakia	149.81	2.0618	4.1913	0.0938	154.00	2.1556	153.95	2.1518	151.91	2.0799	149.85	2.0163
Slovenia	92.694	1.3588	0.9183	0.0202	93.613	1.3790	93.612	1.3789	93.069	1.3618	91.998	1.3321
Solomon Islands	442.40	2.3940	1.5689	0.0188	443.97	2.4128	442.49	2.4046	438.49	2.3832	435.03	2.3636
Somalia	11.005	0.8396	183.31	16.888	194.31	17.728	8.4545	0.5767	0.7809	0.0174	0.5434	0.0104
South Africa	366.23	15.798	262.43	11.050	628.67	26.848	350.22	12.721	184.80	4.6644	153.89	3.5631
South Georgia and the South Sandwich Islands	–	–	0.0301	0.0016	0.0301	0.0016	0.0092	0.0008	0.0018	0.0002	0.0008	0.0001
Spain	514.92	8.6738	260.29	6.3462	775.21	15.020	649.01	11.458	467.75	7.6953	415.26	6.6129
Sri Lanka	479.57	5.3126	18.021	0.5397	497.60	5.8523	487.06	5.6506	379.24	3.8426	341.20	3.3069
Sudan	270.16	15.055	617.10	64.055	887.25	79.110	529.93	39.316	35.267	0.9977	21.039	0.4627
Suriname	2246.8	14.126	1.0263	0.0724	2247.8	14.198	2247.6	14.181	2241.9	13.975	2234.9	13.876
Swaziland	20.595	0.8528	9.2495	0.2727	29.845	1.1255	17.539	0.6415	6.7409	0.1633	5.0563	0.1120
Sweden	1628.5	31.709	26.293	1.0743	1654.8	32.783	1636.4	32.309	1535.1	29.569	1463.5	27.726
Switzerland	104.46	1.4055	5.6926	0.1484	110.15	1.5539	109.64	1.5467	102.22	1.3874	96.757	1.2799
Syrian Arab Republic	2.3844	0.0344	13.250	0.5397	15.634	0.5741	3.7857	0.0653	2.5241	0.0404	2.2534	0.0356

Table 6.8: National inventory of total live carbon (AGB+BGB) in woody vegetation. Continued - part 7

	GlobCover						MODIS					
	forest		shrub/savanna		total		VCF 10%		VCF 25%		VCF 30%	
Country	carbon	area	carbon	area	carbon	area	carbon	area	carbon	area	carbon	area
Tajikistan	0.8854	0.0027	0.1904	0.0106	1.0757	0.0132	0.1504	0.0009	0.0831	0.0003	0.0541	0.0003
Tanzania	1269.9	40.229	279.54	13.540	1549.4	53.769	1284.8	39.778	540.78	12.250	359.01	7.0750
Thailand	1444.1	12.257	419.64	5.3834	1863.7	17.641	1862.0	17.591	1808.3	16.409	1763.3	15.602
Timor-Leste	41.195	0.3498	0.2270	0.0111	41.422	0.3609	41.338	0.3587	40.858	0.3495	39.746	0.3369
Togo	48.743	1.7595	65.398	3.0081	114.14	4.7676	68.224	1.5701	14.778	0.1730	8.9161	0.0989
Tonga	0.0039	0.0003	–	–	0.0039	0.0003	0.0039	0.0003	0.0039	0.0003	0.0039	0.0003
Trinidad and Tobago	43.202	0.4146	0.0497	0.0027	43.252	0.4173	42.809	0.4037	41.131	0.3658	40.480	0.3539
Tunisia	4.8881	0.0613	3.8417	0.1421	8.7297	0.2034	6.4992	0.0872	5.4362	0.0687	4.9120	0.0609
Turkey	663.42	9.8150	290.49	8.5846	953.91	18.400	796.48	12.480	623.84	9.2905	552.35	8.1133
Turkmenistan	–	–	0.3457	0.0214	0.3457	0.0214	0.0040	0.0003	–	–	–	–
Turks and Caicos Islands	0.0177	0.0005	0.0025	0.0002	0.0202	0.0007	0.0202	0.0007	0.0195	0.0006	0.0195	0.0006
Uganda	156.26	4.9435	101.41	5.7430	257.68	10.686	215.05	8.0346	108.75	2.7718	97.577	2.3194
Ukraine	365.94	8.1028	11.378	0.5674	377.32	8.6701	373.57	8.4260	362.53	7.8356	353.95	7.4214
United Arab Emirates	–	–	0.0151	0.0013	0.0151	0.0013	–	–	–	–	–	–
United Kingdom	21.976	0.4761	151.59	6.2413	173.57	6.7174	165.49	6.2321	105.42	3.2391	87.652	2.4986
United Kingdom	0.0357	0.0011	0.4505	0.0120	0.4862	0.0131	0.4862	0.0131	0.4347	0.0111	0.4108	0.0104
United States	17145	277.94	5810.7	212.08	22955	490.02	17546	303.33	15601	244.25	14714	221.74
Uruguay	15.182	0.4452	58.044	2.6840	73.226	3.1292	68.507	2.8333	33.111	0.9524	26.946	0.7187
Uzbekistan	0.3124	0.0094	0.2829	0.0142	0.5953	0.0236	0.2709	0.0083	0.0999	0.0027	0.0257	0.0009
Vanuatu	38.349	0.4656	0.0086	0.0003	38.358	0.4660	38.307	0.4653	38.001	0.4605	37.816	0.4580
Venezuela	6276.7	55.807	92.966	4.8908	6369.7	60.698	6321.0	58.562	6115.5	52.477	6015.7	50.268
Viet Nam	1024.3	7.5948	419.77	5.5052	1444.1	13.100	1441.4	13.028	1400.7	12.026	1368.6	11.441
Virgin Islands British	0.4922	0.0042	0.0011	0.0001	0.4933	0.0043	0.4933	0.0043	0.4922	0.0042	0.4922	0.0042
Virgin Islands U.S.	0.9081	0.0094	–	–	0.9081	0.0094	0.9081	0.0094	0.8972	0.0091	0.8826	0.0088
Wallis and Futuna	0.0127	0.0011	–	–	0.0127	0.0011	0.0127	0.0011	0.0127	0.0011	0.0127	0.0011
Yemen	0.2602	0.0270	26.558	1.2117	26.819	1.2387	1.9199	0.0866	–	–	–	–
Zambia	749.77	32.398	537.73	23.106	1287.5	55.504	1195.5	49.642	548.38	21.033	379.25	14.228

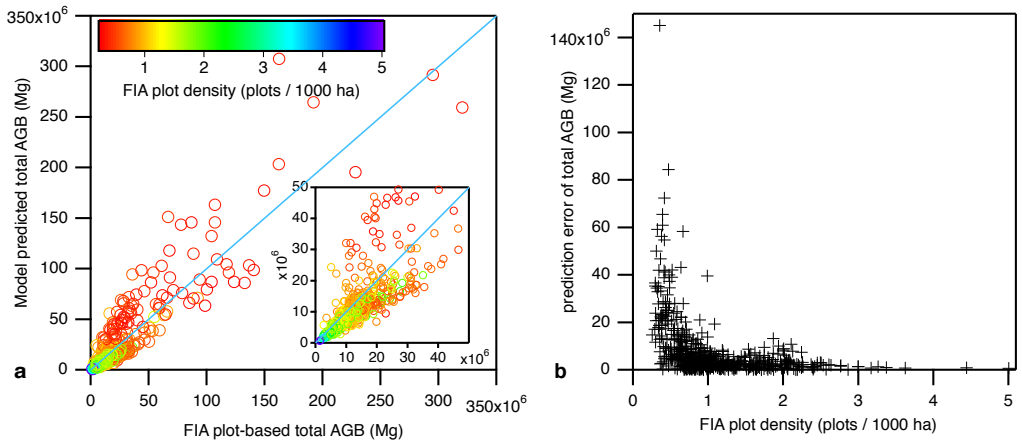

Figure 6.4: US county-level comparison between FIA inventory and model estimated total carbon stock (AGB+BGB). Inset enlarges the lower carbon ranges of the plot. a) Scatterplot of total carbon values. Coloring shows the density of FIA plots within the given county, in terms of number of plots per 1000 ha. b) Prediction error, absolute value of predicted total carbon minus FIA plot-based total carbon, at the county level as a function of FIA plot density within the county.

6.3 US County Level Comparison

The model estimations of carbon stock is also compared with field-based inventory at smaller scales - US county level. Again, to remove the discrepancy due to forest area differences, US county level mean carbon density is first calculated by averaging all the plot-level biomass values in that county, then scaling this by the forested area of the county based on remote sensing data used in this study (Figure 6.4), and finally converting to carbon using a factor of 0.5. Only counties with a minimum of 100 plots are included. This leaves 564 counties located in the contiguous 48 states, ranging in forested area from 20,000 ha to 1.66 million ha. On the county level in the US, our model prediction has R^2 value of 0.83 with an average positive bias of 1.63 Mg/ha. However, figure 6.4 shows that part of this

error comes from under-sampling with the field inventory. Panel a) shows that the counties with higher density of FIA plots tend to be much better correlated with model estimates of carbon total, while panel b) clearly demonstrates the decrease in prediction error as FIA plot density in the county increases.

6.4 Tropics comparison

The tropical forests are the most difficult to validate due to the lack of reliable field inventory data. Unlike the national level and county level comparisons in the previous sections, reported inventory for the tropics are not as reliable[Brown et al., 1989, Gibbs et al., 2007, Saatchi et al., 2011b]. For the comparison here, 3660 geo-referenced field plots across the pan-tropics are compiled (Sandra Brown, Nancy Harris, personal communication). The aboveground biomass values of these plots are compared with the model estimated aboveground biomass at the same location.

The main issue with this approach is the mis-match between the size of the field plot and the size of the model output pixel. Saatchi et al. [2011a] demonstrated that in tropical forests, plot-measured AGB values can have coefficient of variation from 30% to almost 100% within the same forest stand when the plot size is 0.1 ha or less. To reduce the effect of forest heterogeneity, the 3660 plots are checked against the 1km grid, and plots that fall within the same pixel have their AGB values averaged. All grids that do not have at least 5 plots are dropped. After this step, 52 averaged AGB values remain. These 52 averaged AGB values are plotted again the model estimated AGB values for the same location in figure 6.5, with 2 outlier points removed (50 points remaining).

The field plots show moderate correlation between model estimated AGB values and plot-based average AGB values ($R^2 = 0.323$). Given the correlation shown in section 6.3 between model prediction errors and sampling density even at the

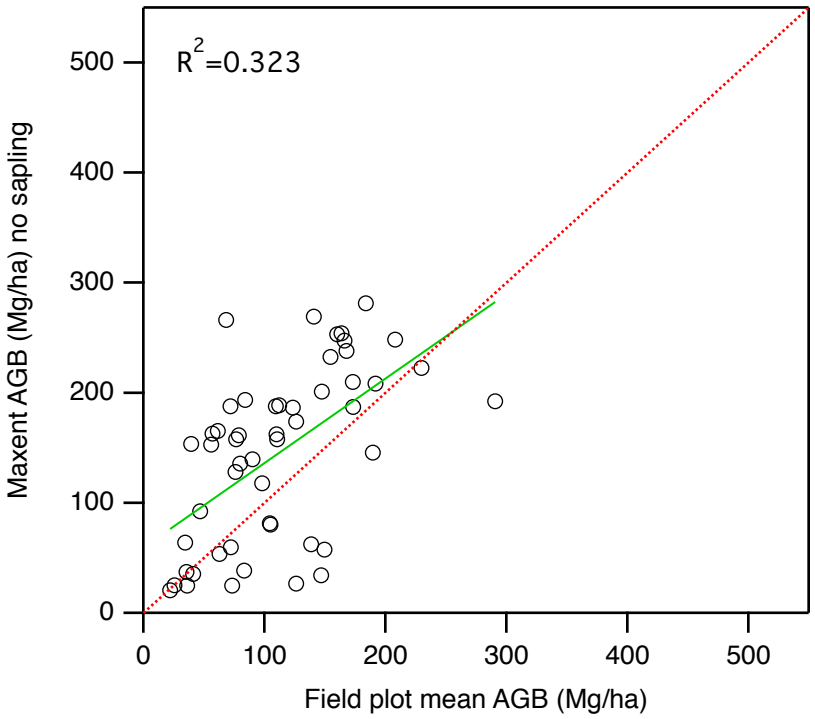

Figure 6.5: Comparison between model estimated pixel-level AGB density and field-measured AGB density for the same locations by average a minimum of 5 field plots where 5 or more are available. Two outlier locations were removed. One-to-one line is drawn in red, a simple linear regression fit line is shown in green, with R^2 value of 0.323

much larger county level, it is likely that a significant portion of the prediction error seen here is due to forest heterogeneity at the smaller field plot scales.

CHAPTER 7

Summary and Discussion

In this dissertation, I have shown the various pieces of the puzzle required to construct the first global spatially explicit biomass map. Chapter 3 showed the processing of the remote sensing data that is required to make them useable, such as the removal of cloud-cover effects from optical data and the size scaling of land-cover map. Next, in chapter 4, GLAS data from IceSAT were used to create global samples of AGB through the use of regional allometric equations developed from field inventory data. The use of regional allometric equations is important to reduce regional biases due to errors in allometry. With the set of global AGB samples, the prediction of global AGB distribution was then performed using the Maximum Entropy method.

Chapter 5 detailed the steps required in using the MaxEnt model. The globe was first divided into continents, then further divided by GlobCover landcover type. Each landcover type or a combination of several types was used as one domain for the MaxEnt model. AGB samples within the domain were divided into bins and each bin was modeled independently using MaxEnt. This was due to the binomial design of the model that required interpreting the final output by combining the probabilities to create an expectation value of AGB which is the model prediction.

Prior probability was introduced to take advantage of the prior information from the GLAS samples, with the Amazon region further divided into sub-regions with local prior distributions using a soil map for division. Tropical regions had

issues with cloud cover and required using MODIS NDVI to identify possibly misclassified pixels.

After the model estimation of aboveground biomass, model uncertainty is calculated at the pixel level to augment the AGB product with a spatially explicit model uncertainty map. Sapling biomass was accounted for using developed relationships. Belowground biomass was then calculated from the AGB (including sapling) using a compilation of root:shoot equations from existing literature.

Finally, the carbon stocks are calculated from the AGB and BGB estimates, with analyses performed on the national and biome levels. The spatial patterns allowed us to see the carbon distributions across the various biomes of the globe as well as latitude ranges. The national carbon stock tables also provided a new reference for inventory reporting, especially for countries that do not have a well developed forestry program. The model estimates compared very well with national inventories from countries with relatively reliable forest inventory programs, which are in the temperate zones. Globally, the total carbon stock in live biomass of forests is estimated to be 311.4 PgC for the year 2005 compared with 302.8 PgC (also for 2005) based on the FAO Forest Resources Assessment report (FRA 2010). The shrubland and savanna biomes add another 25.6 PgC for a total global carbon in live woody vegetation of 337 PgC.

The products created as a part of this dissertation will hopefully help in the efforts to reduce uncertainties in the terrestrial carbon cycle by providing better estimates of carbon emissions due to land-use change and forest regrowth. It can also serve as a reference for nations who do not have an extensive forest inventory program.

References

F Achard, H.D. Eva, H.J. Stibig, P Mayaux, J. Gallego, T. Richards, and J.P. Malingreau. Determination of deforestation rates of the world's humid tropical forests. *Science*, 297(5583):999, 2002.

R Aerts, RGA Boot, and PJM Van der Aart. The relation between above-and belowground biomass allocation patterns and competitive ability. *Oecologia*, 87 (4):551–559, 1991.

Steve Archer, David S Schimel, and Elisabeth A Holland. Mechanisms of shrubland expansion: land use, climate or CO2? *Climatic change*, 29(1):91–99, 1995.

Olivier Arino, Patrice Bicheron, Frederic Achard, John Latham, Ron Witt, and Jean-Louis Weber. GLOBCOVER The most detailed portrait of Earth. *ESA Bulletin-European Space Agency*, (136):24–31, November 2008.

Gregory P Asner, David E Knapp, Eben N Broadbent, Paulo JC Oliveira, Michael Keller, and Jose N Silva. Selective logging in the Brazilian Amazon. *Science*, 310(5747):480–482, 2005.

A Baccini, N Laporte, S J Goetz, M Sun, and H Dong. A first map of tropical africa's above-ground biomass derived from satellite imagery. *Environmental Research Letters*, 3(4):045011, 2008.

A Baccini, S J Goetz, W.S. Walker, N T Laporte, M Sun, D Sulla-Menashe, J Hackler, P S A Beck, R Dubayah, M.A. Friedl, S Samanta, and R A Houghton. Estimted carbon dioxide emissions from tropical deforestation improved by carbon-density maps. *Nature Climate Change*, 2(1):1–4, January 2012.

Timothy R Baker, Oliver L Phillips, Yadvinder Malhi, Samuel Almeida, Luzmila Arroyo, Anthony Di Fiore, Terry Erwin, Timothy J Killeen, Susan G Laurance,

and William F Laurance. Variation in wood density determines spatial patterns in amazonian forest biomass. *Global Change Biology*, 10(5):545–562, 2004.

A P Ballantyne, C B Alden, J B Miller, P P Tans, and JWC White. Increase in observed net carbon dioxide uptake by land and oceans during the past 50 years. *NATURE-LONDON-*, 488(7409):70–72, 2012.

Christopher Baraloto, Suzanne Rabaud, Quentin Molto, Lilian Blanc, Claire Fortunel, Bruno Herault, Nallaret Davila, Italo Mesones, Marcos Rios, Elvis Valderrama, and Paul V A Fine. Disentangling stand and environmental correlates of aboveground biomass in amazonian forests. *Global Change Biology*, 17(8): 2677–2688, May 2011.

William A Bechtold and Paul L Patterson. The enhanced forest inventory and analysis program: national sampling design and estimation procedures. Technical Report SRS-80, United States Department of Agriculture, 2005.

Patrice Bicheron, Pierre Defourny, C Brockmann, L Schouten, C Vancutsem, M Huc, S Bontemps, M Leroy, Frederic Achard, M Herold, F Ranera, and Olivier Arino. GLOBCOVER Products Description and Validation Report. Technical report, April 2008.

Daniel B Botkin and Lloyd G Simpson. Biomass of the North American boreal forest: A step toward accurate global measures. *Biogeochemistry*, pages 161–174, 1990.

Sandra Brown, Andrew J R Gillespie, and Ariel E Lugo. Biomass estimation methods for tropical forests with applications to forest inventory data. In *Forest Science*, pages 881–902. Society of American Foresters, 1989.

Richard T Busing and Takao Fujimori. Biomass, production and woody detritus in an old coast redwood (Sequoia sempervirens) forest. *Plant Ecology*, 177(2): 177–188, April 2005.

Josep G Canadell, Corinne Le Quéré, Michael R Raupach, Christopher B Field, Erik T Buitenhuis, Philippe Ciais, Thomas J Conway, Nathan P Gillett, R A Houghton, and Gregg Marland. Contributions to accelerating atmospheric co2 growth from economic activity, carbon intensity, and efficiency of natural sinks. *Proceedings of the National Academy of Sciences*, 104(47):18866–18870, 2007.

TN Carlson and DA Ripley. On the relation between ndvi, fractional vegetation cover, and leaf area index. *Remote Sensing Of Environment*, 62(3):241–252, 1997.

J Chave, C Andalo, S Brown, M A Cairns, J Q Chambers, D Eamus, H Fölster, F Fromard, N Higuchi, T Kira, J P Lescure, B W Nelson, H Ogawa, H Puig, B Riéra, and T Yamakura. Tree allometry and improved estimation of carbon stocks and balance in tropical forests. *Oecologia*, 145(1):87–99, June 2005.

R T Corlett and R B Primack. Tropical rainforests and the need for cross-continental comparisons. *Trends in Ecology & Evolution*, 21(2):104–110, 2006.

Peter R. Dallman. *Plant life in the world's mediterranean climates : California, Chile, South Africa, Australia, and the Mediterranean Basin.* University of California Press, 1998.

Eric A Davidson and Ivan A Janssens. Temperature sensitivity of soil carbon decomposition and feedbacks to climate change. *Nature*, 440(7081):165–173, March 2006.

C.M. DiMiceli, M.L. Carroll, R.A. Sohlberg, C. Huang, M.C. Hansen, and J.R.G. Townshend. Annual global automated modis vegetation continuous fields (mod44b) at 250 m spatial resolution for data years beginning day 65, 2000 - 2010, collection 5 percent tree cover, 2011.

Jinwei Dong, Xiangming Xiao, Sage Sheldon, Chandrashekhar Biradar, Nguyen Dinh Duong, and Manzul Hazarika. A comparison of forest cover maps

in mainland southeast asia from multiple sources: Palsar, meris, modis and fra. *Remote Sensing Of Environment*, 127(C):60–73, December 2012.

David S Early and David G Long. Image reconstruction and enhanced resolution imaging from irregular samples. *Geoscience and Remote Sensing, IEEE Transactions on*, 39(2):291–302, 2001.

Jane Elith, Steven J Phillips, Trevor Hastie, Miroslav Dudík, Yung En Chee, and Colin J Yates. A statistical explanation of maxent for ecologists. *Diversity and Distributions*, 17(1):43–57, November 2010.

Jingyun Fang, Takehisa Oikawa, Tomomichi Kato, Wenhong Mo, and Zhiheng Wang. Biomass carbon accumulation by japan's forests from 1947 to 1995. *Global Biogeochemical Cycles*, 19(2):n/a–n/a, April 2005.

FIA. *Forest Inventory and Analysis: Sampling and Plot Design*, February 2005.

Alan H Fielding and John F Bell. A review of methods for the assessment of prediction errors in conservation presence/absence models. *Environmental Conservation*, 24(01):38–49, 1997.

Food and Agriculture Orgnization. *Global Forest Resources Assessment 2010 - Main report*. FAO Forestry, 2010.

Holly K Gibbs, Sandra Brown, John O Niles, and Jonathan A Foley. Monitoring and estimating tropical forest carbon stocks: making redd a reality. *Environmental Research Letters*, 2(4):045023, December 2007.

A Grainger. Difficulties in tracking the long-term global trend in tropical forest area. *Proceedings of the National Academy of Sciences*, 105(2):818–823, January 2008.

M C Hansen, S V Stehman, P V Potapov, T R Loveland, J R G Townshend, R S DeFries, K W Pittman, B Arunarwati, F Stolle, and M K Steininger. Humid

tropical forest clearing from 2000 to 2005 quantified by using multitemporal and multiresolution remotely sensed data. *Proceedings of the National Academy of Sciences*, 105(27):9439, 2008.

M C Hansen, P V Potapov, R Moore, M Hancher, S A Turubanova, A Tyukavina, D Thau, S V Stehman, S J Goetz, T R Loveland, A Kommareddy, A Egorov, L Chini, C O Justice, and J R G Townshend. High-Resolution Global Maps of 21st-Century Forest Cover Change. *Science*, 342(6160):850–853, November 2013.

David J Harding. ICESat waveform measurements of within-footprint topographic relief and vegetation vertical structure. *Geophysical Research Letters*, 32(21): L21S10, 2005.

Linda S. Heath and James E Smith. An assessment of uncertainty in forest carbon budget projections. *Environmental Science & Policy*, 3(2):73–82, 2000.

R A Houghton, Forrest Hall, and Scott J Goetz. Importance of biomass in the global carbon cycle. *Journal of Geophysical Research*, 114:G00E03, September 2009.

A Huete, K Didan, T Miura, EP Rodriguez, X Gao, and LG Ferreira. Overview of the radiometric and biophysical performance of the modis vegetation indices. *Remote Sensing Of Environment*, 83:195–213, 2002.

Marc L Imhoff. A theoretical analysis of the effect of forest structure on synthetic aperture radar backscatter and the remote sensing of biomass. *Geoscience and Remote Sensing, IEEE Transactions on*, 33(2):341–352, 1995.

J.C. Jenkins, D.C. Chojnacky, L.S. Heath, and R.A. Birdsey. National-scale biomass estimators for united states tree species. *Forest Science*, 49(1):12–35, 2003.

C O Justice, JRG Townshend, E F Vermote, E Masuoka, R E Wolfe, N Saleous, D P Roy, and J T Morisette. An overview of MODIS Land data processing and product status. *Remote Sensing Of Environment*, 83(1):3–15, 2002.

T Kajimoto, Y Matsuura, M A Sofronov, A V Volokitina, S Mori, A Osawa, and A P Abaimov. Above-and belowground biomass and net primary productivity of a larix gmelinii stand near tura, central siberia. *Tree physiology*, 19(12): 815–822, 1999.

GE Kindermann, I McCallum, and S Fritz. A global forest growing stock, biomass and carbon map based on fao statistics. *Silva Fennica*, 2008.

Akira Komiyama, Jin Eong Ong, and Sasitorn Poungparn. Allometry, biomass, and productivity of mangrove forests: A review. *Aquatic Botany*, 89(2):128–137, August 2008.

MA Lefsky, DJ Harding, M Keller, WB Cohen, CC Carabajal, FD Espirito-Santo, MO Hunter, R de Oliveira, and PB de Camargo. Estimates of forest canopy height and aboveground biomass using icesat (vol 33, art no l05501, 2006). *Geophysical Research Letters*, 33(5):–, 2006.

Michael A Lefsky. A global forest canopy height map from the moderate resolution imaging spectroradiometer and the geoscience laser altimeter system. *Geophysical Research Letters*, 37(15):L15401, August 2010.

Michael A Lefsky, Michael Keller, Yong Pang, Plinio B De Camargo, and Maria O Hunter. Revised method for forest canopy height estimation from geoscience laser altimeter system waveforms. *Journal of Applied Remote Sensing*, 1:–, 2007.

S O Los, J A B Rosette, N Kljun, P R J North, L Chasmer, J C Suárez, C Hopkinson, R A Hill, E van Gorsel, C Mahoney, and J A J Berni. Vegetation height

and cover fraction between 60 ° s and 60 ° n from icesat glas data. *Geoscientific Model Development*, 5(2):413–432, 2012.

Elizabeth C. Losos and Egbert G. Jr. Leigh, editors. *Tropical Forest Diversity and Dynamism: Findings from a Large-Scale Plot Network*. University of Chicago Press, 2004.

Jean-Remy Makana, Corneille N Ewango, Sean M McMahon, Sean C Thomas, Terese B Hart, and Richard Condit. Demography and biomass change in monodominant and mixed old-growth forest of the congo. *Journal of Tropical Ecology*, 27(05):447–461, August 2011.

Peter McKendry. Energy production from biomass (part 1): overview of biomass. *Bioresource technology*, 83(1):37–46, 2002.

E T A Mitchard, S S SAATCHI, I H Woodhouse, G Nangendo, N S Ribeiro, M Williams, C M Ryan, S L Lewis, T R Feldpausch, and P Meir. Using satellite radar backscatter to predict above-ground woody biomass: A consistent relationship across four different african landscapes. *Geophysical Research Letters*, 36(23), December 2009.

Karel Mokany, R John Raison, and Anatoly S Prokushkin. Critical analysis of root : shoot ratios in terrestrial biomes. *Global Change Biology*, 12(1):84–96, 2006.

RB Myneni, RR Nemani, and SW Running. Estimation of global leaf area index and absorbed par using radiative transfer models. *IEEE Transactions on Geoscience and Remote Sensing*, 35(6):1380–1393, 1997.

Christopher S R Neigh, Ross F Nelson, K Jon Ranson, Hank A Margolis, Paul M Montesano, Guoqing Sun, Viacheslav Kharuk, Erik Næsset, Michael A Wulder, and Hans-Erik Andersen. Taking stock of circumboreal forest carbon with

ground measurements, airborne and spaceborne lidar. *Remote Sensing Of Environment*, 137(C):274–287, October 2013.

D M Olson, E Dinerstein, E D Wikramanayake, N D Burgess, G V N Powell, E C Underwood, J A D'amico, I Itoua, H E Strand, and J C Morrison. Terrestrial ecoregions of the world: a new map of life on earth. *BioScience*, 51(11):933–938, 2001.

Y Pan, R A Birdsey, J Fang, R Houghton, P E Kauppi, W A Kurz, O L Phillips, A Shvidenko, S L Lewis, J G Canadell, P Ciais, R B Jackson, S W Pacala, A D McGuire, S Piao, A Rautiainen, S Sitch, and D Hayes. A large and persistent carbon sink in the world's forests. *Science*, 333(6045):988–993, August 2011.

Yude Pan, Richard A Birdsey, Oliver L Phillips, and Robert B Jackson. The structure, distribution, and biomass of the world's forests. *Annual Review of Ecology, Evolution, and Systematics*, 44(1):131010123440000, November 2012.

Genevieve Patenaude, Ronald Milne, and Terence P Dawson. Synthesis of remote sensing approaches for forest carbon estimation: reporting to the Kyoto Protocol. *Environmental Science & Policy*, 8(2):161–178, April 2005.

David A. Perry, Ram Oren, and Stephen C. Hart. *Forest Ecosystems*. Johns Hopkins University Press, 2 edition, 2008.

S Phillips, R Anderson, and R Schapire. Maximum entropy modeling of species geographic distributions. *Ecological Modelling*, 190(3-4):231–259, January 2006.

SJ Phillips and M Dudík. A maximum entropy approach to species distribution modeling. In *Proceedings of the twenty-first edings of the Twenty-First International Conference on Machine Learning*, 2004.

Steven J Phillips and Miroslav Dudík. Modeling of species distributions with

maxent: new extensions and a comprehensive evaluation. *Ecography*, 31(2): 161–175, 2008.

J. Pitman. *Probability*. Springer texts in statistics. Springer, 1993. ISBN 9780387979748.

Sorin C Popescu, Kaiguang Zhao, Amy Neuenschwander, and Chinsu Lin. Satellite lidar vs. small footprint airborne lidar: Comparing the accuracy of aboveground biomass estimates and forest structure metrics at footprint level. *Remote Sensing Of Environment*, 115(11):2786–2797, November 2011.

K G Roques, T G O'connor, and A R Watkinson. Dynamics of shrub encroachment in an African savanna: relative influences of fire, herbivory, rainfall and density dependence. *Journal of Applied Ecology*, 38(2):268–280, 2001.

Casey M Ryan, Mathew Williams, and John Grace. Aboveand belowground carbon stocks in a miombo woodland landscape of mozambique. *Biotropica*, 43(4): 423–432, 2011.

S Saatchi, M Marlier, R L Chazdon, D B Clark, and A E Russell. Impact of spatial variability of tropical forest structure on radar estimation of aboveground biomass. *Remote Sensing Of Environment*, 115(11):2836–2849, 2011a.

Sasan S Saatchi and Kyle C McDonald. Coherent effects in microwave backscattering models for forest canopies. *Geoscience and Remote Sensing, IEEE Transactions on*, 35(4):1032–1044, 1997.

Sassan Saatchi, Y Malhi, B Zutta, W Buermann, L O Anderson, A M Araujo, O L Phillips, J Peacock, H ter Steege, and G Lopez Gonzalez. Mapping landscape scale variations of forest structure, biomass, and productivity in amazonia. *Biogeosciences Discussions*, 6(3):5461, 2009.

Sassan S. Saatchi, Nancy L. Harris, Sandra Brown, Michael Lefsky, Edward T. A. Mitchard, William Salas, Brian R. Zutta, Wolfgang Buermann, Simon L. Lewis, Stephen Hagen, Silvia Petrova, Lee White, Miles Silman, and Alexandra Morel. Benchmark map of forest carbon stocks in tropical regions across three continents. *Proceedings of the National Academy of Sciences of the United States of America*, 108(24):9899–9904, 2011b.

SS Saatchi and M Moghaddam. Estimation of crown and stem water content and biomass of boreal forest using polarimetric sar imagery. In *Ieee Transactions on Geoscience and Remote Sensing*, pages 697–709. CALTECH, Jet Prop Lab, Pasadena, CA 91109 USA, June 2000.

J L Sarmiento and N Gruber. Sinks for anthropogenic carbon. *Physics Today*, 55 (8):30–36, 2002.

Dmitry Schepaschenko, Ian McCallum, Anatoly Shvidenko, Steffen Fritz, Florian Kraxner, and Michael Obersteiner. A new hybrid land cover dataset for russia: a methodology for integrating statistics, remote sensing and in situ information. *Journal of Land Use Science*, 6(4):245–259, December 2011.

Marc Simard, Kegi Zhang, Victor H Rivera-Monroy, Michael S Ross, Pablo L Ruiz, Edward Castañeda-Moya, Robert R Twilley, and Ernesto Rodriguez. Mapping height and biomass of mangrove forests in Everglades National Park with SRTM elevation data. *Photogrammetric Engineering and Remote Sensing*, 72(3):299–311, 2006.

Marc Simard, Naiara Pinto, Joshua B Fisher, and Alessandro Baccini. Mapping forest canopy height globally with spaceborne lidar. *Journal of Geophysical Research-Biogeosciences*, 116:G04021, 2011.

J W Ferry Slik, Gary Paoli, Krista McGuire, Ieda Amaral, Jorcely Barroso, Meredith Bastian, Lilian Blanc, Frans Bongers, et al. Large trees drive forest above-

ground biomass variation in moist lowland forests across the tropics. *Global Ecology and Biogeography*, 21(10):n/a–n/a, July 2013.

James E Smith, Linda S. Heath, and Coeli M Hoover. Carbon factors and models for forest carbon estimates for the 2005–2011 national greenhouse gas inventories of the united states. *Forest Ecology and Management*, 307:7–19, November 2013.

W-T Tsai, M Spencer, C Wu, C Winn, and K Kellogg. Seawinds on quikscat: Sensor description and mission overview. *IEEE*, 3:1021–1023, 2000.

Ivan Valiela, Jennifer L Bowen, and Joanna K York. Mangrove Forests: One of the World's Threatened Major Tropical Environments. *BioScience*, 51(10): 807–815, 2001.

Frank Van Langevelde, Claudius ADM Van De Vijver, Lalit Kumar, Johan Van De Koppel, Nico De Ridder, Jelte Van Andel, Andrew K Skidmore, John W Hearne, Leo Stroosnijder, and William J Bond. Effects of fire and herbivory on the stability of savanna ecosystems. *Ecology*, 84(2):337–350, 2003.

Jakob J Van Zyl. The Shuttle Radar Topography Mission (SRTM): a breakthrough in remote sensing of topography. *Acta Astronautica*, 48(5):559–565, 2001.

G.B. West, J H Brown, and B J Enquist. A general model for the origin of allometric scaling laws in biology. *Science*, 276(5309):122–126, 1997.

Yifan Yu, Sassan Saatchi, Linda S. Heath, Elizabeth LaPoint, Ranga Myneni, and Yuri Knyazikhin. Regional distribution of forest height and biomass from multisensor data fusion. *Journal of Geophysical Research-Biogeosciences*, 115: –, 2010.